PHYSMOD 2024 - Book of Abstracts

Adam Thomas, Alexandrou Giorgos, Alisse Jean, Amon Thomas, Andrewartha Tristan, Azarpeyvand Mahdi, Babin Valery, Badeke Ronny, Barulli Marilina, Beleza Vaz Guilherme, et al.

PHYSMOD Lyon 2024

PHYSMOD 2024

International Workshop on Physical Modelling of Flow and Dispersion Phenomena

Ecole Centrale de Lyon, Ecully, France – August 28-30, 2024

Book of Abstracts

La Région Auvergne-Rhône-Alpes · ÉCOLE CENTRALE LYON · Lyon 1 · INSA INSTITUT NATIONAL DES SCIENCES APPLIQUÉES LYON · cnrs · LMFA

Table of contents

28 Aug 2024

Buoyancy and stratification

PHYSMOD 2024 – International Workshop on Physical Modelling of Flow and Dispersion Phenomena
Ecole Centrale de Lyon, Ecully, France – August 28-30, 2024

Bottom roughness effects on mixing properties of a gravity current

G. Ravizza Garibaldi[1], A. Di Bernardino[2], G. Leuzzi[1], G. Querzoli[3], P. Monti[1]

[1]University of Rome La Sapienza, Faculty of Civil and Industrial Engineering, Department of Civil, Building and Environmental Engineering, Via Eudossiana 18, 00184 Rome, Italy
[2]University of Rome La Sapienza, Department of Physics, P. Aldo Moro 5, 00185 Rome, Italy
[3]University of Cagliari, Faculty of Engineering and Architecture, Department of Civil, Environmental Engineering and Architecture, Via Marengo 2, 09123 Cagliari, Italy

Abstract

The objective of this work is to provide experimental evaluation of turbulence parameters for a gravity current flowing over roughness elements. Such parameters can be of interest in turbulence closure models, as well as increase knowledge on turbulent mixing for different environmental compartments, such as atmospheric or oceanic flows.

The experiments are conducted in a water tank 7.4 m long (x-axis), 0.35 m high (z-axis) and 0.25 m wide (y-axis). The tank is divided into two separate sections by a movable gate. The left side of the channel is filled with a mixture of salt and fresh water (heavier fluid), whose density is higher than that of the fresh water (lighter fluid) contained in the right section (Figure 1). The water depth in the two volumes is H=0.25 m, the density difference $\Delta\rho$=6.9 g/l. The left volume is premixed with a fluorescent dye (Rodhamine-WT). The experiment starts by removing the gate, which allows the denser fluid to flow from left to right under the lighter fluid. Velocity and dye concentration are measured simultaneously on the vertical section (x-z plane) passing through the longitudinal axis of the channel. Feature Tracking and Planar Laser-Induced Fluorescence techniques were used to provide simultaneous velocity and density measurements along a vertical plane passing through the longitudinal axis of the tank.

The acquisition facility consists of a green laser (5 W, wavelength $532 \cdot 10^{-9}$ m) that illuminates the acquisition plane (~0.002 m thick), and two synchronized cameras, which acquire 100 frames per second with a resolution of 1024x1280 pixels. The two cameras are aligned to optimize framing of the area of interest (0.072 m high, z-axis, and 0.088 m wide, z-axis) and to reduce image distortion. The first camera captures the positions of non-buoyant particles (~$20 \cdot 10^{-6}$ m in diameter) premixed in both fluids and allows assessment of instantaneous velocity fields by image analysis-based feature-tracking. A Gaussian interpolation algorithm is applied at each instant to the scattered samples in the x-z plane to obtain the instantaneous velocity field on a regular 102x128 array, which corresponds to a spatial resolution of ~0.0007 m. Fluid density is determined in each pixel by laser-induced planar fluorescence, by which it is possible to relate density with the measured brightness (related to the fractional volume of the coloured fluid), which, in turn, is proportional to the salt concentration. The instantaneous concentration field is mapped onto the instantaneous velocity field using an affine transformation that takes into account the different viewpoint of the two cameras. Each array of roughness elements used for the experiments is composed of parallelepipeds of base $1.5 \cdot 10^{-2}$ m

glued onto the bottom of the channel in an aligned pattern (Figure 1). The height of the obstacles varies between $1.5 \cdot 10^{-2}$ m and $2.0 \cdot 10^{-2}$ m; their average height is $h=1.75 \cdot 10^{-2}$ m. Three arrangements corresponding to plan area indices, $\lambda_P=A_P/A_T=0.2$, 0.3 and 0.4, are investigated. Here, A_P is the plan area occupied by the obstacles and A_T is the array area. After the passage of the gravity current front, a quasi-stationary regime lasting nearly 90 s occurs, during which statistics of the variables are determined. In particular, streamwise (u) and vertical mean velocity components, velocity variances, vertical momentum flux, as well as mean density and vertical density flux are determined on the 102x128 array by applying the canonical Reynolds averaging method. From the density and velocity fields and the turbulent mass and momentum fluxes, the vertical profiles of turbulent diffusivities of mass, $<K_\rho>$, momentum, $<K_M>$, obtained using first order closure, and the inverse of the turbulent Schmidt number, $<Sc_t^{-1}>=< K_\rho >/< K_M >$, were determined for the three λ_P ($<\cdot>$ refers to horizontal averaging). To analyse the role played by the roughness elements, the values of the variables obtained for the three λ_P have been averaged among them and compared to those determined in the case of smooth bottom (no roughness elements).

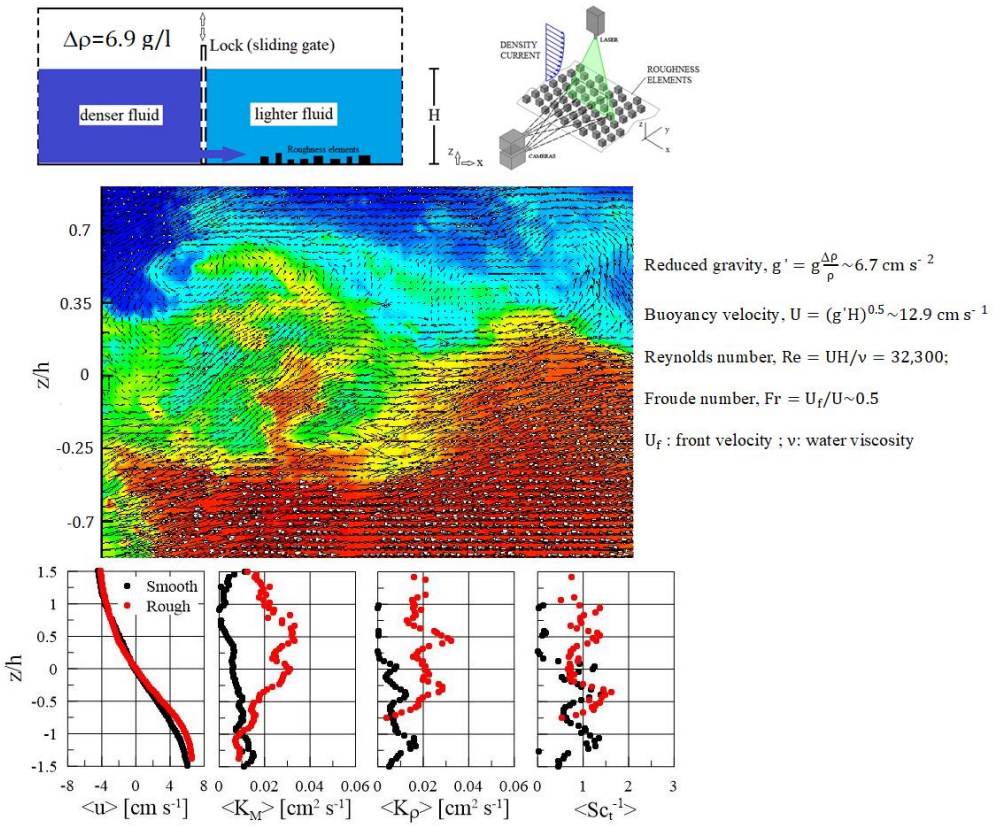

Figure 1: Sketch of the experimental apparatus (above), snapshot of an instantaneous velocity (vectors) and density field (colour map, red refers to denser fluid) for λ_p=0.3 (middle), and some of the vertical profiles obtained for the smooth (black symbols) and the rough (red symbols) case, where the latter refers to the average calculated for the three rough cases. z/h=0 corresponds to the height where the streamwise velocity changes its sign (~0.12 m above the channel bottom).

Figure 1 (middle panel) shows a snapshot of the instantaneous velocity and density fields during the breaking of a Kelvin-Helmholts billow forming after the passage of the front. On average, the depth of the interfacial layer is ~2h=0.035 m for the rough case, while it is considerably lower for the smooth one. The bottom panel shows a clear dependence of both $<K_\rho>$ and $<K_M>$ on the surface characteristics (i.e., rough or not), but this is not reflected in Sc_t^{-1}, which remains, albeit fluctuating, around the unit value.

PHYSMOD 2024 – International Workshop on Physical Modelling of Flow and Dispersion Phenomena
Ecole Centrale de Lyon, Ecully, France – August 28-30, 2024

Dispersion of Passive and Dense Plumes over a Step-Change in Wall Roughness

C. Deebank, M. Placidi, M. Carpentieri

Centre for Aerodynamics and Environmental Flow, Faculty of Engineering and Physical Sciences, University of Surrey, Guildford, UK

The majority of the literature on atmospheric dispersion, to date, considers boundary layers with homogenous surface roughness morphologies. However, in many scenarios in nature this is not the case. For example, wind flow over farmland encountering an urban area or ocean winds blowing over a coastline. This discontinuity - or step-change - in the characteristics of surface roughness will generate an internal boundary layer (IBL) within the existing boundary layer as the flow adjusts to the new surface conditions. The IBL (in a smoother to rougher case) is characterised by a region of more turbulent 'adjusted flow' close to the surface within the existing boundary layer that grows in height with downstream distance.

This presentation will discuss a series of IBL dispersion experiments carried out in the EnFlo wind tunnel at the University of Surrey. The work aims to study the effect of an IBL on the dispersion of passive and dense gas plumes released both upstream and downstream to the newly-developed IBL. The IBL was generated using the method detailed by Ding et. al. (2023); a step-change in roughness length, with an upstream section of relatively lower roughness length to a downstream section of higher roughness length. Passively buoyant (air) and dense (CO_2) plumes are released from a ground level point source in three separate locations: 1m upstream from, 1m downstream from and at the step change location. Time-resolved concentration measurements were taken via a single FFID mounted on a 3-axis traverse (Figure 1).

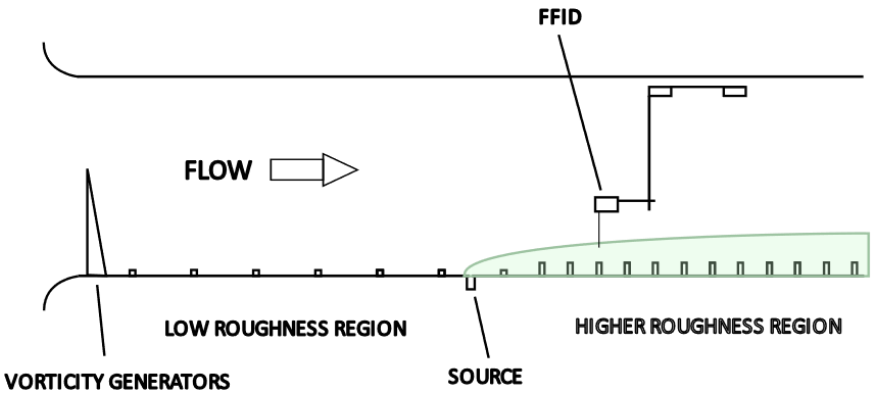

Figure 1: Diagram of EnFlo Tunnel test section showing experimental setup used

Profiles were taken at seven streamwise locations, one vertical and two lateral (one in roughness sublayer, one in the log-law region), to observe the plume lateral and vertical growth rate as well as the behaviour of concentration within the plume, both in terms of its mean and higher-order properties.

Initial results show an increase in plume lateral and vertical spread immediately behind the step change (Figure 2). In this case, the plume width is calculated by fitting a Gaussian curve to mean concentration profiles and extracting its standard deviation. As the distance from the step change increases, the growth rate decaysbut remains greater than it was before step change; this is likely due to the higher wall roughness driving increased turbulence levels within the boundary layer. Concentration fluctuations are also seen to exhibit a significant increase downstream of the step change. These trends occur in both the passively buoyant and dense plumes.

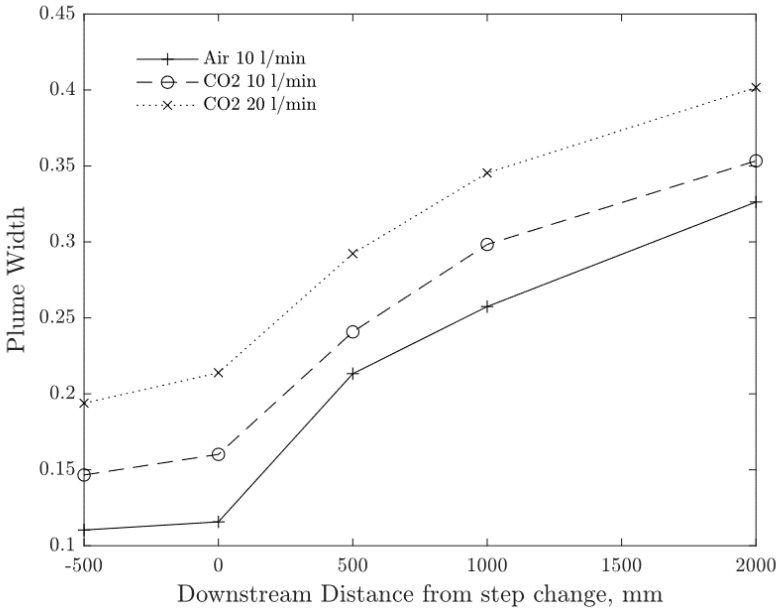

Figure 2: Non-dimensionalised plume width in the roughness sublayer plotted against streamwise distance from the step change

The presentation will explore these results in more detail, as well as discuss the behaviour of higher-order concentration statisitics within the IBL.

References

Ding, S. S. Et al (2023). Neutrally- and stably-stratified boundary layers adjustments to a step change in surface roughness. *Experiments in Fluids* 64. 86.

PHYSMOD 2024 – International Workshop on Physical Modelling of Flow and Dispersion Phenomena
Ecole Centrale de Lyon, Ecully, France – August 28-30, 2024

Gravity currents advancing on heated walls: experimental and numerical analysis

S. Lanzini[1], M. Marro[1], S.Vaux[2], M. Creyssels[1], J. Jay[3], P. Salizzoni[1,4]

[1] Ecole Centrale de Lyon, CNRS, INSA Lyon, Univ Claude Bernard Lyon 1, LMFA, UMR5509, 36 Av. Guy de Collongue, Ecully 69130, France
[2] Institut de Radioprotection et de Sûreté Nucléaire (IRSN), PSN-RES, SA2I, LIE, Cadarache, 13115 St Paul-Lez-Durance, France
[3] Thermal Center of Lyon (CETHIL-UMR CNRS 5008) INSA Lyon, Villeurbanne, France
[4] Department of Environmental, Land and Infrastructure Engineering (DIATI), Politecnico di Torino, Corso Duca degli Abruzzi 24, 10129 Turin, Italy

Introduction

A gravity current is generated when a layer of fluid with density ρ, travels into an ambient fluid with a different density ρ_0. Such currents are ubiquitous in geophysical (winds, oceanic currents, pyroclastic clouds), industrial (liquid and gas releases), and environmental domains. The current fronts have been characterized in literature in terms of advancing velocity, height, and entrainment and mixing with the ambient fluid. Notably, front properties were described in previous studies evaluating the effects of the Richardson number at source (Sher and Woods 2017), different wall slopes, and the presence of free-slip or no-slip boundary condition at the wall. The goal of this work is to extend the understanding of the phenomenon imposing a boundary condition that has not yet been studied, namely, the presence of a constant heat flux at the wall. This condition is useful to investigate, for example, the interaction of an atmospheric gravity current with heating emitted from the earth's ground or, referring to the upside-down problem, how hot smokes generated by a fire in a road tunnel advance below the cold ceiling.

Methods and Results

The analysis is performed by combining novel laboratory experiments and numerical simulations**.** The experimental installation (Figure 1 (a)) consists of a 4-meter long and 30-cm wide rectangular channel, in which the lower wall can be warmed by means of 8 resistor fabrics (Figure 1 (b)). These elements, each measuring 500cmx30cm, heat uniformly the entire area of the lower wall through Joule effect. The heating power is controlled by adjusting the voltage supplied to each resistor. The dense gravity current is created by a mixture of air and CO_2 that is introduced into a tranquilization chamber and then at channel inlet with a constant mass flux. The mixture is seeded with micronic olive oil droplets and is visualized by means of laser tomography.

The numerical analysis is performed with 3D large-eddy-simulations that are used to solve Favre-filtered Navier Stokes equation along with energy conservation and species transport equations. We use the numerical code CALIF3-ISIS developed at the French Institut de Radioprotection ed Surete Nucleaire (IRSN).

A new non-dimensional number, $\hat{B}$, is defined to evaluate different heating intensities. This is obtained considering the ratio between the vertical buoyancy flux per unit area, B_φ, induced by the imposed heat flux per unit area φ, and the horizontal buoyancy flux per unit area that generates the current, B_{CO2}. The latter is computed as $B_{CO2} = u_s g(\rho_s - \rho_0)/\rho_0$, where g is the gravitational acceleration and u_s and ρ_s are the inlet velocity and density, respectively.

The advancing front velocity is investigated in both experiments (Figure 1(c)) and simulations (Figure 1(d)) while the entrainment and mixing processes are studied only through simulations. We find that, regardless of the Richardson number at the inlet, the advancement velocity is reduced in the case with heated wall compared to the adiabatic-wall case. The slowdown of the front in the heated case is due to its interaction with the vertical hot plumes created by natural convection. The mixing with hot-air plumes causes a reduction in the buoyancy of the front, which can lead, for sufficiently intense heating, to a null advancing velocity and to the lifting of the current.

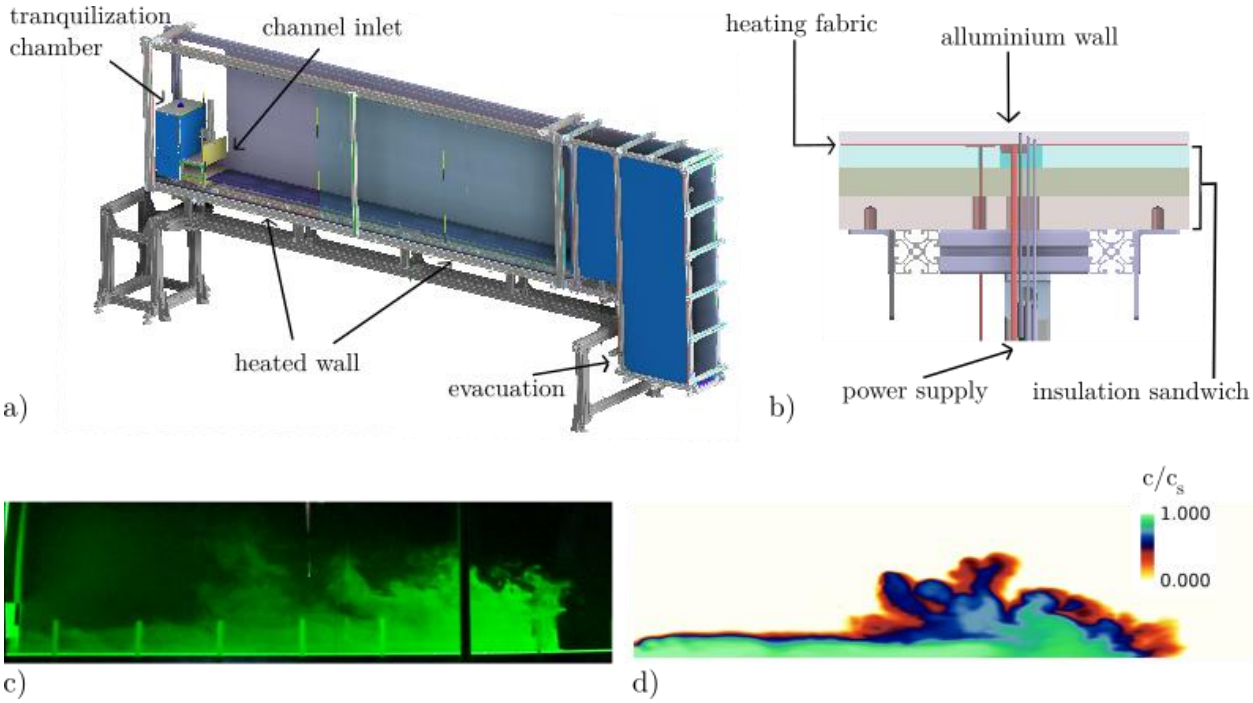

Figure 1: Panel a) shows an outline of the experimental facility and panel b) shows a detail of the heated wall. Panels c) and d) rapresent an experimental and numerical visualization of a current with $\hat{B} = 0.02$. The color scale in panel d) is the local concentration normalized with the concentration at the source

References

Sher D., Woods A.W. Mixing in continuous gravity currents. *Journal of Fluid Mechanics*. 2017;818:R4. doi:10.1017/jfm.2017.168

PHYSMOD 2024 – International Workshop on Physical Modelling of Flow and Dispersion Phenomena
Ecole Centrale de Lyon, Ecully, France – August 28-30, 2024

Investigation of the influence of atmospheric stability on pollutant concentration using field observation data

Takumi Tachibana[1], Ryuichiro. Yoshie[2], Yingli Xuan[2]

[1]Wind Engineering Institute Co., Ltd. Kanda Jinbo-chou 1-14-3, 101-0051 Chiyoda, Tokyo, Japan
[2]Tokyo Polytechnic University, Department of Engineering, Iiyama Minami 5-45-1, 243-0297 Atsugi, Japan

Abstract

Hu and Yoshie (2020) proposed SER_C* (Stability Effect Ratio of Normalized Pollutant Concentration) as an index that expresses the stability effect on pollutant concentration. SER_C* represents the ratio of normalized pollutant concentration under non-neutral atmospheric stability conditions to that under neutral conditions. Their analysis revealed that SER_C* generally increases as Pasquill atmospheric stability shifts from class A to G. However, the standard deviation was large at each class. One of the reasons of this large deviation may be the inadequate representation of atmospheric stability by Pasquill's classification. Therefore, in this study, we decided to investigate SER_C* using the Bulk Richardson number (R_b) to classify atmospheric stability. First, R_b was determined using observation data and the results of Weather Research and Forecasting model (WRF) analysis. Then we investigated SER_C* based on nitrogen oxides (NOx) concentration data observed at 36 Roadside Air Pollution Monitoring Stations in Tokyo. As a result, the value of SER_C* increases as R_b increases. In unstable atmospheric conditions, the standard deviation of SER_C* is smaller when classified by R_b compared to Pasquill's classification. However, the standard deviation of SER_C* in neutral and stable state was still large. The uncertainty in the NOx emissions assumption may have led to a larger standard deviation of SER_C*.

Classification of Atmospheric stability

In this study, the Bulk Richardson number (R_b) by equation (1) was utilized for atmospheric stability classification. The R_b was determined using wind speed and temperature observed at H=200 m, and ground surface temperature analyzed by WRF (Yoshie at al., 2023).

$$R_b = \frac{g(\theta_H - \theta_G)H}{\theta_a U_H^2} \quad (1)$$

where g is acceleration of gravity [m s^{-2}], H is reference height [m], θ_H is representative potential temperature [K] and θ_G is ground surface temperature [K], θ_a is average of potential temperature below 200 m height [K], U_H is wind speed at reference height [m s^{-1}]. For R_b<0, the atmospheric stability is unstable, and R_b>0, the atmospheric stability is stable. R_b=0 represents a neutral condition.

Statistical data analysis of SER_C* based on observational data

There are 36 Roadside Air Pollution Monitoring Stations in Tokyo, Japan, and pollutant concentrations are constantly monitored (Bureau of Environment 2024). We used hourly values of NOx from June 2018 to May 2019. The procedure of statistical data analysis is as follows. Step 1. Define hourly

atmospheric stability classes based on the R_b. Step 2. For each station, normalize NOx concentration using the below equation (2). But in the actual procedure, only CU [ppb m s^{-1}] was calculated for C^* because H and Q would be eliminated after the following assumption and procedure. Step 3. For each station, group C^* based on day of week and hour. We assume that the NOx emission rate Q is the same if the day of week and hour are the same. Step 4. For each station, Classify the C* grouped in step 3 by 16 wind direction at H=200 m. Step 6. For each station, select C_n^* under neutral conditions for each day of week, hour, wind direction. Step 7. For each station, divide all C^* values by C_n^* to get SER_C* that expresses the stability effect on NOx each day of week, hour, wind direction.

$$C^* = \frac{CU_H H^2}{Q} \quad (2)$$

$$SER\_C^* = \frac{C^*}{C_n^*} \quad (3)$$

Where C^* is non-dimensional normalized NOx concentration, C is the observed NOx concentration [ppb], Q is emission rate [m^3 s^{-1}], C_n^* is C^* under neutral atmospheric conditions.

Results

All averaged value of SER_C* (36 stations) are plotted as a function of R_b in Figure 1. The numbers of data for each plot are written in Figure 1. SER_C* value is larger than 1 under stable atmospheric conditions, equal to 1 under neutral condition and smaller than 1 under unstable atmospheric conditions. Although not shown in this figure, the trend in the change in SER_C* with respect to stability is more pronounced when atmospheric stability is classified by R_b rather than Pasquil's stability class, as compared to the results of Hu and Yoshie (2020). Additionally, when the atmospheric stability is unstable, the standard deviation of SER_C* is small. However, the standard deviation of SER_C* in neutral and stable conditions are still large. One reason for this is the assumption that NOx emissions would be the same for the same day of the week and time of day. This uncertainty may have increased the standard deviation of SER_C*.

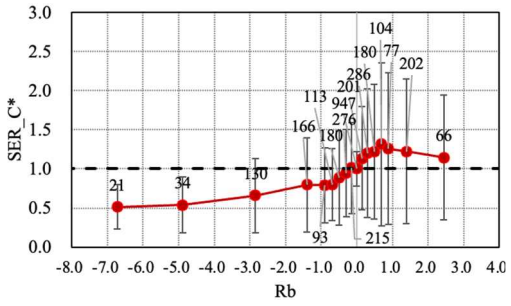

Figure 1: SER_C (average of 36 stations) as a function of Bulk Richard son number (R_b)*

Acknowledgement

This work was supported by JSPS KAKENHI Grant Number 21H01498.

References

Hu, T., Yoshie, R. (2020). Effect of atmospheric stability on air pollutant concentration and its generalization for real and idealized urban block models based on field observation data and wind tunnel experiments. *Journal of Wind Engineering & Industrial Aerodynamics*, Vol, 207.

Bureau of Environment (2024). Tokyo Metropolitan Government JP Website.

Yoshie, R., Tachibana, T., Xuan, Y. (2023) Investigation of atmospheric stability in Tokyo using observation data and analysis data by WRF. *The 16the International Conference on Wind Engineering*.

PHYSMOD 2024 – International Workshop on Physical Modelling of Flow and Dispersion Phenomena
Ecole Centrale de Lyon, Ecully, France – August 28-30, 2024

Passive scalar dispersion in stable boundary layers

P. Salizzoni[1], M. Marro[1], P. Hayden[2], M. Carpentieri[2]

[1] Ecole Centrale de Lyon, CNRS, Universite Claude Bernard Lyon 1, INSA Lyon, LMFA, UMR5509, 69130, Ecully, France
[2]EnFlo Laboratory, School of Mechanical Engineering Sciences, University of Surrey, Guildford, GU2 7XH, UK

Introduction

Atmospheric stratification significantly influences plume dispersion, with non-neutral stratified conditions (stable and convective) prevailing for more than 70% of the time (e.g., Wood et al., 2010). Despite this, laboratory experiments examining the effects of thermal stratification on scalar dispersion have been exceedingly rare. To address this gap, wind tunnel experiments were conducted in stable boundary layers developing over a rough wall.

Methods

The experiments were conducted in the EnFlo Lab Wind Tunnel at the University of Surrey, an open-circuit wind tunnel designed specifically for environmental fluid dynamic experiments. The wind tunnel is equipped with twin fans that power its engine, and dispersion in stable boundary layers is achieved via a suck-through mechanism. It has an overall length of 27.2 meters, with a working section measuring 20 meters in length, 3.5 meters in width, and 1.5 meters in height. The airspeed range of the tunnel spans from 0.3 m/s to 3 m/s.

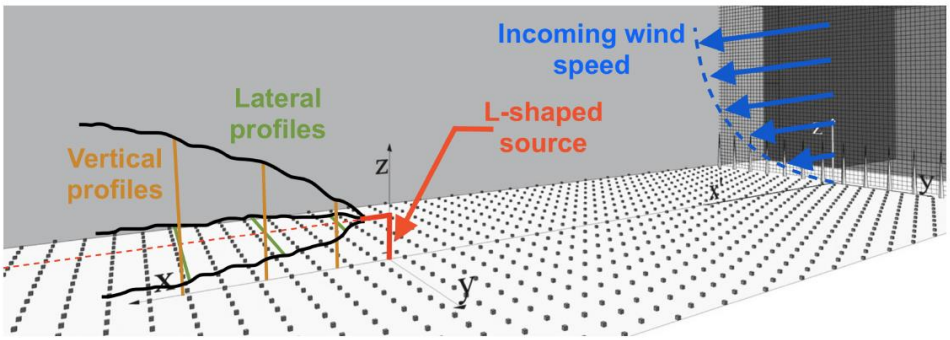

Figure 1: Experimental layout.

We have reproduced the experimental set up used by Fackrell and Robins (1982) in their seminal work, and recently reproduced by Nironi et al. (2015). An L-shaped source was placed in a fully-developed turbulent boundary layer (Figure 1) with varying Richardson number Ri_b. Simultaneous measurements of concentration, temperature and velocity were performed. The stratified boundary layer and its different stability conditions are obtained through a specific temperature profile at the inlet of the test section and cooling the wind tunnel floor. The temperature profile at the inlet is imposed with 15 heaters, each formed by a group of 9 tubes. Each group is spaced by 0.1 m along the vertical direction.

Moreover, the sidewalls of the test section are heated as well to help the inlet heater keep the correct vertical temperature gradient for all the testing section length.

Results

A full characterisation of the flow field has been performed as a preliminary task, analyzing single point velocity statistics, focusing on second turbulent kinetic energy production and dissipation phenomena. Expected characteristics of turbulence suppression by means of stratification have been observed. Moreover, length scales and time scales with have been computed using an Eulerian approach. A good agreement has been observed with the boundary layers simulated for this work and other boundary layers in previous studies (Marucci et al, 2018). Subsequently, we analysed concentration field as induced by releases emitted by two source sizes of different size and placed in flows with different stratification strengths (as well as the reference neutral case). The statistical moments of the concentration measurements were analysed up to the fourth order. A comparison between probability density function of concentration and the gamma distribution has shown a good agreement. Moreover, turbulent fluxes and turbulent diffusion coefficients have been computed by means of standard gradient diffusion hypothesis. Based on these data we could evaluate the dependence of the turbulent Schmidt number (see Figure 2) and of characteristic mixing time scales on different stability conditions.

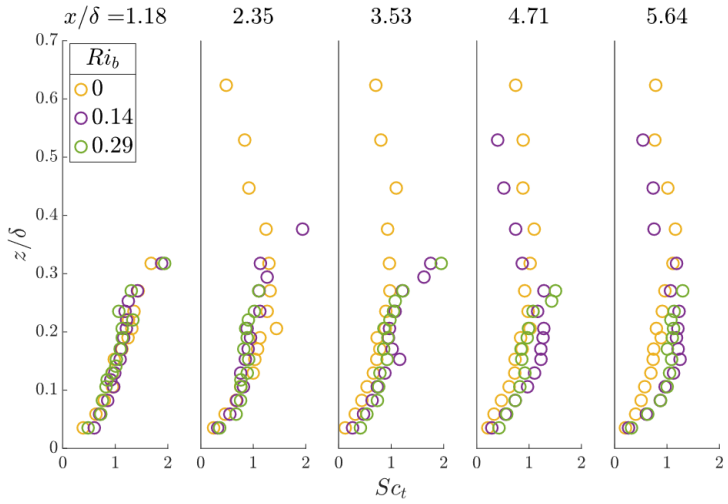

Figure 2: Evolution of the turbulent Scmidt number at varying downstream distance from the source for three startification conditions, as quantified by the bulk Richardson number Ri_b.

References

Fackrell J., Robins A. (1982). Concentration fluctuations and fluxes in plumes from point sources in a turbulent boundary layer. Journal of Fluid Mechanics 117, 1–26.

Marucci D., Carpentieri M., Hayden P.(2018). On the simulation of thick non-neutral boundary layers for urban studies in a wind tunnel, International Journal of Heat and Fluid Flow 72, 37-51

Nironi C., Salizzoni P., Marro M., Mejean P., Grosjean N., Soulhac L. (2015). Dispersion of a passive scalar fluctuating plume in a turbulent boundary layer. part i: Velocity and concentration measurements. Boundary-layer meteorology 156(3), 415–446.

Wood, C. R., Lacser, A., Barlow, J. F., Padhra, A., Belcher, S. E., Nemitz, E., Helfter, C., Famulari, D. & Grimmond, C. S. B. (2010) Turbulent flow at 190 m height above london during 2006-2008: a climatology and the applicability of similarity theory. Boundary-Layer Meteorology 137 (1), 77–96.

PHYSMOD 2024 – International Workshop on Physical Modelling of Flow and Dispersion Phenomena
Ecole Centrale de Lyon, Ecully, France – August 28-30, 2024

Pollutant Dispersion of Ship Emissions under Realistic Operating Conditions: Focus on Methodology

S. Gillmeier[1], E.W.M. Roosenboom[2], L.F. Sánchez Castro[3], J. Muralha[4], G. Beleza Vaz[4], T. Andrewartha[3]

[1] Eindhoven University of Technology, Department of the Built Environment, Groene Loper 3, 5612 AE Eindhoven, The Netherlands
[2] Damen Naval, De Willem Ruysstraat 99, 4381 NK Vlissingen, The Netherlands
[3] Knud E. Hansen, Lundegaarden, Claessensvej 1, DK-3000 Elsinore, Denmark
[4] blueOASIS, R. Prudêncio Franco da Trindade 4, 2655-344 Ericeira, Portugal

Abstract

Air pollution is recognized by the WHO as one of the greatest health risks. Although emissions of key air pollutants have decreased over the past decades, air quality remains poor in many areas (European Environment Agency, 2022). Among others this concerns the shipping industry and port areas. In situations where vessels operate in open sea or manoeuvre in harbours, various wind conditions might occur, possibly resulting in the exposure of crew or passengers on deck to noxious pollutants (e.g., Kennedy, 2019). For harbour operation, not only particulate matter remaining on deck is critical, but emitted pollutants can also be transported into the urban environment, resulting in locally increased concentrations of hazardous pollutants (e.g., Toscano et al., 2021). There is overall consensus for development into green(er) alternatives for fossil fuels and zero emission shipping within the shipping industry. This, however, is a long-term ambition (International Maritime Organization, 2022) and until then emissions will still need to be critically assessed. This work deals with the effect of neutral maritime-like atmospheric boundary layer (ABL) wind conditions on the exhaust gas dispersion of a vessel under realistic operational conditions: (i) in isolation, (ii) in proximity to a second vessel and (iii) nearby harbour infrastructure.

The vessel under investigation is a generic version of a representative service offshore vessel (length: 84 m; beam: 17 m), typically used for the construction and maintenance of wind farms in open sea. Such vessels usually have multiple exhaust pipes, located in close proximity to one another in a single casing. For the wind tunnel experiments, the exhaust pipes are combined into a single unit, and pollutants are released from one circular pipe of 0.76 m inner diameter (full-scale). The model hull is milled from Polyurethan while other more complex parts on deck are 3D powder printed from PA12. The sharp railings are cut from aluminium to guarantee sharp edges and flow separation. To emit pollutants from the exhaust a printed stainless steel pipe connection is inserted in the model. Figure 1 shows a drawing of the actual vessel (a) and a picture of the simplified wind tunnel model (b).

Measurements are conducted in the closed-circuit Atmospheric Boundary Layer Wind Tunnel at Eindhoven University of Technology at a reduced geometric scaling ratio of 1:100. With this geometric scale, neutral atmospheric flow conditions over sea can be replicated in the wind tunnel while keeping the densimetric Froude number in experiments and reality similar, following VDI-3783 (2000) guidelines. To guarantee Froude number similitude, a velocity scale of 1:10 is chosen.

Pollutants are released at a reduced-scale velocity of 0.88 m/s which corresponds to 25% of Maximum Continuous Rating (MCR) engine load. With an assumed full-scale wind velocity of about 10 m/s in 20 m height above water (Dutch Offshore Wind Atlas, 2019) relatively low approach flow velocities of about 1 m/s at exhaust height are required for the experiments. The resulting Reynolds number is about 11,200 based on the vessel's beam (0.17 m - reduced-scale).

Pollutant concentrations (in ppm) are measured at 34 locations on deck of the vessel and 18 locations in the near field using a HFR400 fast flame ionisation detector from Cambustion Ltd.

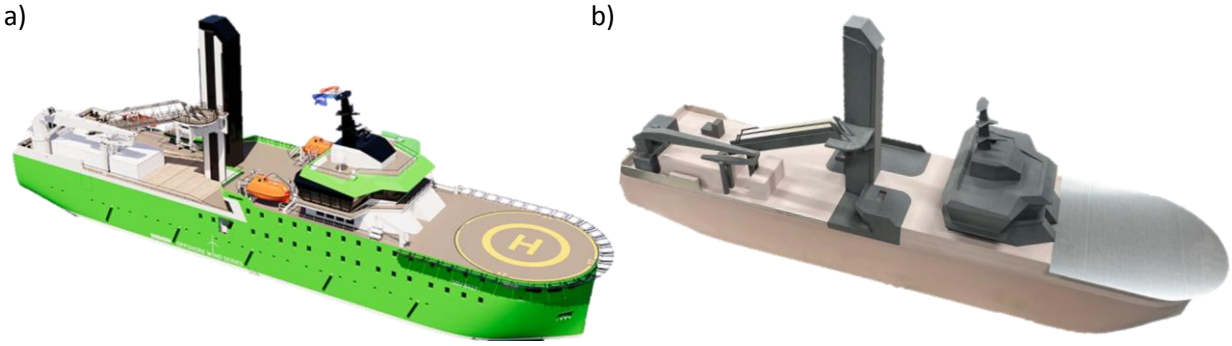

Figure 1: Drawing of a generic service operation vessel (a) and picture of simplified wind tunnel model replicated at a geometric scaling ratio of 1:100 (b).

It is hypothesized that the exposure of pollutants at the investigated locations will vary significantly with wind direction and that the presence of an additional vessel or harbour like infrastructure will strongly influence the dispersion of pollutants. Findings from this work are expected to raise awareness to improve Industry 4.0 design mechanisms. In addition, obtained data will provide a validation database for numerical models and thereby can contribute to improve tools for risk-assessment of ship exhaust gas dispersion.

Acknowledgement

This work is supported by the Engineering Research Infrastructures for European Synergies (ERIES) project (www.eries.eu), which has received funding from the European Union's Horizon Europe Framework Programme under Grant Agreement No. 101058684. This is ERIES publication number C20.

References

Dutch Offshore Wind Atlas, (2019). 10 year average wind speed for different heights – 20m. Available: https://www.dutchoffshorewindatlas.nl/atlas/image-library/image-library/wind-speed-parameter-f.

European Environment Agency, (2022). Air Quality in Europe. Available: https://www.eea.europa.eu//publications/air-quality-in-europe-2022.

International Maritime Organization, (2022). Next steps to deliver IMO GHG strategy. Available: https://www.imo.org/en/MediaCentre/PressBriefings/Pages/18-MEPCGHGprogramme.aspx.

Kennedy, R.D. (2019). An investigation of air pollution on the decks of 4 cruise ships. A Report for Stand.earth.

Toscano, D., Marro, M., Mele, B., Murena, F., Salizzoni, P., (2021). Assessment of the impact of gaseous ship emissions in ports using physical and numerical models: The case of Naples, Building and Environment, 196.

VDI-3783, (2000). Verein Deutscher Ingenieure. Environmental Meteorology – Physical modelling of flow and dispersion Processes in the atmospheric boundary layer – Application of wind tunnels.

PHYSMOD 2024 – International Workshop on Physical Modelling of Flow and Dispersion Phenomena
Ecole Centrale de Lyon, Ecully, France – August 28-30, 2024

Two-dimensional particle image velocimetry measurements in a wind tunnel model of the Jack Rabbit II field tests

P. V.d.F. Lopes[1], C.T. Smith[1], T. O. Spicer[1]

[1]IUniversity of Arkansas, Ralph E. Martin Department of Chemical Engineering, 3202 Bell/CHEG, Fayetteville, AR 72701, U.S.A.

Abstract

The field-scale Jack Rabbit II (JR-II) Mock Urban Environment (MUE) was reproduced in 50:1 scale physical model in the wind tunnel of the University of Arkansas. Field-scale releases of chlorine (liquefied ambient temperature) were all vertically downward from a 15 cm opening in the dissemination vessel which could contain up to 9,000 kg of chlorine. The downward releases formed a radially symmetric wall jet over the 25 m diameter concrete pad on which the releases were made. In the field scale tests, chlorine concentration measurements were made in the MUE in addition to video recordings from various perspectives. After demonstrating that a suitable model of the highly turbulent release flow could be made in the wind tunnel, this paper summarizes 2D Particle Imaging Velocimetry (PIV) measurements made before and during a surrogate chlorine release, which are the first measurements made under these circumstances.

In preparation for modelling the chlorine releases in the wind tunnel, field scale measurements of the upwind velocity profile were compared to velocity measurements made in the wind tunnel model using 3D Laser Doppler Velocimetry (LDV), and the agreement was found to be good. Figure 1a shows a typical comparison between field and wind tunnel measurements upwind of the MUE. The surface roughness in the model was simulated using billboard surface roughness elements measuring 3.8 cm by 3.8 cm perpendicular to the wind tunnel floor placed in a staggered arrangement with 60 cm between rows and 60 cm between elements in the same row. Upwind of the surface roughness elements, the boundary layer was established using Irwin spires.

After the approach wind field was verified, a technique to model the two-phase chlorine release in the wind tunnel was developed based on the radially symmetric, ground level wall jet formed in the field scale releases. In the wind tunnel, denser-than-air gas was released from an area source at floor level with a covering disk that formed a wall jet at the edge of the field-scale concrete pad. The height of the disk corresponded to the field-scale cloud depth at the edge of the concrete pad. In the field scale releases, the chlorine cloud was already diluted with air, which would impact the cloud density and momentum. In the wind tunnel model, the disk height, gas density, and gas release rate were varied by trial and error to reproduce the flow observed in the field scale releases. Validation of the wind tunnel model flow was made by comparison of the times of arrival at various locations in MUE at field and tunnel scale. In addition to 50:1 physical scaling, Froude number scaling was applied to the time scale between model and field scales. The wind tunnel model was developed using the data from JR II Trial 4. JR II Trial 5 was used to validate the modelling methodology. For further information, see Spicer & Smith (2020).

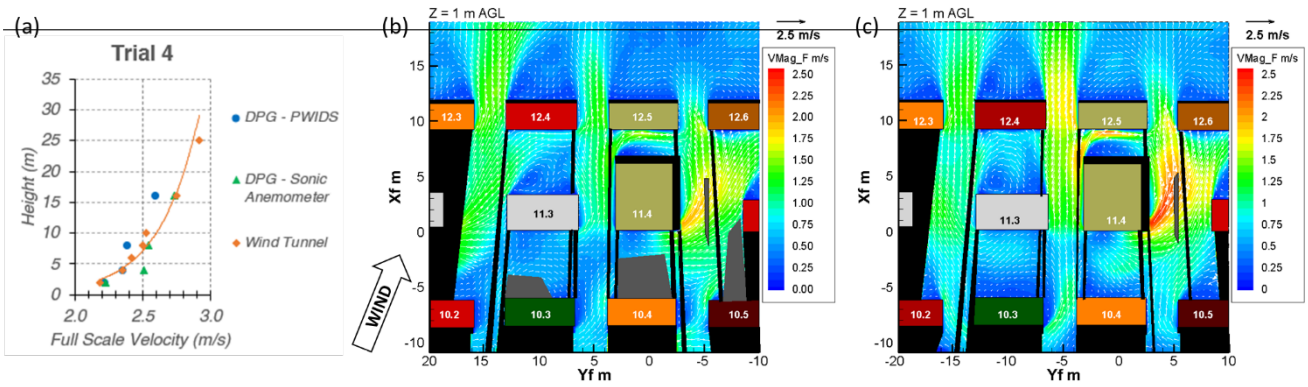

Figure 1. (a) Velocity profile comparisons between field and scale models for JR-II Trial 4. Average velocity magnitude at 1 m AGL horizontal plane in Trial 4 conditions for (b) pre-release and (c) release conditions. Black areas are laser sheet shadows from edges, and gray areas have insufficient signal.

The focus of this research is a subsequent study of the flow field in the MUE using PIV. One measurement campaign was made using a vertical laser sheet through the centreline of the MUE aligned with the wind direction. A second campaign was made using a horizontal laser sheet parallel to the wind tunnel floor at a field-scale height of 1 m above ground level (AGL), and in these experiments, the laser was located downwind of the MUE to avoid displacement of flow through the MUE. Horizontal sections of some CONEX containers in the MUE were made from clear casting epoxy resin so that the laser sheet passed through those CONEX containers, allowing measurements inside the MUE. In both campaigns, measurements were made using the characteristic ambient flow (pre-release) and during the time when the simulated chlorine release was ongoing (release). In both campaigns, average velocity and vorticity were measured using PIV output every 0.1 s.

Figures 1b and 1c show an example comparison between pre-release and release measurements for Trial 4 conditions from the horizontal laser sheet campaign. PIV results show the general flow complexity in the downwind rows of the MUE. The uncertainty for the average vector magnitude for these PIV measurements is between 1.3% and 2.7%. The major difference observed is the increase in velocity in the channels at the sides of CONEX 11.4, especially in the wider channel (increase in velocity around 30%) between CONEX containers 11.4 and 11.5. CONEX 11.4 is three times taller than the surrounding CONEX. This acceleration is likely due to the redirection of the released gas arriving at CONEX 11.4 which favoured the wider gap to the right of the tall building and was also influenced by the wind direction. An increase in velocity from the corners of the model buildings is also observed on both sides of CONEX containers 10.3 and 12.5. For further information, see Lopes (2023). The data sets from these wind tunnel tests are well suited for validation of computational models because of the measured contrast between ambient wind conditions and measured velocities during a release. These velocity measurements could not be made during the chlorine releases because of the corrosive nature of chlorine.

References

Lopes, P.V.d.F. (2023). Investigation of the Flow Field in the Jack Rabbit II Mock Urban Environment Field Tests Using a 1:50 Scale Wind Tunnel Model. [Doctoral dissertation, University of Arkansas]. ScholarWorks@UARK.

Spicer, T. & Smith, C.T. (2020). *Jack Rabbit II Mock Urban Environment Trials: Wind Tunnel Model Investigation and Validation.* U.S. Department of Homeland Security Science & Technology (DHS S&T) Chemical Security Analysis Center (CSAC).

PHYSMOD 2024 – International Workshop on Physical Modelling of Flow and Dispersion Phenomena
Ecole Centrale de Lyon, Ecully, France – August 28-30, 2024

Unravelling the Impact of Urban Morphology on Non-Isothermal Flow Dynamics: Insights from High-Resolution Experimental Investigations

Yunpeng Xue [1*], Yongling Zhao [2], Shuo-Jun Mei [3], Yuan Chao [4, 5] and Jan Carmeliet [2]
[1] Future Resilient Systems, Singapore-ETH Centre, ETH Zurich, Singapore
[2] Department of Mechanical and Process Engineering, ETH Zürich, Zürich, Switzerland
[3] School of Atmospheric Sciences, Sun Yat-sen University, Zhuhai, China
[4] Department of Architecture, National University of Singapore, Singapore
[5] NUS Cities, National University of Singapore, Singapore

Abstract

Understanding the intricate relationship between urban morphology, airflow dynamics, and thermal effects is crucial for improving urban planning, climate mitigation strategies, and environmental sustainability. However, elucidating these relationships, particularly in the context of non-isothermal flow driven by buoyancy effects, remains a significant challenge. In this study, we conducted comprehensive experimental investigations aimed at unravelling the impact of urban morphology on non-isothermal flow dynamics. Utilizing eight 3-D parametric urban models that closely mimics real-world urban configurations, we integrated buoyancy effects into our experimental setup to capture the intricate interplay between heat transport and fluid flow. Leveraging advanced measurement techniques such as Particle Image Velocimetry (PIV) and Laser-Induced Fluorescence (LIF) in a large closed-circuit water tunnel, we obtained high-resolution data on heat and fluid flow behaviours across various urban configurations. The experimental setup of the PIV/LIF measurements in the water tunnel are presented in Figure 1.

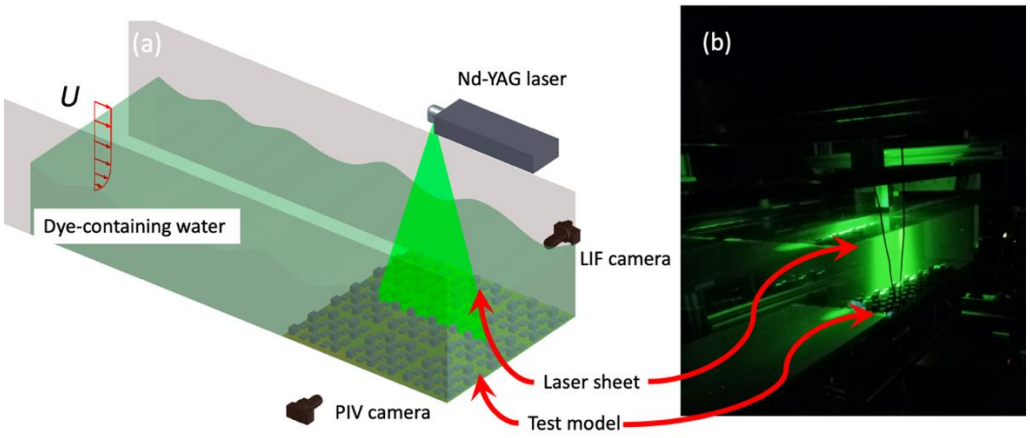

Figure 1. The experimental setup of the PIV/LIF measurements in the water tunnel.

We captured high-resolution flow velocity and temperature data in street canyons, allowing us to compare flow patterns across eight different urban morphology models. For instance, the streamwise and vertical velocity components, as well as the temperature rise along the canyon centreline as functions of height, are normalized by the freestream velocity and summarized in Figure 2. Our findings

reveal a detailed development process of non-isothermal urban flow, highlighting key phenomena such as heat plume generation from the ground, the formation of buoyant updrafts, and the spatial distribution of temperature gradients along the flow.

For example, Figure 3 presents a temporospatial plot of the temperature along the canyon centreline, showing the generation and updraft of unsteady heat plumes. By analysing buoyant flow properties—such as flow updraft, canyon ventilation, and temperature—in different urban models, we discuss the impacts of morphology factors like canyon width, height, and symmetry.

Our study contributes to a deeper understanding of the complex relationship between urban morphology, thermal effects, and flow dynamics in non-isothermal urban environments. By elucidating these interactions, we provide valuable insights that can inform sustainable urban design practices and climate mitigation strategies

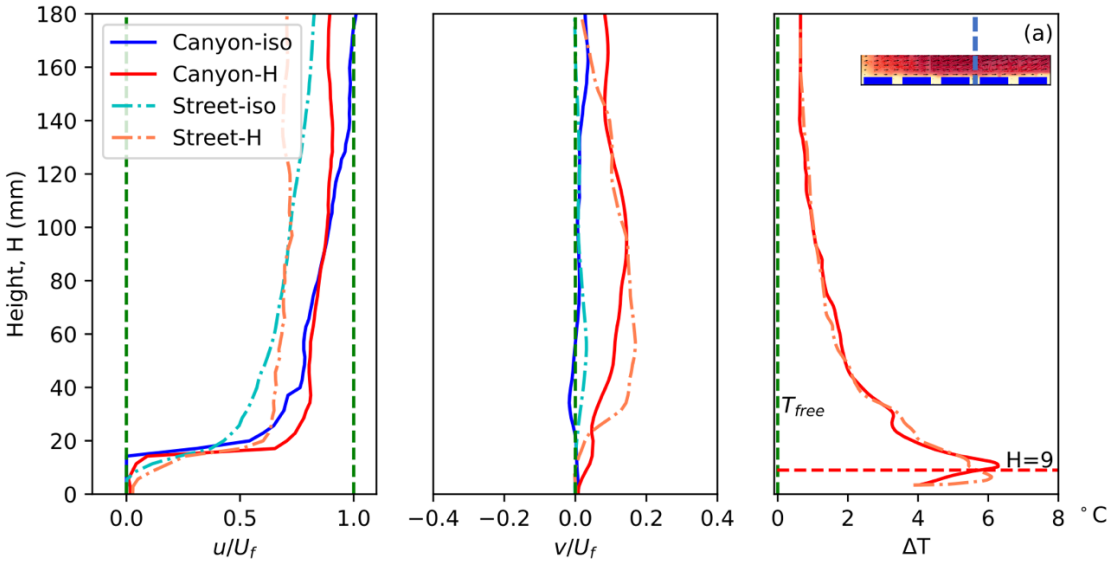

Figure 2. Normalised streamwise velocity, vertical velocity and the temperature rise along the centrelines in urban morphology (a).

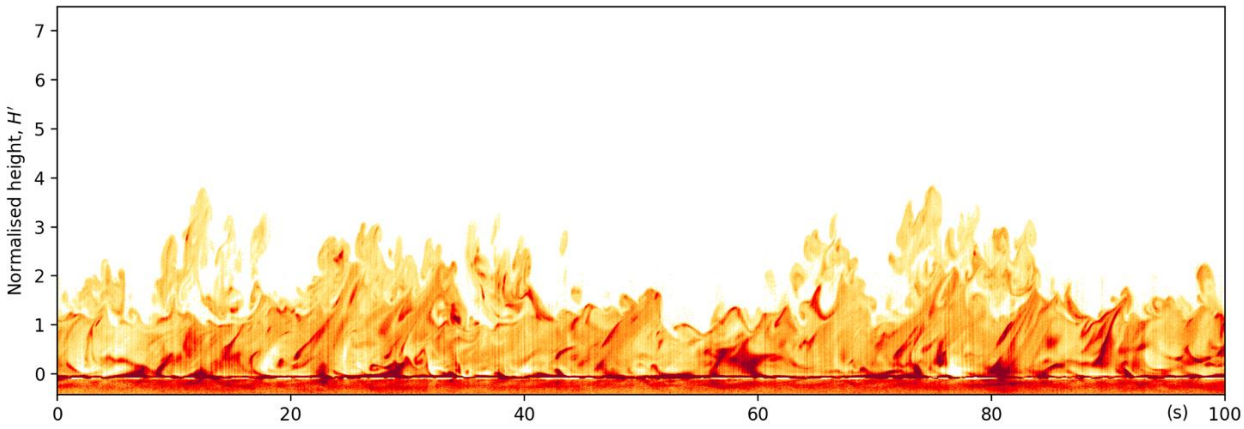

Figure 3. The temporospatial plot of the fluctuating temperature profile along the canyon centreline.

Urban greening

PHYSMOD 2024 – International Workshop on Physical Modelling of Flow and Dispersion Phenomena
Ecole Centrale de Lyon, Ecully, France – August 28-30, 2024

Flow and dispersion in a tree-lined perpendicular street canyon

S. Fellini [1], A.V. Del Ponte [1,2], M. Marro[2], L. Soulhac[2], L. Ridolfi[1], P. Salizzoni[1,2]

[1] Politecnico di Torino, DIATI, Corso Duca Degli Abruzzi 24, 10129, Torino, Italy.
[2] Univ Lyon, Ecole Centrale de Lyon, CNRS, Univ Claude Bernard Lyon 1, INSA, LMFA, UMR5509, 69130 Ecully, France.

Abstract

Despite advancements in environmental legislation, air pollution in cities remains a significant health risk. Understanding pollutant transport between urban canyons and the atmosphere is crucial for effective urban planning, necessitating both numerical and experimental research (Zhao et al., 2023). Trees play a critical role in urban canyon ventilation. While greener cities improve the urban microclimate and mitigate climate change, the effect of trees on pollutant dispersion is debated. Trees can inhibit air circulation, reducing ventilation and potentially increasing pollutant concentrations at pedestrian level (Gromke et al., 2009; Carlo et al., 2024). This study employs wind tunnel experiments to investigate the effect of trees on the turbulent flow field and pollutant concentration within a street canyon oriented perpendicularly with respect to the prevailing wind (Fellini et al., 2022, Del Ponte et al. 2024).

The experiments were conducted in the wind tunnel at Ecole Centrale de Lyon, featuring a test section 12 m long, 2 m high, and 3.5 m wide. An idealized urban geometry at a 1:200 scale was created with a canyon oriented perpendicularly to the wind, with an H/W ratio of 0.5. Two rows of plastic tree model, were placed along the street sides. The tree models' drag coefficients and aerodynamic porosity were measured to ensure aerodynamic similarity. Vehicle emissions were simulated using a linear ethane gas source at street level. The incident flow was controlled and measured to represent an urban atmospheric boundary layer. Concentration fields within the canyon were measured using a Flame Ionization Detector (FID), while velocity fields were obtained using a Laser Doppler Anemometry (LDA). The latter was coupled with the FID for synchronous concentration and velocity measurements. The experiments were characterized by a Reynolds number based on the obstacle height ($Re_H = U_H H/\nu$) of 12500.

The presence of trees significantly alters the concentration pattern within the canyon, transitioning from a nearly two-dimensional to a three-dimensional distribution, depending on tree density. Peaks in concentration alternate with low-pollutant regions, particularly in the canyon's lower portion, suggesting significant spatial variation in pedestrian exposure. Despite this alteration, the average pollution levels and overall ventilation efficiency do not exhibit a specific trend with tree density.

The vertical exchange at the canyon roof, governed by both mean flow and turbulent fluctuations, does not change with tree density. However, vegetation-induced reduction in turbulent mass fluxes within the canyon may account for the observed heterogeneity in pollutant concentration. Spectral

analysis of vertical velocity and turbulent mass fluxes indicates a decrease in energy content of large-scale structures with increasing tree density.

These findings underscore the importance of considering the aerodynamic properties of vegetation in street canyons and contributes valuable experimental data for understanding the intricate interactions between vegetation, airflow, and pollutant dispersion in urban environments, providing a basis for more effective urban design and validation of numerical studies.

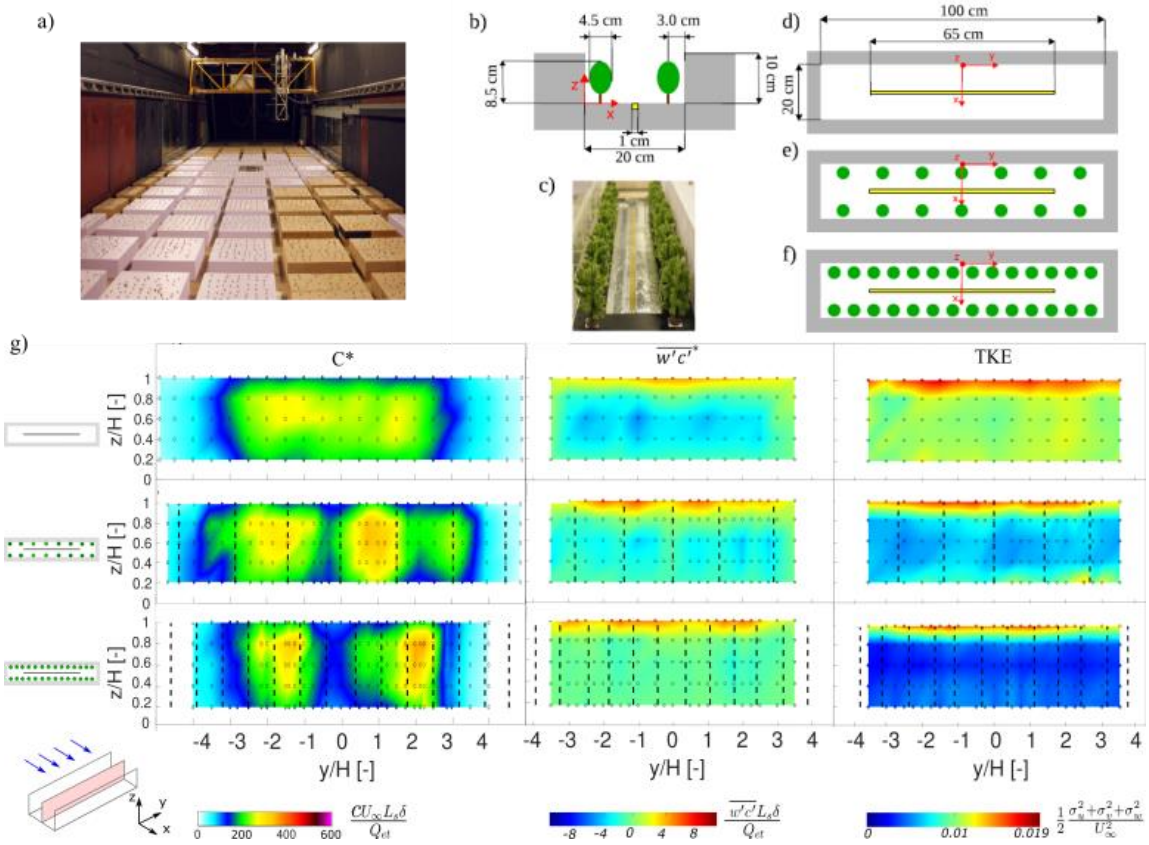

Figure 1: a) The modeled urban canopy in the wind tunnel. Sketch (b) and photo (c) of the front view of the street. Top view of the street canyon model for different tree density configurations (d-f). g) Average concentration fields, vertical turbulent mass fluxes, and turbulent kinetic energy fields in the central section of the canyon for an increasing number of trees in the side rows.

References

Zhao, Y., Chew, L. W., Fan, Y., Gromke, C., Hang, J., Yu, Y., ... & Carmeliet (2023). J. Fluid tunnel research for challenges of urban climate. *Urban Climate*, 51, 101659.

Fellini, S., Marro, M., Del Ponte, A.V., Barulli, M., Soulhac, L., Ridolfi, L. & Salizzoni, P. (2022). High resolution wind-tunnel investigation about the effect of street trees on pollutant concentration and street canyon ventilation, *Building and Environment*, 226(109):763.

Del Ponte, A.V., Fellini, S., Marro, M., van Reeuwijk, M., Ridolfi, L. & Salizzoni, P. (2024). Influence of Street Trees on Turbulent Fluctuations and Transport Processes in an Urban Canyon: A Wind Tunnel Study, *Boundary-Layer Metheorology*, 190:6.

Gromke, C. & Ruck, B. (2009). On the Impact of Trees on Dispersion Processes of Traffic Emissions in Street Canyons, *Boundary-Layer Metheorology*, 131(1):19–34.

Carlo, O. S., Fellini, S., Palusci, O., Marro, M., Salizzoni, P., & Buccolieri, R. (2024). Influence of obstacles on urban canyon ventilation and air pollutant concentration: An experimental assessment, *Building and Environment*, 250, 111143.

PHYSMOD 2024 – International Workshop on Physical Modelling of Flow and Dispersion Phenomena
Ecole Centrale de Lyon, Ecully, France – August 28-30, 2024

Turbulent flow field within an urban canyon with vegetation for any wind directions

A.V. Del Ponte[1, 2], S. Fellini[1], M. Marro[2], L. Soulhac[2], L. Ridolfi[1], P. Salizzoni[2]

[1]Politecnico di Torino, DIATI, Corso Duca Degli Abruzzi 24, 10129, Torino, Italy.
[2]Univ Lyon, Ecole Centrale de Lyon, CNRS, Univ Claude Bernard Lyon 1, INSA, LMFA, UMR5509, 69130 Ecully, France.

Introduction

The greening of cities is known as a promising strategy to mitigate the impacts of climate change. However, the aerodynamic effect of vegetation on urban canyon ventilation is not well understood and its benefits on the air quality are debated. For example, recent studies report that the presence of trees within a canyon, perpendicular to the external wind flow, causes an around 30% increase of pollutant concentration at the pedestrian level (*Fellini et al. 2022*) and a significant decrease of turbulent kinetic energy (*Del Ponte et al. 2024*). However, the effect of the wind direction or canyon geometry on the flow filed within canyons with trees is poorly investigated. *Gromke and Ruck 2012* is the only work investigating the influence of wind direction and canyon height-to-width ratio on the mean concentration field within a vegetated canyon. In this framework, we present the results of an experimental campaign aimed at investigating the turbulent flow field within a canyon with trees, considering different wind directions.

Experimental setup

The experiments were performed in the closed-circuit wind tunnel of the École Centrale de Lyon (figure 1a). In the test section, we reproduced a regular street network covering the floor with blocks of constant height and spacing. A neutrally-stratified boundary layer, of thickness 0.9 m and with a free-stream velocity (U_∞) of 5 m/s, develops above the obstacles. Within the street network we selected a squared street 3.5 m long, 0.1 m high (H) and 0.1 m wide, as reference canyon. The street intersections were hindered, allowing for a two-dimensional flow field within the canyon. The aerodynamic effect of vegetation was modelled using plastic miniatures of trees, with a trunk 2 cm high and a crown 6.5 cm high and 4.5 cm wide. We considered two vegetation configurations, an empty canyon and a canyon with two parallel rows of trees, along the side walls. Both canyons were oriented with angles of 0°, 30° (see figure 1b), and 60°, with respect to the external wind flow. The turbulent flow field was measured on a two-dimensional transversal section of the canyon, using a Laser Doppler Anemometer.

Results and discussion

The flow field within the canyon parallel to the external wind is dominated by an advective motion along the street axis, while, when the canyon is oriented with an angle, the flow shows a complex helicoidal structure. As a consequence, in the empty canyon the mean longitudinal velocity progressively decreases with the increase of the inclination angle, while the transversal mean

velocity deviates from zero, following a recirculating structure (see figure 1d, for the 30° wind direction). When the canyon is oriented parallel to the external wind flow, the presence of trees causes an around 80% decrease in the mean longitudinal velocity in between the trees and a 30% decrease of it above the tree crowns. For the 30° and 60° wind directions, trees weaken the transversal recirculation, mostly in the lower part of the canyon (figure 1e, for the 30° wind direction), as well as they hinder the axis parallel flow. This hindering effect is less marked in the downwind upper corner of the 30° rotated canyon (figure 1f), while it affects the entire transversal section of the 60° rotated canyon. The interaction between the external flow and the tree crowns leads to an increase in the flow velocity fluctuations, with respect to the empty canyon, in the upper part of the parallel canyon and along the downwind wall of the rotated canyons. Conversely, around the trees the flow velocity fluctuations are dampened: they decrease of around 10% for the 0° and 30° wind directions and around 40% for the 60° inclination. The experimental data provide useful information to model the urban microclimate and to validate analytical models that simulate pollutant dispersion in urban-like geometries, like *SIRANE* (*Soulhac et al. 2008, 2011*).

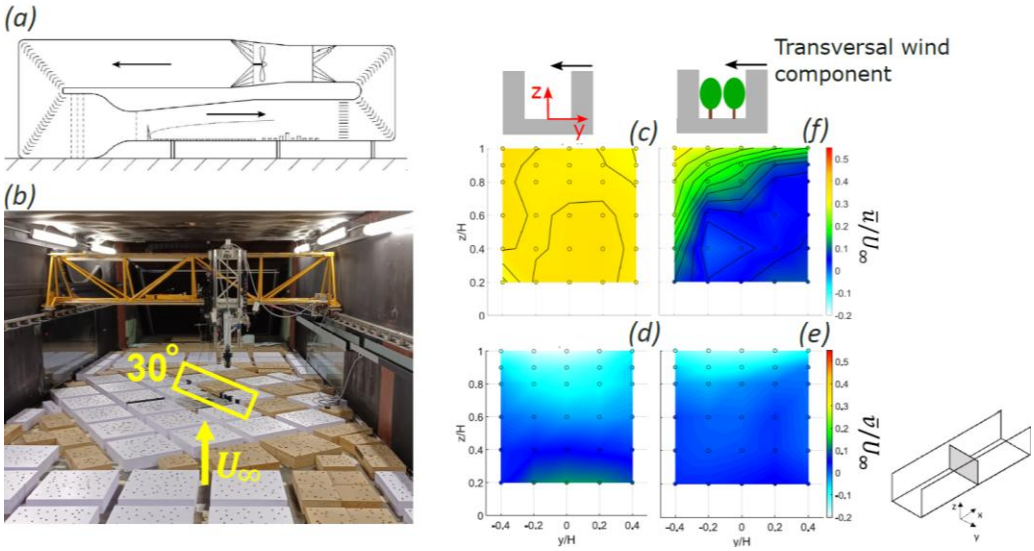

Figure 1: (a) Wind tunnel. (b) Urban network with the street canyon rotated 30° with respect to the wind direction. Mean longitudinal and transversal velocity in the empty (c,d) and vegetated (f,e) canyons, rotated of 30° with respect to the wind direction (see the yellow arrow in panel b).

References

Soulhac, L., Perkins, R. & Salizzoni, P. (2008) Flow in a Street Canyon for any Wind Direction. *Boundary-Layer Meteorology*, 126:365-388.

Soulhac, L., Salizzoni, P., Cierco, F.X. & Perkins, R. (2011) The model SIRANE for atmospheric urban pollutant dispersion; part I, presentation of the model. *Atmospheric Environment*, 45, 7379-7395.

Gromke, C. & Ruck, B. (2012) Pollutant concentrations in street canyons of different aspect ratio with avenues of trees for various wind directions. *Boundary-Layer Meteorology,* 144:41-64.

Fellini, S., Marro, M., Del Ponte, A.V., Barulli, M., Soulhac, L., Ridolfi, L. & Salizzoni, P. (2022) High resolution wind-tunnel investigation about the effect of street trees on pollutant concentration and street canyon ventilation. *Building and Environment*, 226(109):763.

Del Ponte, A.V., Fellini, S., Marro, M., van Reeuwijk, M., Ridolfi, L. & Salizzoni, P. (2024) Influence of Street Trees on Turbulent Fluctuations and Transport Processes in an Urban Canyon: A Wind Tunnel Study. *Boundary-Layer Metheorology*, 190:6.

PHYSMOD 2024 – International Workshop on Physical Modelling of Flow and Dispersion Phenomena
Ecole Centrale de Lyon, Ecully, France – August 28-30, 2024

Wind tunnel measurements on the interaction between an isolated tree and the atmospheric boundary layer

L. Grandoni[1], M. Michard[1], N. Grosjean[1], P. Salizzoni[1,2]

[1]Ecole Centrale de Lyon, CNRS, Universite Claude Bernard Lyon 1, INSA Lyon, LMFA, UMR5509, 69130, Ecully, France
[2]Department of Environmental, Land and Infrastructure Engineering (DIATI), Politecnico di Torino, Corso Duca degli Abruzzi 24, 10129 Turin

Introduction

Vegetation in urban areas brings benefits from a thermal and aesthetic point of view, however its effect on street ventilation and on pollutant dispersion is still debated. Therefore, detailed measurements are needed to study the aerodynamic properties of the vegetation. Several measurement campaigns have been carried out in the literature to assess the interaction between an isolated tree and the surrounding airflow, e.g., Gromke et al. (2008) and Manickathan et al. (2018). In these works, wind tunnel experiments are carried out and the flow field around the tree is analysed for different tree drag coefficient and porosity values. The aim is to understand which are the parameters to be considered to reproduce real scale tree behaviour by means of laboratory scale tree models. Also, these kinds of results are useful to model the presence of the vegetation in CFD simulations. In the present work the interaction between an isolated tree with different porosity values and the atmospheric boundary layer is investigated by means of classic 2D low-speed Particle Image Velocimetry (PIV), 2D high-speed PIV, stereoscopic PIV and volumetric Particle Tracking Velocimetry (PTV). Several approaching wind speeds are considered. The effect of both tree porosity and approaching wind speed on the flow field around the tree and on the wake can be assessed. Besides, a direct estimation of Lagrangian turbulence statistics can be obtained by means of volumetric PTV measurements, which is particularly useful for Lagrangian modelling of pollutant dispersion.

Materials and Methods

The tree model is located into the wind tunnel of the Laboratoire de Mécanique des Fluides et Acoustique of the Ecole Centrale de Lyon, which makes it possible to reproduce a neutral atmospheric boundary layer. Rigid plastic trees for railway modelling about 0.085 m high and 0.045 m wide are used. The thickness of the boundary layer is about 0.5 m. Drag coefficient and aerodynamic porosity - ratio between air velocity behind the tree and of the approaching wind - of the tree model with lower porosity is measured with a uniform approaching wind in Fellini et al. (2022). The higher porosity tree is obtained by defoliating the lower porosity one. For the sake of brevity, the details of the measurement techniques and of the experimental setup are not provided here.

Results

Mean and turbulent velocity field at several longitudinal vertical planes upstream and downstream the isolated tree can be obtained by PIV measurements. Mean velocity magnitude field and streamlines

downstream two trees characterized by different porosity are depicted in Figure 1. The different tree porosity has an important effect on the mean velocity topology. Particularly, a recirculation zone forms downstream the tree with lower porosity, whereas the airflow seems to pass through the branches without forming recirculation zones in the case of the higher porosity tree. Also, PIV data allow us to analyse how turbulence properties of the approaching boundary layer are modified by the presence of trees with different porosity. Even though a shear layer with high turbulence level forms at the tree height in all the cases considered, higher values of Reynolds stresses are observed for lower tree porosity (not shown for brevity). Turbulence length scales can also be obtained from PIV data. As a future perspective, mean and turbulent flow characteristics can be compared to the ones observed on real trees, e.g. by Angelou et al. (2022). Particularly, the latter assessed turbulent transport in the wake of an isolated tree in its natural environment. Volumetric PTV measurements provides tracer particles trajectories and the three components of Lagrangian velocity and acceleration, from which Lagrangian turbulence statistics can be computed. Panel c of Figure 1 shows the variance of the displacement of particle trajectories starting from two points $\mathbf{x}_{0,\mathrm{A}}$ (in the shear layer) and $\mathbf{x}_{0,\mathrm{B}}$ (in the recirculation zone) for the less porous tree. The three components of the displacement are reported. Bold and capital letters refer to vector and Lagrangian quantities, respectively. The flow appears to be inhomogeneous and anisotropic. Higher values of displacement variance for particles departing in the shear layer are due to the higher turbulence level in this zone.

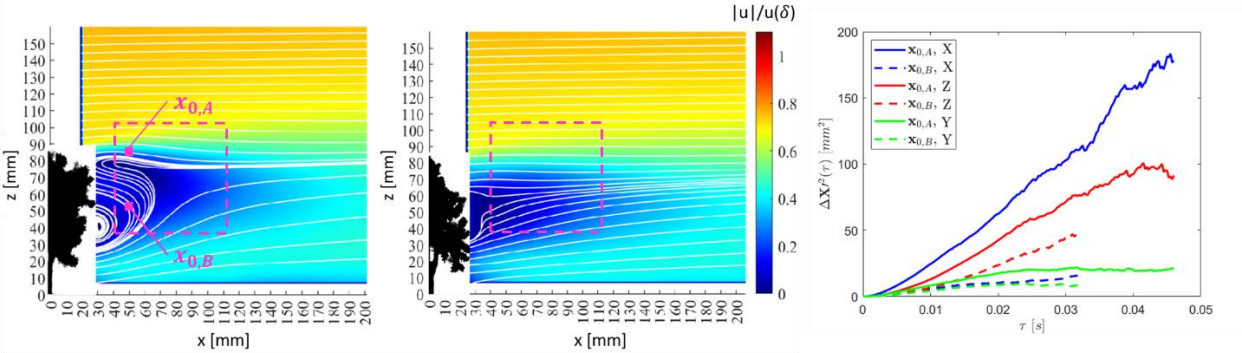

a. b. c.

Figure 1: Mean velocity magnitude field and streamlines downstream the less porous (a) and more porous (b) tree (from low-speed 2D PIV data). The pink dashed square indicates the PTV measurement area. Panel c: variance of the tree displacement components of particle trajectories starting from the two points $\boldsymbol{x}_{0,A}$ and $\boldsymbol{x}_{0,B}$ (from PTV data).

References

Angelou, N., Mann, J. & Dellwik, E. (2022). Wind lidars reveal turbulence transport mechanism in the wake of a tree. Atmospheric Chemistry and Physics, 22(4), 2255-2268.

Fellini, S., Marro, M., Del Ponte, A.V., Barulli, M., Soulhac, L., Ridolfi, L. & Salizzoni, P. (2022). High resolution wind-tunnel investigation about the effect of street trees on pollutant concentration and street canyon ventilation, Building and Environment, 226, 109763

Gromke, C. & Ruck, B. (2008). Aerodynamic modelling of trees for small-scale wind tunnel studies. Forestry: An International Journal of Forest Research, 81(3), 243-258.

Manickathan, L., Defraeye, T., Allegrini, J., Derome, D., & Carmeliet, J. (2018). Comparative study of flow field and drag coefficient of model and small natural trees in a wind tunnel. Urban Forestry & Urban Greening, 35, 230-239.

PHYSMOD 2024 – International Workshop on Physical Modelling of Flow and Dispersion Phenomena
Ecole Centrale de Lyon, Ecully, France – August 28-30, 2024

Experimental investigation of influence of tree-like structures on urban canyon airflow: A comparative study under isothermal and variable thermal conditions

G. Alexandrou[1], P. Mouzourides[1], H. Li[2,3], Y. Zhao[2], J. Carmeliet[2], M. K.-A. Neophytou[1]

[1]Laboratory - Isle of Excellence of Environmental Fluid Mechanics, Department of Civil & Environmental Engineering, University of Cyprus, Nicosia, Cyprus
[2]Department of Mechanical and Process Engineering, ETH Zürich, Zürich, 8093, Switzerland
[3]The Sustainable Design Group, Department of Architecture, University of Cambridge, Cambridge, UK

Abstract

The Urban Heat Island (UHI) phenomenon impacts human thermal comfort, building energy use, and overall sustainability (Deilami et al., 2018). Urban green infrastructure, including trees, green roofs, and facades, is essential for combating UHI effects. Trees, in particular, help regulate temperatures and improve air quality through shading and evapotranspiration process, reducing the need for indoor air conditioning. However, trees in urban canyons can also influence airflow dynamics, sometimes acting as obstacles that hinder lateral airflow and increase pollutant concentration inside the canyon. Understanding these effects is essential for designing sustainable urban environments. Our study investigates how urban trees, with varying height ratios relative to buildings, affect airflow in street canyons. This study also investigates the extent of Roughness Sub-Layer (RSL) and friction velocities. The main goal is to understand how urban trees affect airflow patterns, air exchange, and turbulence dynamics within and above urban canyons.

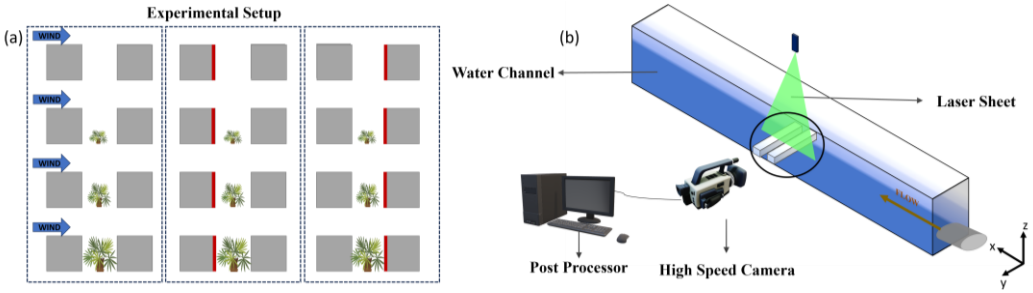

Figure 1: (a) Illustration of the different scenarios and (b) schematic of the PIV setup.

To explore the impact of urban tree planting on microclimate dynamics, we conducted experiments using Particle Image Velocimetry (PIV) technique in a controlled water channel at the University of Cyprus (Figure 1). The experimental setup involved an idealized symmetric urban street canyon, allowing for a detailed examination of airflow dynamics. We employ a non-dimensional analysis (Mouzourides et al., 2022) of the PIV measurements to assess the interplay between buoyant and inertial forces in the presence of tree obstacles of varying tree-to-building height ratios (at h_t/H = 0, 0.25, 0.5 and 1). Notably, the position of the heated surface (whether on the leeward or windward side) affect the vortex structure and its positioning. Additionally, the study examines the influence of

trees on normalized vertical velocities at rooftop level, a parameter critical to the canyon's "breathability" (Kubilay et al., 2017). The volumetric ventilation rate at the canyon's roof-level opening, referring to the rate of air exchange influenced by both convective and turbulent components, is examined for its relevance to pollutant and scalar removal (Li et al., 2022). A key aspect of this research is the study of friction velocity (u*), which is essential in fluid mechanics as it indicates shear stress in terms of velocity. Although measuring u* in urban-like geometries can be challenging, this study uses two approaches to determine its value: (i) the logarithmic-law method and (ii) the method based on the maximum value of measured *RS*.

The findings reveal a notable influence of tree size on vortical flow within the canyon. Smaller trees (h_t/H = 0.25) are observed to change the location of vortex formation, while larger trees (h_t/H = 0.5 and 1) lead to the creation of recirculation cells around trees (Figure 2).

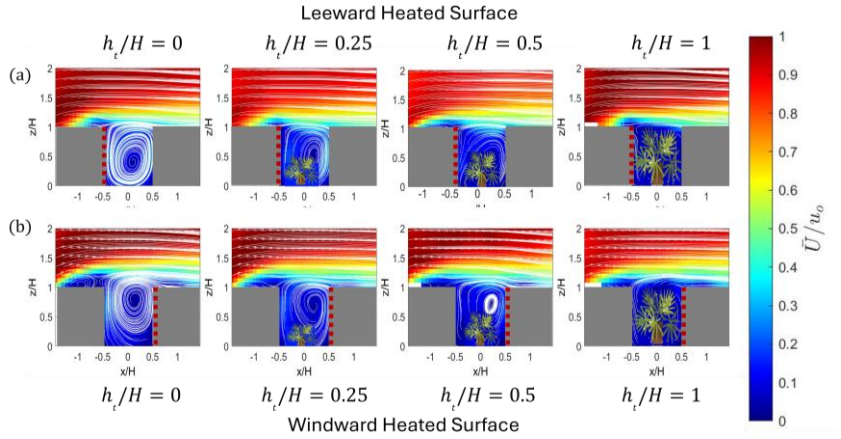

Figure 2: Mean flow field for (a) leeward heated surface and (b) windward heated surface.

This study found that in urban canyons with $h_t/H = 1$ and a leeward heated surface, air flow changes from air removal to air entrainment. In contrast, with windward heated surface, air removal stays consistent, regardless of tree size. Furthermore, analysing *RS*, vertical profiles revealed that the RSL ranges from 1.10H to 1.60H, with a significant increase in windward heated surface scenarios. These results suggest that tree height and heated surface orientation affect airflow dynamics in urban canyons, offering valuable insights for urban design.

This study provides insights into the effects of urban trees on microclimate dynamics within street canyons, demonstrating how tree height and orientation of heated surfaces can influence airflow and temperature patterns. The findings have implications for urban design and planning, suggesting that strategic tree placement can contribute to mitigating the UHI effect and improving urban sustainability. Future work could explore additional variables such as tree species, leaf density, and other environmental factors that may impact microclimate dynamics.

References

1. K. Deilami, Md. Kamruzzaman, Y. Liu, Urban heat island effect: A systematic review of spatio-temporal factors, data, methods, and mitigation measures, International Journal of Applied Earth Observation and Geoinformation, vol. 67, pp. 30-42, 2018.
2. Mouzourides P, Marakkos C, Neophytou MKA. Urban street canyon flows under combined wind forcing and thermal buoyancy. Phys Fluids. 2022;34(7).
3. A. Kubilay, M.K.-A. Neophytou, S. Matsentides, M. Loizou, J. Carmeliet, The Pollutant Removal Capacity of an Urban Street Canyon and its Link to the Breathability and Exchange Velocity. Procedia Engineering, 2017;180.
4. H. Li, Y. Zhao, B. Sützl, A. Kubilay, J. Carmeliet, Impact of green walls on ventilation and heat removal from street canyons: Coupling of thermal and aerodynamic resistance. Building and Environment. 2022;214

PHYSMOD 2024 – International Workshop on Physical Modelling of Flow and Dispersion Phenomena
Ecole Centrale de Lyon, Ecully, France – August 28-30, 2024

Flow past a building with surface greening: comparison of PIV and LDV in two wind tunnels

V. Pappa[1], C. Gromke[2], D. Bouris[1]

[1]National Technical University of Athens, School of Mechanical Engineering, 9 Heroon Polytechnioy, 15773, Zografos, Greece
[2]Karlsruhe Institute of Technology, Institute for Water and Environment, Laboratory of Building and Environmental Aerodynamics, Kaiserstrasse, 12, 76128 Karlsruhe, Germany

Abstract

In the context of studying vegetation effects on flow in the urban environment, twin studies of the flow past a cube shaped building (H=110 mm) were performed in the wind tunnels of the Karlsruhe Institute of Technology (KIT), (cross section 2x1m) and the National Technical University of Athens (NTUA), (cross section 3.5x2.5m). Identically shaped buildings were used, exposed to comparable upstream atmospheric boundary layer (ABL) profiles in terms of mean velocity, turbulence intensity and integral length scales. Simulated vegetation was placed on the building's upstream face or roof. Measurements were performed with Laser Doppler Velocimetry (LDV) at KIT and 2D-3C (and 2D-2C) Particle Image Velocimetry (PIV) at NTUA.

For characterising the upstream flow in both wind tunnels, hot wire anemometry was used to measure mean and fluctuating quantities and the integral length scales were calculated. Results are presented in Figure 1, along with the indicative regions of the turbulence intensity for moderately rough and rough terrains (VDI, 2000). The agreement of the vertical distribution of the ABL quantities in the two wind tunnels is notable, at least up to twice the building height (z_{ref}=H). The slight differences in the profiles lead to Reynolds numbers (based on building height and upstream velocity at the same height) of Re_H=23,500 at KIT and Re_H=16,500 at NTUA, both above the reported $Re_{H,crit}=10^4$ limit for Re number independence (VDI, 2000).

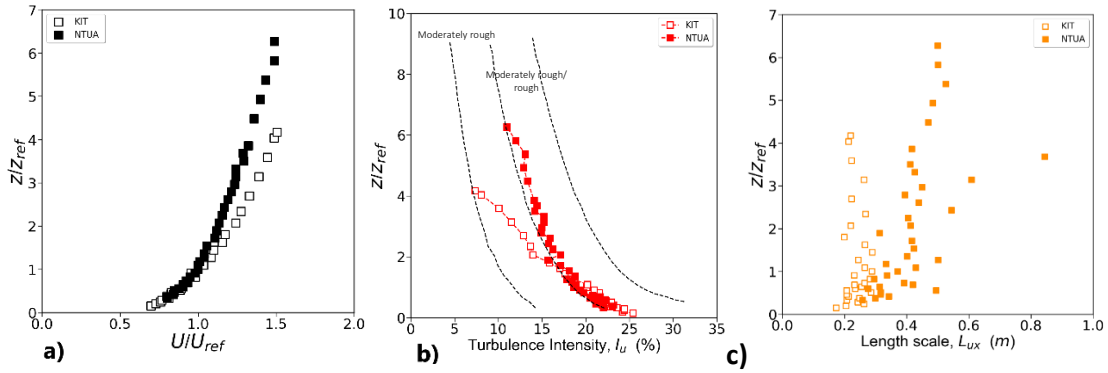

Figure 1: Boundary layer properties in the KIT and NTUA wind tunnels, calculated from the streamwise velocity component a) mean velocity, b) turbulence intensity, c) integral length scale

Vegetation on the building surfaces was modelled with reticulated, open cell foam of varying density (10-60 PPI), whose pressure loss coefficient was independently measured at KIT and NTUA and corresponds to dense hedges or ivy, based on dynamic similarity (Gromke, 2011) at a scale of 1:300.

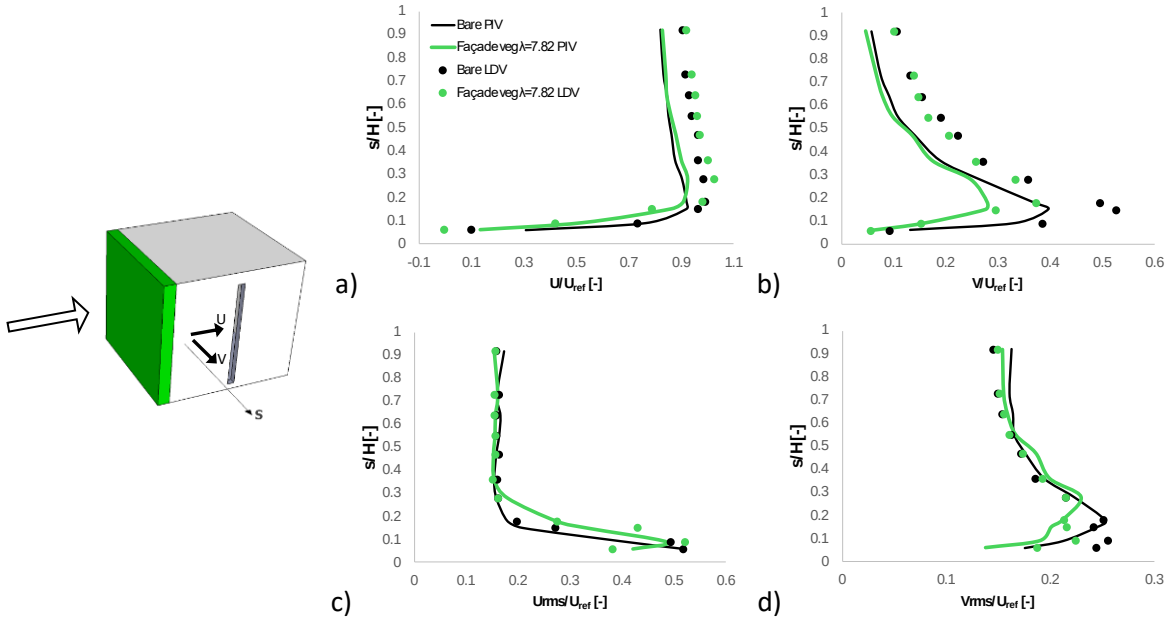

Figure 2: PIV and LDV results, with and without vegetation, along a horizontal profile (s) halfway up the sidewall and 0.1H from the leading edge: streamwise a) mean, c) rms and lateral b) mean, d) rms

Indicative results from LDV and PIV are presented in Figure 2 along a horizontal profile outside the building (s/H=0 at the wall), 0.1H from the leading edge and halfway up the building's side wall. The differences in the measured mean and rms velocities among the two methods are less than 10% of the upstream velocity at the building height (U_{ref} =U_H) with or without facade vegetation. It is important to note that the two measurement sets both show that upstream facade vegetation reduces the lateral mean velocity next to the side wall (Figure 2b) and dampens lateral velocity fluctuations (Figure 2d). The effect on the streamwise component is present mainly in an increase of the rms values (Figure 2c) near the wall.

Overall, the two measurement sets indicate the same qualitative trends of flow structure while vegetation effects and quantitative results are in close agreement. The full set of data is publicly available (Pappa et al. 2023) and provides an opportunity to analyse the effects of building outer surface vegetation on the flow field as well as differences arising from measurement techniques, experimental conditions and wind tunnel configurations.

Acknowledgements

Funding was provided by the EU under (PR# 101079125) TWEET-IE: Twin Wind tunnels for Energy and the EnvironmenT - Innovations and Excellence.

References

Gromke C. (2011) A vegetation modeling concept for building and environmental aerodynamics wind tunnel tests and its application in pollutant dispersion studies. *Environmental Pollution* 159.8-9, 2094–2099.

Pappa, V., Gromke, C., & Bouris, D., (2023). Twin test 1: Effect of vegetation on urban flows. PIV data from NTUA WT experiment and LDV from KIT WT experiment *(1.0.0) [Data set].* DOI: 10.5281/zenodo.10019002

VDI 3783/Part 12 (2000) Environmental Meteorology. Physical Modelling of Flow and Dispersion Processes in the Atmospheric Boundary Layer. Application of Wind Tunnels. *Beuth Verlag GmbH*, 10772 Berlin

Indoor air circulation

PHYSMOD 2024 – International Workshop on Physical Modelling of Flow and Dispersion Phenomena
Ecole Centrale de Lyon, Ecully, France – August 28-30, 2024

Laboratory-scale modeling of air velocity and pollutant concentration fields in an amphitheatre classroom

A. Pini[1], G. Leuzzi[1], A. Pelliccioni[2], G. Querzoli[3], P. Monti[1]

[1]University of Rome La Sapienza, Faculty of Civil and Industrial Engineering, Department of Civil, Building and Environmental Engineering, Via Eudossiana 18, 00184 Rome, Italy
[2]Italian Workers' Compensation Authority (INAIL), Department of Occupational and Environmental Medicine, Epidemiology and Hygiene, Monte Porzio Catone, 00078 Rome, Italy
[3]University of Cagliari, Faculty of Engineering and Architecture, Department of Civil, Environmental Engineering and Architecture, Via Marengo 2, 09123 Cagliari, Italy

Abstract

This work aims to study natural circulation and pollutant dispersion within an amphitheatre-shaped university classroom by means of a laboratory-scale model of an indoor environment at the University of Rome "La Sapienza". The work is part of the VIEPI (Integrated Evaluation of Indoor Particulate Exposure) Project, whose main objectives include assessment of indoor air quality (Pelliccioni et al., 2020).

The experiments were conducted using a 1:20 scale model (65x56.5x27.5 cm) of the room and a hydraulic network designed to ensure the desired flow rate (Figure 1). The working fluid is water. The flooring and fixed furniture of the room were built by 3D printing. The side walls and ceiling were made of 0.01 m thick transparent plexiglass sheets to allow optical access from the outside. On the wall behind the room desk, the two doors (8 cm high and 5 cm wide) communicating with the outside, were reproduced. Through these openings, inflow and outflow mimicking natural, isothermal, steady-state ventilation, were set. The isothermal assumption is feasible to describe the case of an empty room. A constant flow rate, ~$9 \cdot 10^{-4}$ $m^3 s^{-1}$, was fixed at the inlet door (which corresponds to an average velocity U~0.22 ms^{-1}), while the Reynolds number Re=UD/ν was ~21,000, were ν is kinematic viscosity of water and D is the door diagonal. Note that this Reynolds number, despite high, does not guarantee the dynamic similarity with the real case in the whole domain. The experiments carried out to acquire the velocity field were conducted along five vertical planes (A-E).

The acquisition facility consists of a 1000 W, white halogen lamp, emitting a light sheet ~0.02 m thick illuminating the acquisition plane and a camera (1024x1280 pixels in resolution) acquiring 250 frames per second. The camera acquires the positions of the particles passively transported by the fluid and allows the evaluation of the instantaneous velocity fields on interrogation areas (vertical sections) of the room by means of a feature-tracking algorithm based on image analysis on a regular 92 (horizontal) x 47 (vertical) array, which corresponds to a ~5 mm spatial resolution. The mean and the variance of the velocity components and the turbulent momentum flux were calculated on each grid cell. To investigate pollutant dispersion inside the classroom, a mixture of water and fluorescein – here considered representative of any passive pollutant – of known concentration enters from the inlet door. From the grey levels of the image pixels along the section, the time histories of the

concentration values as well as the mean concentration field in correspondence of each pixel of the interrogation area can be detected. The streamlines corresponding to the mean velocity field measured in some of the vertical sections are depicted in Figure 1.

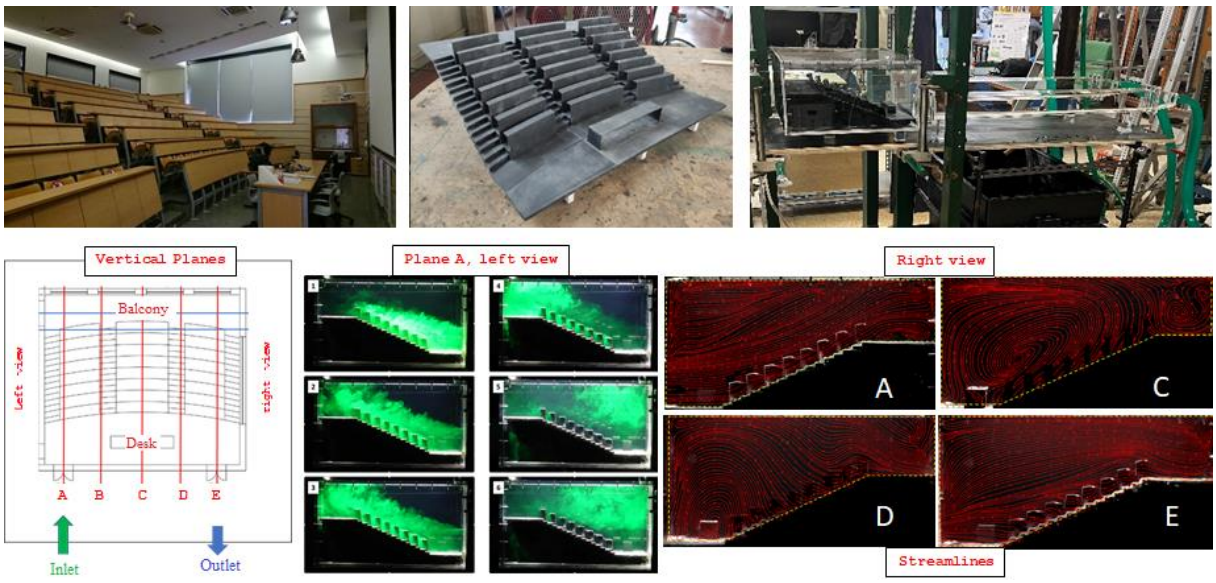

Figure 1: The classroom, its 1:20 scale model, and the experimental set up (above). Examples of instantaneous concentration fields during filling (1-3) and emptying (4-6) phases of the tracer (fluorescein), and examples of streamlines along planes A, C, D and E (below).

The flow entering the classroom is visible in the section passing through the centreline of the inlet door (plane A, right view). It assumes the characteristics of a jet and it is initially horizontal. Then, the flow bends upward and runs parallel to the inclined plane formed by the benches. At the balcony the velocity magnitude is about one tenth of that at the door mainly due to horizontal spreading of the jet (not shown). Two vortices form above the balcony, one near the ceiling and one near the floor. The axis of the latter lies horizontally on the balcony (normally to the plane of the picture), and becomes larger, as it can be seen from the vertical section passing through the centre of the classroom (plane C, right view). Also evident is the presence of a large structure, rotating anticlockwise, which rises up the slope formed by the benches and descends near the wall behind the desk. Plane E (right view, the one passing through the outflow door) shows how the downward flow is approximately parallel to the benches. It is notable that the flow is considerably slow over the entire plane, ~0.01 ms^{-1} at most, while the velocity increases near the exit door.

Figure 1 also shows six snapshots of the flow taken at a fluorescein release in the corridor connected to the inlet door. Fluorescein concentration, which can be considered representative of any passive pollutant, can be estimated from the brightness level of the image pixels, which is linearly proportional to the fluorescein concentration. Panels 1-3 and 4-6 refer to the filling and the emptying phases, respectively. Visual inspection of the images shows how the tracer, once it enters the classroom, is mostly captured by the large swirling structure shown by the streamlines, and tends to recirculate in the upper part of the classroom for a long time. On the other hand, the lower part of the room is less polluted. Emptying times are therefore highly dependent on location within the room and can differ by as much as a factor of three (not shown).

References

Pelliccioni, A., et al. (2020). Integrated evaluation of indoor particulate exposure: The viepi project. *Sustainability*, 12(22), art. no. 9758 , 1-25.

PHYSMOD 2024 – International Workshop on Physical Modelling of Flow and Dispersion Phenomena
Ecole Centrale de Lyon, Ecully, France – August 28-30, 2024

Natural ventilation and stochastic wind fluctuations: preliminar experimental results

T. Di Renzo[1, 2], R. Vesipa[1], L. Ridolfi[1], P. Salizzoni[2], M. Marro[2]

[1]DIATI, Politecnico di Torino, C.so Duca degli Abruzzi 24, 10129 Torino, Italy
[2]Laboratoire de Mécanique des Fluides et d'Acoustique, University of Lyon, CNRS UMR 5509 École Centrale de Lyon, INSA Lyon, Université Claude Bernard, 36, avenue Guy de Collongue, 69134 Ecully, France

Introduction

Due to the interest in the possible energy saving and the relevance of the air quality of enclosed spaces, the study of natural ventilation has received growing attention over the last decades.

The natural ventilation is the phenomenon for which the warm stale air produced in enclosed spaces (e.g., in a room) rises toward the ceiling and accumulates generating a stratification between the buoyant layer (warmer and less dense) and the cool layer (of ambient air). If an opening is present at the ceiling level of the room, the buoyant air is expelled. Due to mass conservation, cooler air enters in the room from the exterior ambient through another opening. This phenomenon takes place due to the pressure difference between the interior and the exterior of the room caused by the accumulation of buoyant air. The presence of an external wind may radically modify the pressure gradient between interior and exterior; thus, the flow rate of air expelled from the room can be either enhanced or decreased by the wind, depending on its direction.

Due to the relevance of an external wind to naturally ventilated systems, several studies (e.g., Coomaraswamy & Caulfield, 2011) investigated its effect on the dynamics of the system. Almost all past works focused on the deterministic dynamics induced by an external wind with negligible velocity fluctuations, showing the resulting bistability in the dynamics of the system. In real cases, the situation is even more complex, as wind velocity exhibits stochastic fluctuations due to atmospheric turbulence. In a previous work (Vesipa et al., 2023), the effects of a fluctuating wind on the dynamics of a naturally ventilated system were investigated numerically. A structural change in the time averaged behaviour of the system was shown: the buoyant layer which accumulates at the ceiling turns out to be denser and thicker. This experimental work aims to investigate the effects of stochastic fluctuations of wind velocity, to validate the numerical solutions with the experimental results.

Physical model

As in Vesipa et al. (2023), we consider a room of height H which contains a point buoyancy source at floor level. The room has two openings, one at ceiling level and one at floor level. From the buoyancy source a warm turbulent plume arises, which generates a stratification whose interface is placed at height h from the floor. The buoyant air accumulated at the ceiling induces the stack effect, which drives the natural ventilation of the room.

The presence of an external wind which opposes the stack effect alters the dynamics. If the wind is not strong enough to overcome the stack effect, the stratification and the forward flow are maintained, but the buoyant layer becomes thicker and denser. If the wind is strong enough to overcome the stack effect, the flow changes direction. If the reverse flow persists, the buoyant fluid mixes with the ambient air completely ($h = 0$).

Experimental setup and results

The effect of wind fluctuations was investigated by performing an experimental campaign in a wind tunnel at École Centrale de Lyon. The room was simulated by using a cubic box. The buoyant layer was reproduced by injecting carbon dioxide: since carbon dioxide has larger density than air, a stratification takes place, but the experimental setup is upside down with respect to the physical problem. To allow visualization, the carbon dioxide was seeded with oil droplets and laser tomography was performed. The effect of external wind having fluctuations of different magnitude (i.e., different σ_u/u, where σ_u is the standard deviation of the wind velocity and u is the mean wind velocity. The density and the height of the buoyant layer were measured, by means of a flame ionisation detector (FID, cf. Vidali et al., 2022) and processing videos taken with a camera, respectively. Experimental setup is shown in panel 1.a, where the zoom is a picture of the box used for the experiments. Results of the non-dimensional interface level $\hat{h} = h/H$ of the buoyant layer are plotted in panel 1.b, as a function of the wind parameter *W* (that is the square of a Froude number). As expected by Vesipa et al. (2023), as the magnitude of the wind velocity fluctuations increases (higher σ_u/u), the buoyant layer enlarges, and the mean value of its interface level decreases. Such a deviation from the case of a constant wind ($\sigma_u/u = 0$) increases as the mean value of *W* increases.

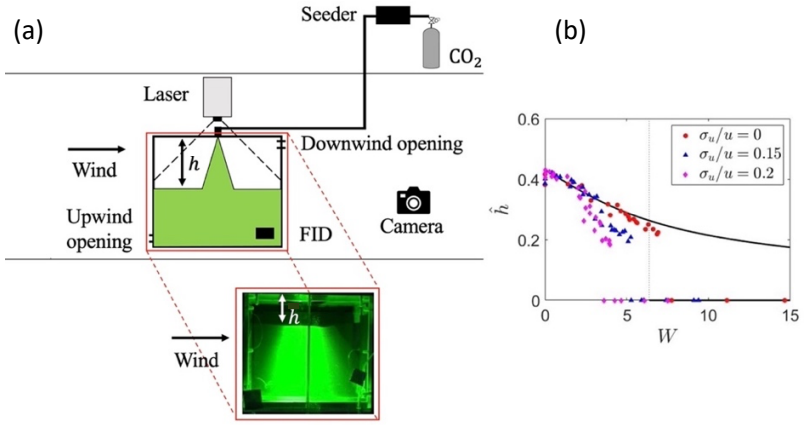

Figure 1: Panel (a): experimental setup. Panel (b): theoretical behaviour in case of constant wind (black lines) and experimental results (markers) of the non-dimensional interface elevation $\hat{h}$.

References

Coomaraswamy, I. A., & Caulfield, C. P. (2011). Time-dependent ventilation flows driven by opposing wind and buoyancy. *Journal of Fluid Mechanics*, 672. 33-59.

Vidali, C., Marro, M., Correia, H., Gostiaux, L., Jallais, S., Houssin, D., Vyazmina, E, & Salizzoni, P. (2022). Wind-tunnel experiments on atmospheric heavy gas dispersion: Metrological aspects. *Experimental Thermal and Fluid Science*, 130. 110495

Vesipa, R., Ridolfi, L., & Salizzoni, P. (2023). Wind fluctuations affect the mean behaviour of naturally ventilated systems. *Building and Environment*, 229. 109928.

PHYSMOD 2024 – International Workshop on Physical Modelling of Flow and Dispersion Phenomena
Ecole Centrale de Lyon, Ecully, France – August 28-30, 2024

Wind tunnel study on the effect of wind directions on the indoor airflow pattern for a naturally ventilated pig barn with an outdoor exercise yard

Xuefei Wu[1], David Janke[1], Sabrina Hempel[1], Thomas Amon[1, 2], Qianying Yi[1]

[1]Department of Sensors and Modelling, Leibniz Institute for Agricultural Engineering and Bioeconomy (ATB), Max-Eyth-Allee 100, 14469 Potsdam, Germany
[2]Institute for Animal Hygiene and Environmental Health, Department of Veterinary Medicine, Free University Berlin, Robert-von-Ostertag-Str. 7-13, 14163 Berlin, Germany

Abstract

A naturally ventilated pig barn with an outdoor exercise yard (Pig Barn$_{outdoor-yard}$) shows potential for improving animal welfare and meat quality by allowing pigs to sleep in the housing area and excrete or play in the outdoor exercise yard. To ensure a thermally comfortable environment and good air quality inside Pig Barn$_{outdoor-yard}$, proper ventilation is essential. To gain a deeper understanding of the ventilation inside Pig Barn$_{outdoor-yard}$, the airflow pattern inside the barn was depicted, since the airflow pattern is directly related to the pathways for heat and pollutant removal and is related to the ventilation efficiency. However, evaluating the ventilation performance is challenging due to the complex configurations, such as the presence of the outdoor exercise yard and large ventilation openings. Additionally, variable directions of the outside wind combined with the unique configuration of Pig Barn$_{outdoor-yard}$ further complicate the ventilation dynamics. Therefore, the objective of this study is to assess the relationship between external wind directions and the airflow pattern inside Pig Barn$_{outdoor-yard}$.

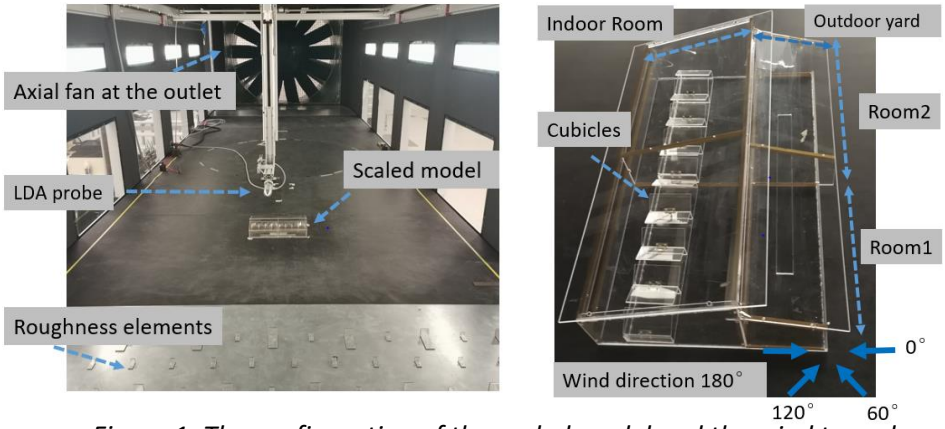

Figure 1: The configuration of the scaled model and the wind tunnel

The wind tunnel was used to carry out the study because it can fully control environmental conditions and independently adjust specific parameters. A 1:50 scaled model of Pig Barn$_{outdoor-yard}$ was constructed (Fig. 1) based on a real pig barn in Germany. The airflow pattern inside the scaled model was measured in an atmospheric boundary layer wind tunnel using 2-dimensional Laser Doppler Anemometry (LDA). Before the measurement of the airflow pattern, the wind profile above

the farmland was reconstructed in the wind tunnel, and the Reynolds number independence test was performed inside the scaled barn model. Subsequently, the airflow pattern in the yard and the indoor housing area in a horizontal plane at the height of 12 mm above the floor (equivalent to 0.60 m in full scale, corresponding to the level of the animal-occupied zone) was measured under wind directions of α = 0°, 60°, 120°, and 180° (shown in Fig. 1). The results showed that:

1. An atmospheric boundary layer wind over farmland terrain was successfully generated for a 1:50 scaled model of Pig $Barn_{outdoor\text{-}yard}$. A freestream velocity of 10.0 m s^{-1}, demonstrating acceptable Reynolds number independence for the airflow pattern, was determined for the wind tunnel experiment.

2. The horizontal vector fields at 0.60 m in full scale are depicted in Fig. 2. Table 1 presents the statistical results of the measured velocity in the yard and the indoor room, where a larger standard deviation (SD) indicates poorer airflow homogeneity. The airflow pattern under different wind directions revealed the following:

(2.1) The inclined wind caused relatively high-speed wind to be unevenly distributed in the yard at 60° and in the indoor room at 120°, and the high-speed wind enhances air exchange, while areas with low-speed wind might lack fresh air for the animal occupants. The parallel wind resulted in lower speed airflow inside both the yard and the indoor room. (2.2) The exercise yard was the windward part at wind angles of 0° and 60°, and the indoor room was the windward part at 120° and 180°. Better velocity homogeneity was always observed in the leeward part of the barn compared to the windward part. Improved airflow uniformity generally corresponded to decreased average velocities under all wind directions. (2.3) The combined effect of the barn configuration and wind directions shaped different airflow patterns in the animal-occupied zone, highlighting the potential impact of the pig barn with an outdoor exercise yard on airflow re-organization.

3. The pig barn with an outdoor yard exhibited different airflow patterns compared to conventional buildings, offering valuable insights into the natural ventilation of animal houses.

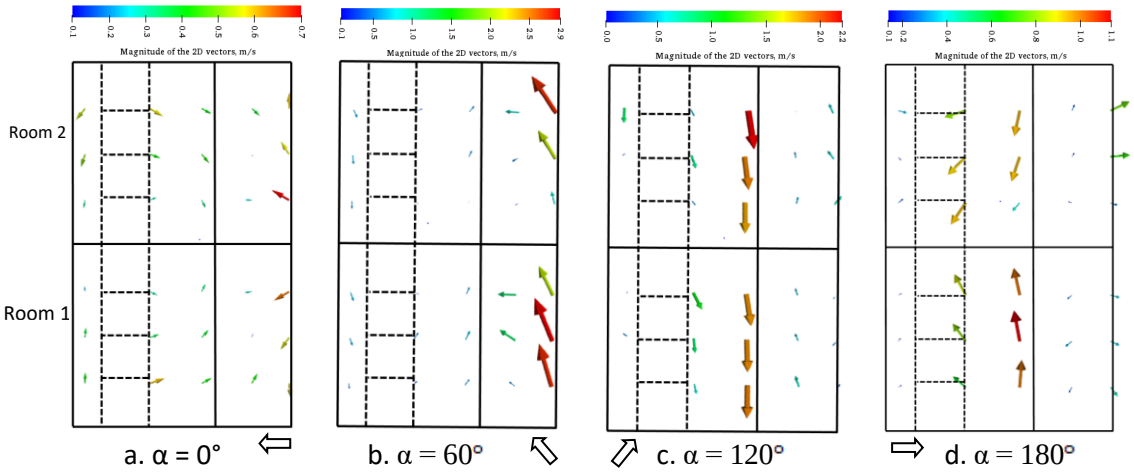

Figure 2: Airflow patterns at a horizontal plane at 0.6 m high in full scale above the barn floor (Note: black arrows indicate the freestream wind directions)

Room number	Housing area	Wind directions α (°)							
		0		60		120		180	
		V.avg (m s^{-1})	SD (m s^{-1})	V.avg (m s^{-1})	SD (m s^{-1})	V.avg (m s^{-1})	SD (m s^{-1})	V.avg (m s^{-1})	SD (m s^{-1})
Room 1	Exercise yard	0.26	0.24	1.20	1.00	0.45	0.21	0.31	0.07
	Indoor room	0.42	0.10	0.37	0.20	0.95	0.82	0.65	0.74
Room2	Exercise yard	0.27	0.20	1.75	0.97	0.40	0.16	0.38	0.27
	Indoor room	0.38	0.10	0.47	0.12	0.97	0.74	0.63	0.34

Table 1. Average velocity (V.avg) and standard deviation (SD) of the airflow velocity in the yard and the indoor room

Poster session

PHYSMOD 2024 – International Workshop on Physical Modelling of Flow and Dispersion Phenomena
Ecole Centrale de Lyon, Ecully, France – August 28-30, 2024

Dispersion of gas and aerosols within urban canopy

H. Chaloupecká[1], M. Mamula[1], J. Suchánek [2], J. Wild[3,4], R. Kellnerová[1], Z. Zelinger[2]

[1]Institute of Thermomechanics, Czech Academy of Sciences, Dolejškova 5, 18200 Praha, Czech Republic
[2]J. Heyrovský Inst. of Physical Chemistry, Czech Academy of Sciences, Dolejškova 3,18200 Praha, Czech Republic
[3]Faculty of Mathematics and Physics, Charles University, Ke Karlovu 3, 12116 Praha, Czech Republic
[4]Faculty of Safety Engineering,VSB-Technical University of Ostrava, Lumírova 13, 70030 Ostrava, Czech Republic

Abstract

Aerosols are widespread in our daily routines. We find them in both natural phenomena, like raindrops, and human activities, like car exhausts. They impact climate, health, manufacturing activities, and transportation. Exposure to aerosols can be detrimental to human health, with particular risks to the respiratory and cardiovascular systems. Most dispersion studies utilizing wind-tunnel modelling are engaged in dispersion of gases in complex terrain. However, only few studies are interested in dispersion of aerosols. Nevertheless, this dispersion can be very different from the gas, especially for huge particles. Hence, this study investigates dispersion of both, aerosols and gas, within urban canopy. The canopy used was a part of a European town modelled in the scale of 1:200 placed in a wind-tunnel with neutral stratification. A point ground level source was placed in the middle of a street lined by a relatively high block of flats and a low school building. The concentration time series were measured by the HFR500 fast flame ionisation detector of Cambustion for the gas and with the sensor SPS30 Sensirion for the aerosols. The results revealed that the dispersion field exhibits for both contaminants the presence of the isolated roughness flow regime. However, in other aspects the dispersion for both substances differ.

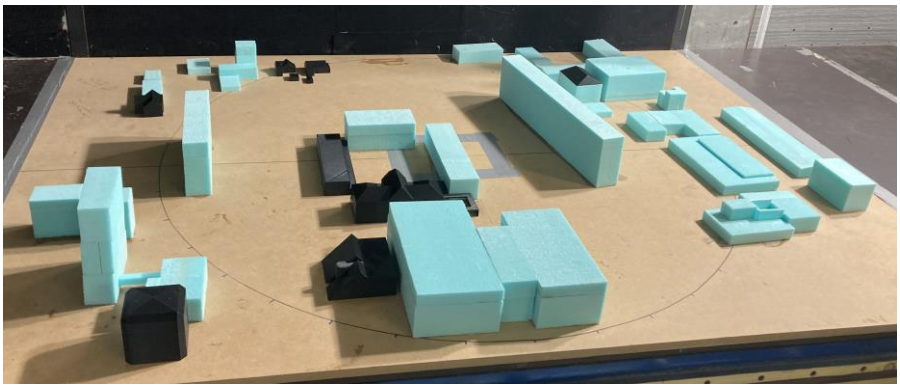

Figure 1: The model in the wind tunnel utilized in the experiments.

Funding

This research was funded by the Technology Agency of the Czech Republic, grant SS03010139 and the Institute of Thermomechanics, Academy of Sciences, Czech Republic—RVO: 6138998.

PHYSMOD 2024 – International Workshop on Physical Modelling of Flow and Dispersion Phenomena
Ecole Centrale de Lyon, Ecully, France – August 28-30, 2024

Turbulent transport characteristics of coherent structures in ideal vegetation morphology based on wind tunnel experiments

Guoliang Chen[a], Chun-Ho Liu[a], Ziwei Mo[b]
a *Department of Mechanical Engineering, The University of Hong Kong*
b *School of Atmospheric Sciences, Sun Yat-sen University*

In this paper, turbulent coherent structures are examined using the phase-space algorithm (Wu et al., 2022), in which the freestream velocity fluctuation, acceleration, and jerk affect the three axes of the detection ellipsoid. Moreover, geometric scale factor ($0 \le k \le 1$) is used to magnify or reduce the size of detection ellipsoid. The flows and turbulence over vegetation canopies of different roughness are studied by wind tunnel experiments (Mo et al., 2022; Fig. 1). Mean wind speed and fluctuating velocities (streamwise and vertical directions) are measured by a constant-temperature hot-wire anemometer (CTA) with 2,000 Hz sampling frequency. The drag coefficient C_d (= $2u^{*2}/U_\infty^2$) is calculated from the friction velocity u^* and freestream velocity U_∞ (Mo and Liu, 2018)). The vertical momentum flux $u'w'$ is divided into four quadrants according to the positive and negative characteristics of streamwise u' and vertical w' fluctuating velocities, namely outward interaction Q_1 (u' > 0 and w' > 0), ejection Q_2 (u'< 0 and w' > 0), inward interaction Q_3 (u' < 0 and w' < 0) and sweep Q_4 (u' > 0 and w' <0). Exuberance η (= $(S_1+S_3)/(S_2+S_4)$) is defined to compare the transport efficiency, while S_i (= $(u'w')_{Qi}/(u'w')$) quantifies the contribution from the i-th quadrant Q_i to the spatio-temporal average of vertical momentum flux $u'w'$. Generally, in the entire roughness sublayer (RSL), increasing drag coefficient C_d in (idealized) vegetation morphology (staggered arrays in Fig. 2a, 2b, 2c, and aligned arrays in Fig. 2d, 2e, 2f) improves transport efficiency of coherent structures in vegetation canopies. At the same wind speed and density, staggered arrays are more efficient than aligned arrays in terms of transport. It is especially obvious in the low-frequency band at low vegetation density. The increase in wind speed under staggered arrays has little effect on transport performance. However, at higher wind speeds, the transport efficiency η increases with increasing vegetation density regardless of aligned or staggered arrays. At the same time, the critical frequency (the maximum frequency within the same transport efficiency range) also increases, in particular in the lower RSL near the top of vegetation canopy. It is thus indicated that the increase in density promotes high-frequency, small-scale turbulence to enhance transport processes.

Keywords: Drag coefficient C_d, Momentum flux, Phase-space algorithm, Scaling factor k, Transport efficiency η, Wind tunnel experiment.

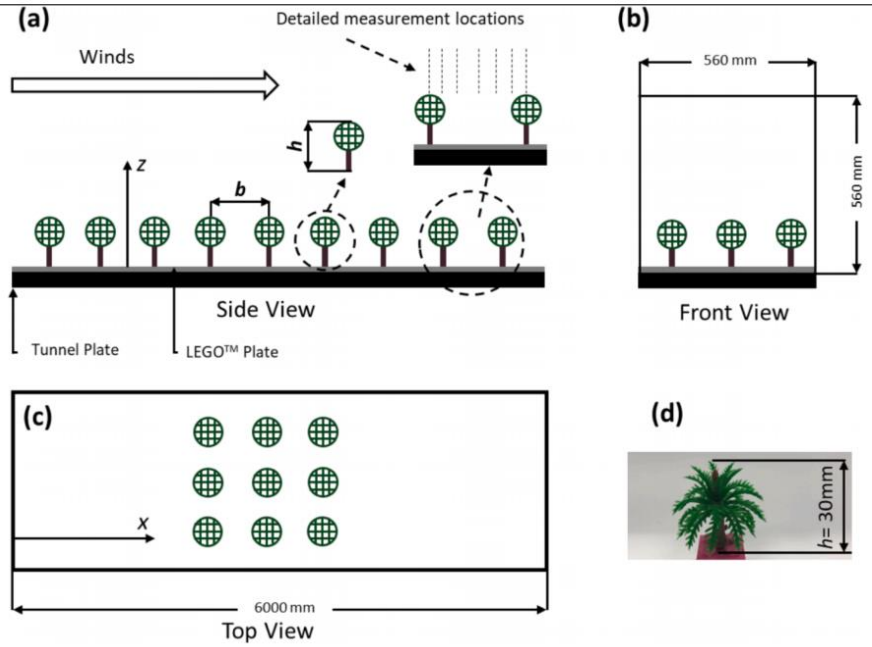

Fig. 1. Schematic of the test section with models of vegetation canopy. (a) Front view; (b) side view; (c) top view; and (d) photograph of a unit of plastic tree model.

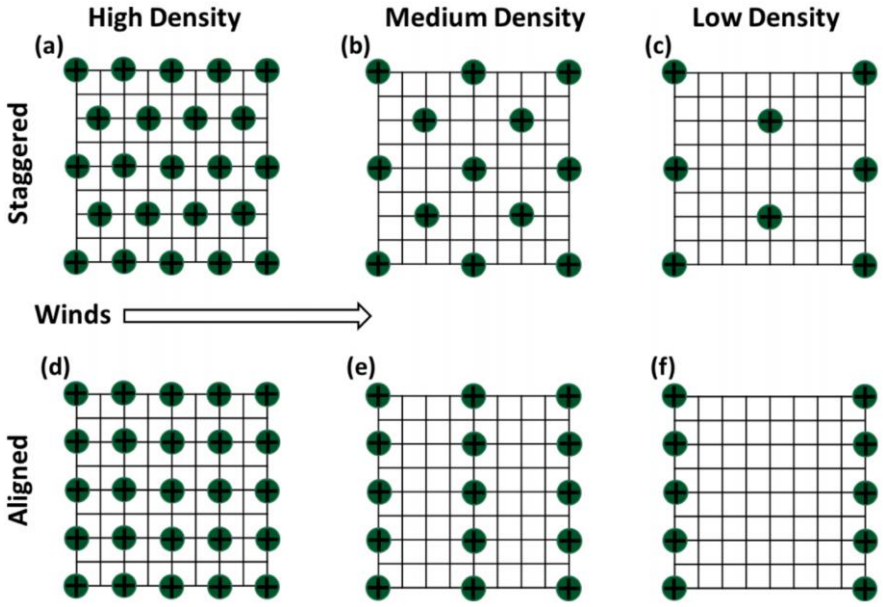

Fig. 2. Layout of the vegetation canopy models being configured in staggered and aligned patterns.

References

Wu, J., Krynkin, A., & Croft, M. (2022) Objective phase-space identification of coherent turbulent structures in 1D time series. Journal of Hydraulic Research, 60, 811–825. https://doi.org/10.1080/00221686.2022.2064344

Mo, Z., & Liu, C. H. Geosocial Letters. (2018). Wind tunnel measurements of turbulent boundary layer flows over arrays of ribs and cubes. 5:16 https://doi.org/10.1186/s40562-018-0115-x

Mo, Z., Liu, C. H., Chow, H. L., Lam, M. K., Lok, Y. H., Ma, S. W., Wong, F. L., & Yip, P. Y. (2022). Roughness sublayer over vegetation canopy: A wind tunnel study. Agricultural and Forest Meteorology, 316, Article 108880. https://doi.org/10.1016/j.agrformet.2022.108880

PHYSMOD 2024 – International Workshop on Physical Modelling of Flow and Dispersion Phenomena
Ecole Centrale de Lyon, Ecully, France – August 28-30, 2024

Exploring the influence of wind patterns on SUHI: a case study on Italian cities

*Antonio Esposito [1, *], Gianluca Pappaccogli [1], Pietro Salizzoni[2], Giuseppe Maffeis[3], Riccardo Buccolieri [1]*

[1]Dipartimento di Scienze e Tecnologie Biologiche ed Ambientali, University of Salento, S.P. 6 Lecce-Monteroni, 73100 Lecce, Italy

[2]Laboratoire de Mécanique des Fluides et d'Acoustique, University of Lyon, CNRS UMR 5509, Ecole Centrale de Lyon, INSA Lyon, Université Claude Bernard, 36, Avenue Guy de Collongue, 69134 Ecully, France

[3]TerrAria s.r.l., via Melchiorre Gioia 132, 20125 Milan, Italy

Abstract

Urban environments are increasingly becoming hotspots in the face of climate change, with the intensification of extreme heat events posing significant challenges to human health and well-being (Basu and Samet, 2002; Tan et al., 2007). Among the complex factors contributing to urban heat, the urban heat island effect (UHI) stands out as a prominent phenomenon, increasing temperatures within cities compared to their surrounding rural areas. In this context, understanding the dynamics of the urban heat island, particularly the surface urban heat island (SUHI), becomes crucial for developping effective mitigation strategies and enhancing urban resilience (Abdulateef & Al-Alwan, 2022, Irfeey et al, 2023).

In this context, the present study aims to assess the intensity of SUHI in relation to different wind patterns by describing the geometry of the city through urban morphological parameters. For this purpose, land surface temperature (LST) data from the sentinel-3 and wind pattern data from ERA5 reanalyses (spatial resolution 0.25x0.25°) are used, whereas the city geomatics are properly described at the same spatial resolution as the LST data (i.e. 1x1km). Specifically, the cities of Milan, Turin and Lecce are considered, over a period including the summer seasons (JJA) during the years 2022-2023. The SUHI study points out that the optimal conditions for a peak in the phenomenon occur during calm wind conditions at night, and especially in more densely urbanised areas. At the same time, this phenomenon becomes minor for wind intensities greater than 6.5 ms-1, demonstrating its effect mainly in the more suburban areas of the city (Figure 1). Furthermore, wind direction shows a significant impact on the distribution of SUHI in cities. It has been observed that northerly winds mitigate SUHI intensity, while southerly winds tend to intensify it. Additionally, efforts are made in this study to consider the effects of albedo and shading in explaining the variations in SUHI intensities among different cities. By analysing the SUHI phenomenon among different cities and considering urban geometry, this study provides valuable insight for enhancing the understanding of factors affecting SUHI intensity and supporting the improvement of urban thermal environments through informed urban planning, mitigation systems, and the promotion of human well-being and thermal comfort.

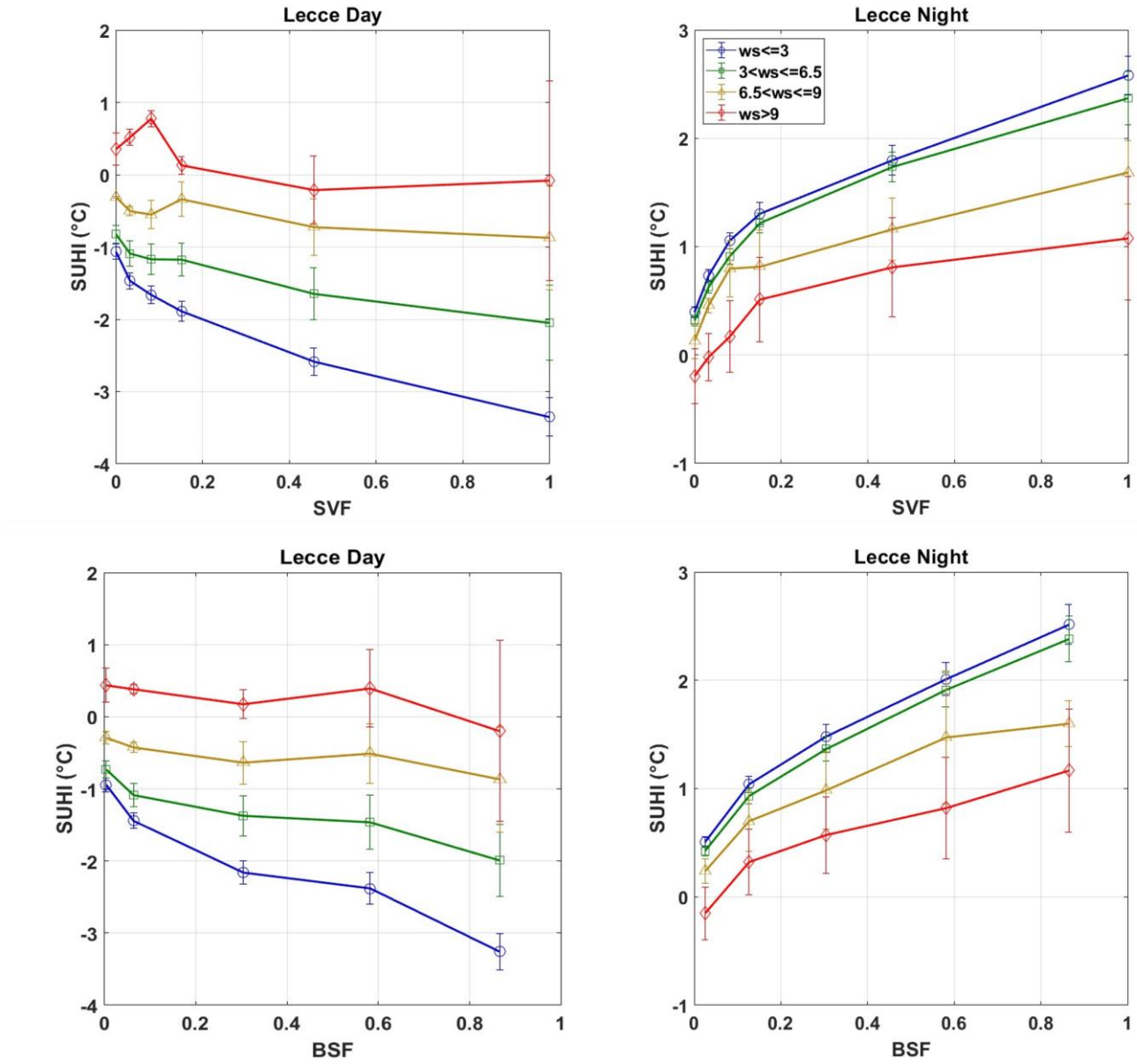

Figure 1. Example of the relationship between morphological parameters and SUHI in the city of Lecce according to different wind speed classes. Above SVF - sky view factor, below BSF - building surface fraction.

References

Abdulateef M.F., Al-Alwan H.A.S. (2022). The effectiveness of urban green in frastructure in reducing surface urban heat island. Ain Shams Engineering Journal, 13 (1), Article 101526.

Basu, R., and Samet, J. (2002). Relation between elevated ambient temperature and mortality: A review of the epidemiologic evidence. Epidemiol. Rev. 24, 190–202.

Irfeey, A.M.M.; Chau, H.-W.; Sumaiya, M.M.F.; Wai, C.Y.; Muttil, N.; Jamei, E. Sustainable Mitigation Strategies for Urban Heat Island Effects in Urban Areas. Sustainability 2023, 15, 10767.

Tan, J., Zheng, Y., Song, G., Kalkstein, L. S., Kalkstein, A. J., and Tang, X. (2007). Heat wave impacts on mortality in Shanghai, 1998 and 2003. Int. J. Biometeorology 51, 193–200.

29 Aug 2024

Quality assurance and improvement of experimental techniques

PHYSMOD 2024 – International Workshop on Physical Modelling of Flow and Dispersion Phenomena
Ecole Centrale de Lyon, Ecully, France – August 28-30, 2024

FFID matters

A. Robins, P. Hayden

EnFlo, School of Mechanical Engineering Sciences, University of Surrey, UK

Abstract

Cambustion Ltd. introduced the new HFR500 FFID in 2020, which prompted us to ask of its performance relative to the previous HFR400 and, for that matter, the original FFID that is described in Fackrell (1980). Existing data and some new runs were used to examine not only the intercomparison, but also the performance relative to the theory developed in Fackrell's paper. The set of available experiments is summarised below.

A HFR500, no filters, 10000Hz sampling, digital filtering to 400Hz, two FFIDs on the traverse
B HFR500, no filters, 400Hz, two FFIDs on the traverse
C HFR500, 1 filter, 400Hz, two FFIDs on the traverse
D HFR500, 2 filters, 400Hz, two FFIDs on the traverse
E HFR500, no filters, 10000Hz, digital filtering to 400Hz, two FFIDs on the traverse
F HFR400, no filters, 10000Hz, digital filtering to 400Hz, one FFID on the traverse
E/L HFR500, no filters, 10000Hz, digital filtering to 400Hz, one FFID on the traverse, effect of tube length
E/U HFR500, no filters, 10000Hz, digital filtering to 400Hz, one FFID on the traverse, effect of ambient flow speed
E/Δp HFR500, no filters, 10000Hz, digital filtering to 400Hz, one FFID on the traverse, effect of sampling flow rate

Cases A to D treated means of handling the somewhat greater noise levels seen with the HFR500, E and F investigated sensitivity to installation conditions (i.e. one or two FFIDs mounted on the traverse arm), as well as comparison between the 400 and 500. Cases E/L, E/U and E/Δp examined the effects of sampling tube length, ambient flow speed and sample flow rate. These latter three sets of experiments were guided by the performance relationships developed by Fackrell (1980). Further tests, to be completed prior to Physmod 2024, were then planned to treat the questions that arose from these studies in a more systematic manner.

The experiments were (and will be) carried out in a H = 1m deep, neutral boundary layer, mostly with a 2ms^{-1} reference speed. As an example of the intercomparisons, the figure below shows dimensionless concentration fluctuation variances measured in an elevated plume, source height h = 0.34H, using the HFR400 as the reference and showing results for the HFR500 in Cases A to E. The instruments were operated in their default conditions (for the EnFlo Lab.). Concentrations, C, were made dimensionless, C^*, using the reference flow speed, the emission rate and the source height.

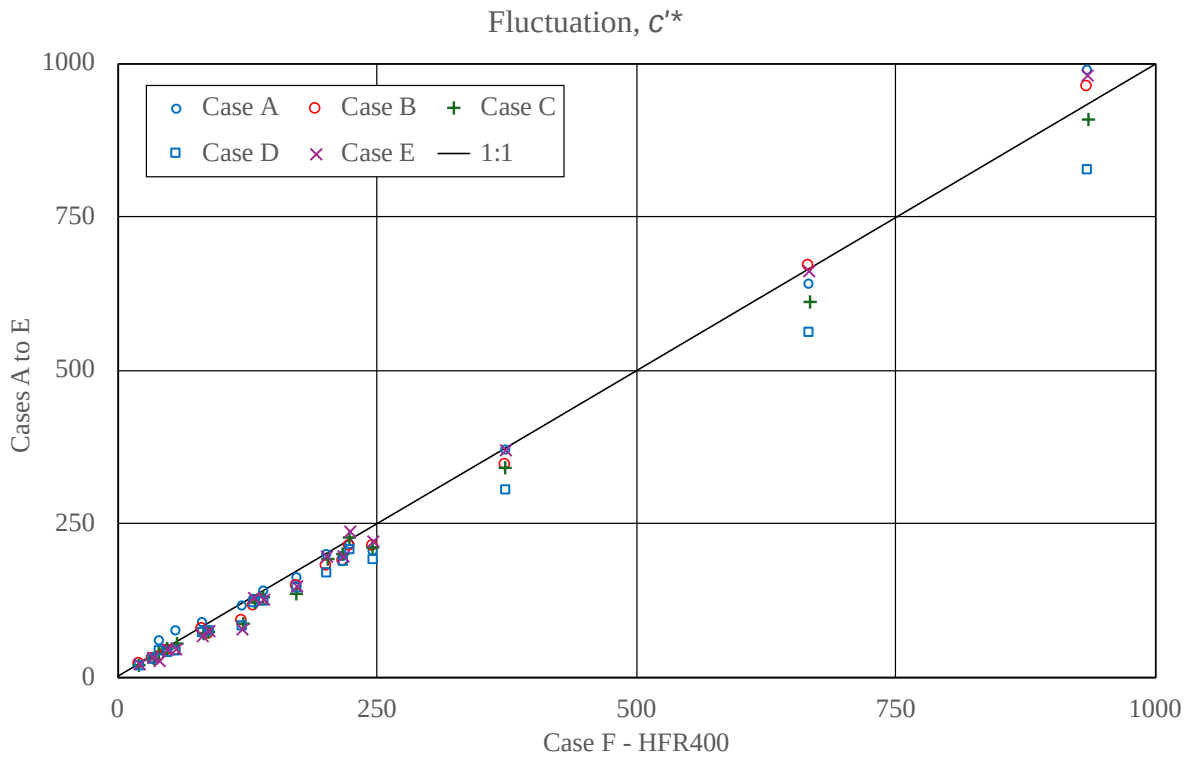

Figure 1: Intercomparisons of dimensionless concentration fluctuation variances measured in an elevated plume, h/H = 0.34. The effect of the filter options can be seen by comparing results for cases B, C and D. Overall, the scatter around the 1:1 line is somewhat larger than hoped for (a target of a few percent), given that a 5-minute averaging time was used.

There are other matters to consider, including procedures for calibration, background and drift corrections, and the treatment of lone spikes in the signal.

We hope that this presentation will encourage a general discussion amongst those present that might lead to preferred best-practice guidance for FFID use in wind tunnels.

Reference

Fackrell, JE (1980). A flame ionisation detector for measuring fluctuating concentration. *J. Phys. E: Sci. Instrum., Vol*. 13, 888-893.

PHYSMOD 2024 – International Workshop on Physical Modelling of Flow and Dispersion Phenomena
Ecole Centrale de Lyon, Ecully, France – August 28-30, 2024

A viable alternative to FFID for tracer concentration measurement

P. Hayden, D. M. Birch

Centre for Aerodynamics & Environmental Flow, University of Surrey Department of Mechanical Engineering Sciences, Guildford, GH2 7XH, United Kingdom

Abstract

The physical modelling of dispersion in turbulent plumes requires the time-domain measurement of a representative tracer gas. The only technology currently able to do this is the fast-flame ionization detector (FFID), which measures ionization within the sample after exposure to a hydrogen combustion flame, and is sensitive to hydrocarbons only. The FFID instrument has a response bandwidth of up to 200 Hz (Marucci & Carpentieri 2020), but is itself complex and costly; the sensing head is large and generates significant waste heat, while the umbilical must include lines for not only power and signal, but also fuel. The potential for interference in experimental measurement campaigns is therefore high.

Pellistor sensors, on the other hand, measure hydrocarbon concentration through catalytic effects, and are entirely electrical. These are a mature technology; they are commonly used in safety applications, and are readily available from commercial suppliers. Although these sensors are significantly smaller than FFID heads, they tend to have a larger sensing volume. More importantly, though, they tend to have very low bandwidths (order 0.01 Hz), which renders them unusable for characterizing fluctuations in turbulent plumes. To address these shortcomings, a novel enclosure and dynamic calibration process has been developed for these off-the shelf-sensors.

First, an Alphasense CH-A3 pellistor sensor was fitted with a sealed cap which provided a small-volume plenum over the sensing surface, miminizing the volume of the measured sample. Inlet and outlet channels allowed samples of gas to enter via a small-diameter inlet, flow across the sensing surface in the plenum, and then exit under an applied pressure difference. Next, a calibration apparatus was constructed which was capable of producing a flow of arbitrary concentration varying in time. A solution of air and propane was fed at constant pressure into the sensor plenum, with a computer-controlled servovalve controlling the flow rate of propane. Great care was taken to balance the gas system back-pressures, and to ensure that the gases were well-mixed before introduction into the plenum. The servovalve was then actuated sinusoidally in time, resulting in a sinusoidal variation in propane concentration within the sensor plenum. The concentration in the plenum was simultaneously monitored with a fast-response FFID in order to provide a calibration reference. The concentration amplitudes were adjusted with the frequencies (up to 3500 PPM) to ensure sufficient signal-to-noise ratio.

Signals from the pellistor were obtained at a range of concentration frequencies from 0.2 Hz to 3 Hz. The dynamic response was then mapped in the spectral domain, yielding the frequency-dependent

gain and phase shift requried for dynamic calibration. Figure 1(a) compares the self-scaled concentrations obtained from the pellistor and the FFID at freqencies of 0.2 Hz and 1 Hz, and shows good agreement: this represents an increase in bandwidth of at least two decades. Note that these signals were obtained from the analogue sensing element without any pre-amplification or signal conditioning.

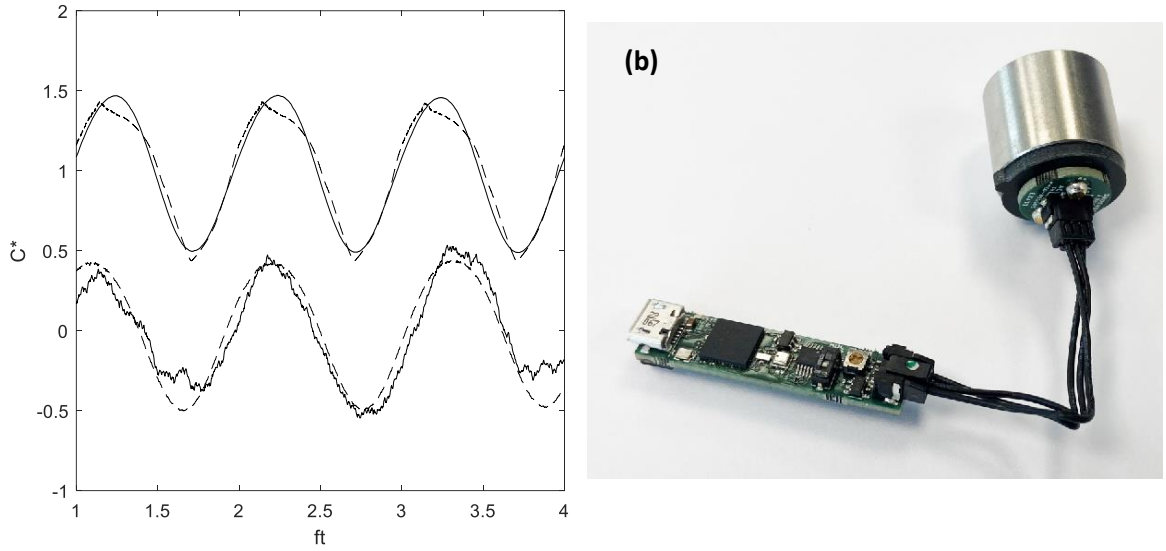

Figure 1: (a) preliminary calibrated dynamic response (solid, pellistor; dashed, FFID); (b) Prototype digital pellistor concentration sensor.

A bespoke miniature analogue signal conditioning and USB data acquisition system was developed for the sensor (figure 1b), to improve signal-to-noise ratio and enable operation at higher frequencies, and a compact probe body for the integrated sensor unit is being designed.

Also, since most commercially-available pellistor sensors are intended for use in safety applications, they will have a semi-porous barrier between the sample gas and the catalytic surface in order to comply with ATEX requirements (EU directive 99/92/EC). This barrier is expected to have a significant effect on dynamic response, and aftermarket removal of the barrier or reduction of its thickness is also being explored in order to further improve the bandwidth.

The small size and low cost of these sensors (relative to FFIDs) will enable the deployment of spatially-resolved rakes of concentration probes, allowing simultaneous spatial correlations in concentration and/or significantly reducing the wind tunnel run time required by a single scanning FFID probe. Furthermore, the improved bandwidth would enable pellistors to be used to evaluate higher order concentration statistics up to a bandwidth of at least 3 Hz so far. With either analogue or digital outputs available, the instrument can also be integrated with existing velocity measurement systems in order to resolve mass fluxes.

References

Marucci, D. and Carpentieri, M. (2020). "Dispersion in an array of buildings in stable and convective atmospheric conditions". Atmos. Env. 222, 117100.

PHYSMOD 2024 – International Workshop on Physical Modelling of Flow and Dispersion Phenomena
Ecole Centrale de Lyon, Ecully, France – August 28-30, 2024

PIV as an alternative to LIF systems for wind experiments: a study on street canyon pollution

Š. Nosek[1], Z. Babuková[1], R. Kellnerová[1], M. Jakubcová[1], Z. Jaňour[1],

[1]Institute of Thermomechanics of the CAS, Fluid Dynamics, Dolejškova 1402/5, 18200, Czech Republic

Abstract

Measurements of planar turbulent pollution fluxes in wind tunnel experiments are rare as they require laser-induced fluorescence systems in combination with particle image velocimetry (PIV). The need for time-resolved measurements of turbulent in-plane pollutant fluxes requires expensive lasers for the LIF systems, which operate at different wavelengths than the PIV lasers. Another problem is the need for fluorescent markers such as acetone or anisole, which are hazardous substances.

This study presents an alternative for measuring planar turbulent pollutant fluxes, namely the PIV system. We used the time-resolved PIV system in the same conventional way as for velocity measurement, but instead of filling the incoming flow with the seeding particles, the particles were injected through the ground-level line source in the centre of the studied street canyon. Since the wind tunnel had an open circuit, there was no background concentration of particles during the measurement. After the camera had recorded sufficient double images, these images were subjected to velocity and concentration post-processing. The classical adaptive PIV methods were used for velocity post-processing, while image processing methods such as pixel resampling and Gaussian filtering were used for concentration post-processing. Finally, since the pixel value is linearly proportional to the particle concentration, the absolute concentration values were calculated using the calibration coefficient, the ratio between the average ethane concentration measured with the fast flame ionisation detector (FFID) and the average pixel value of the region of interest.

We validated the results of the PIV concentration measurements in two ways. First, we compare the concentration contours obtained from the FFID measurements with those obtained from the PIV system for two different street canyon aspect ratios. Second, we compare the turbulent, advective, and total vertical pollutant fluxes at the roof level of the street canyon, having an aspect ratio of 1, with those calculated in the LES study by Michioka et al. (2014) (see Figure 1). Although the geometry of the buildings was different (the width of the buildings was three times larger in the current study), the results show that the PIV system can be used as a reliable method to measure planar pollutant fluxes and to analyse the dynamics of the concentration, e.g. by dynamic mode decomposition, within the urban canopy.

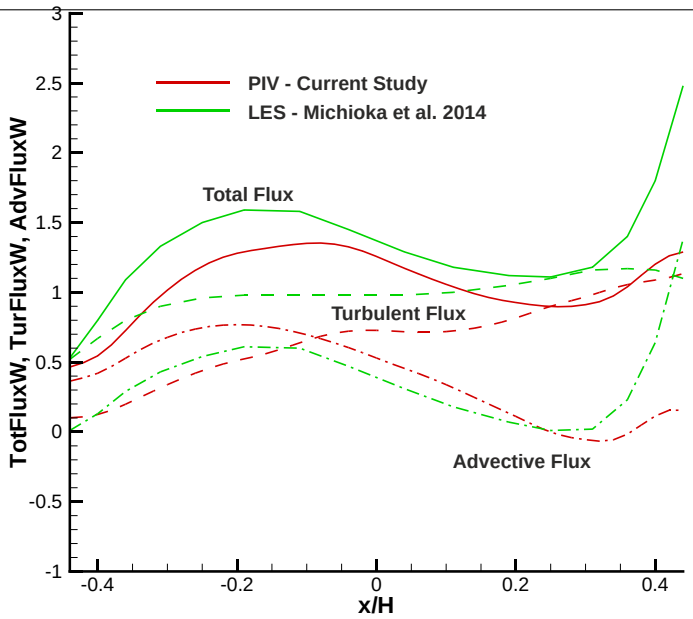

Figure 1: Comparison of the horizontal profiles of the mean dimensionless vertical pollution fluxes at the roof height of the street canyon with aspect ratio 1 between the current study (red lines) and the LES study (green lines) by Michioka et al. (2014). The solid, dashed and dash-and-dotted lines represent the total, turbulent and advective pollutant fluxes respectively. The position of the ground-level line source for both studies was at x/H = 0.

References

Michioka, T., Takimoto, H. & Sato, A. (2014) Large-Eddy Simulation of Pollutant Removal from a Three-Dimensional Street Canyon. *Boundary-Layer Meteorology*, 150- 259–275.

PHYSMOD 2024 – International Workshop on Physical Modelling of Flow and Dispersion Phenomena
Ecole Centrale de Lyon, Ecully, France – August 28-30, 2024

Multiscale inhomogeneous grids for experimental atmospheric boundary layer generation: a comparison with spires

T. Huret[1], C. Vassilicos[1], G. Tanguy[1], L. Jacquin[2], Q. Gallas[3]

[1]Univ. Lille, CNRS, ONERA, Arts et Métiers Institute of Technology, Centrale Lille, UMR 9014 -LMFL – Laboratoire de Mécanique des Fluides de Lille -Kampé de Fériet, F-59000 Lille, France
[2]DAAA, ONERA, Université Paris-Saclay, F-92120 Meudon, France
[3]ONERA-The French Aerospace Lab, 31410 Mauzac, France

Abstract

A common practice for both research and industrial applications involving the generation of a neutral atmospheric boundary layer (ABL) in a wind tunnel consists in associating a roughness fetch with an upstream array of "spires" (Irwin, 1981). This passive method enables to tailor the mean velocity profile on the basis of quantitative guidelines. At the expense of a further time-consuming trial-and-error design process, these devices can be adjusted to generate representative turbulent intensity profiles, but no representative trends of the integral length scale profile.

In parallel, the downstream evolution of regular and fractal grid-generated turbulence has been recently shown to scale with a wake-interaction model (Gomez-Fernandez *et al*., 2012) which can be used to predict basic properties of downstream turbulence profiles in case of zero mean shear. If this scaling law were to apply to grid-generated shear flow, it would enable the independent tailoring of turbulent intensity and mean velocity profiles without trial-and-error. In order to investigate these ideas experimentally, our work makes use of Multiscale Inhomogeneous Grids (MIG), a new type of passive device defined to vary the turbulence scaling parameters with altitude, while enabling a tailoring of the mean velocity profile. Examples of MIGs are illustrated in Figure 1.

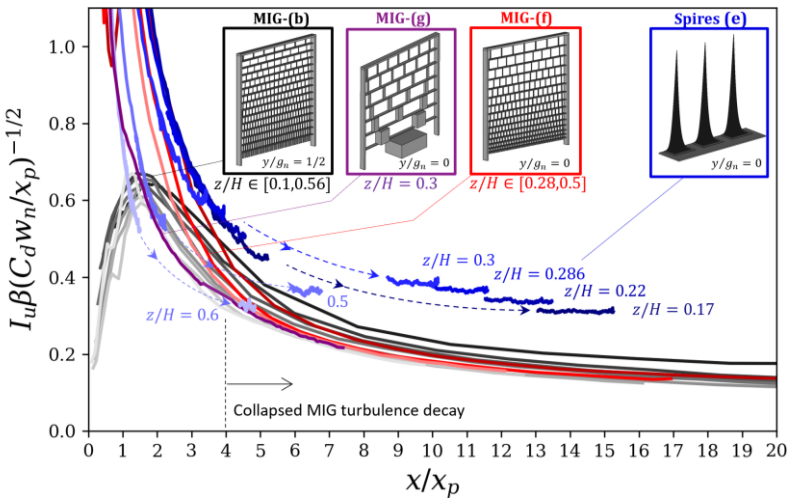

Figure 1: Normalized streamwise profiles of turbulent intensity I_u=u'/U downstream of both discrete MIG grids (b,g,f) and a continuous MIG grid (e). Each device is designed to reproduce the same

logarithmic mean flow over the full-height H of the wind tunnel. Each profile is obtained at a given altitude z/H corresponding to a given local mean shear (lighter color means higher altitude and smaller mean shear). The axes are normalized by: x_p a wake-interaction length scale, C_d the drag of a grid's bar in isolation, w_n the width of the grid bar and β=2.88 (Gomes-Fernandes et al., 2012).

A general MIG design algorithm is developed for the generation of a prescribed mean flow profile. It is experimentally validated for the design of MIGs aiming to generate full-depth and part-depth neutral atmospheric boundary layer configurations. The devices are studied over both smooth and rough walls in the SCL-PIV wind tunnel of ONERA Lille using both Hot-Wire Anemometry (HWA) and stereo Particle Image Velocimetry (S-PIV). This validation process reveals the existence of a defective grid regime for specific local geometric configurations of MIGs. A set of criteria on local geometric parameters (i.e. local obstruction and local mesh aspect ratio) is suggested to avoid this defective grid regime. These criteria extend to MIGs the obstruction-based criterion usually considered when designing parallel-bar arrays or square mesh grids (Rose, 1966).

The turbulence intensity decay downstream of the designed MIGs is then studied by scaling its streamwise profile measured downstream of each vertical level of the grid by the corresponding wake-interaction parameters for zero shear grid flows (Figure 1). As expected, this scaling reveals a remnant effect of the local mean shear. However, it provides a satisfactory collapse of profiles having similar mean shear conditions, thereby justifying the usefulness of this scaling model for grid-generated shear flows.

Moreover, our work reveals that spires can be conceptually designed and studied as "continuous MIG grids", with the expectation that the wake-interaction scaling would be as relevant for spires as it is for discrete MIGs. However, it appears in Figure 1 that turbulence decay downstream of spires does not collapse with turbulence decay downstream of discrete MIGs, even with comparable generated mean shear. A physical mechanism of a different nature appears to be at play downstream of spires in the development of turbulence intensity, despite their conceptual proximity to MIGs.

Indeed, a different turbulence production regime is observed for these two types of devices. On the one hand, spires generate one single intense shear layer with a very large Turbulence Kinetic Energy (TKE) production rate at z/H=0.3. This shear layer is separated from the naturally growing boundary layer by a well-mixed highly turbulent region. The mean shear layer decays and converges to the prescribed logarithmic mean flow profile at x=6H. On the other hand, downstream of discrete MIG grids, less intense TKE production regions are spread at each level across the height of the grid. These differences suggest (i) a spire TKE production mechanism of a different nature than planar wake-interactions alone –e.g. through massive recirculation bubbles or wakes oscillations—, and potentially (ii) a spires-generated flow structure that may enhance the interaction with the naturally-growing boundary layer. Future studies will investigate these possible mechanisms and their relation to wake-interaction mechanisms, as the resulting understanding may help improve the design process of both discrete MIG grids and continuous spires for ABL generation.

References

Irwin, H. P. A. H. (1981). The design of spires for wind simulation. *Journal of Wind Engineering and Industrial Aerodynamics,* 7(3), 361-366.

Gomes-Fernandes, R., Ganapathisubramani, B., & Vassilicos, J. C. (2012). Particle image velocimetry study of fractal generated turbulence. *Journal of Fluid Mechanics*, 711, 306-336.

Rose, W. G. (1966). Results of an attempt to generate a homogeneous turbulence shear flow. *Journal of Fluid Mechanics*, 25(1), 97-120.

PHYSMOD 2024 – International Workshop on Physical Modelling of Flow and Dispersion Phenomena
Ecole Centrale de Lyon, Ecully, France – August 28-30, 2024

Time Resolved Surface Pressure and Concentration Correlations in an Atmospheric Boundary Layer

J. Schmeer[1], M. Placidi[1], D. M. Birch[1]

[1]University of Surrey, Faculty of Engineering and Physical Sciences, School of Mechanical Engineering Sciences, Centre for Aerodynamics and Environmental Flow, Guildford, UK

Abstract

Understanding flow patterns in the urban canopy layer is important for pollutant dispersion studies in the interest of environmental impact and human health due to the associated effects of poor air quality. Surface pressure measurements are often used to capture mean flow structures, and concentration measurements are used to detect plume dispersion.

However, to date there has been little work on time-resolved pressure histories, nor has there been any investigations of correlations between concentration and surface pressure in the atmospheric boundary layer. To that end, a highly instrumented model building (the 'Smart Cube') has been developed for use in the University of Surrey's Environmental Flow wind tunnel to investigate spatially resolved instantaneous surface pressure fluctuations. The Smart Cube model is validated by comparing mean pressure measurements to published data from previous work (including Castro and Robins, 1977).

A dynamic pressure calibration technique has been developed to enable the use of ultra-low range pressure scanners (Surrey Sensors Ltd. model DPS14-160P, having a full-scale range of 160 Pa and bandwidth of 1 kHz) for time-resolved pressure measurements in flows with free-stream velocities of 2.5 ms^{-1}. With pressure measurements resolved in both space and time, flow structures could be investigated for the case of a single cube and staggered cube array (which approximates an urban morphology), at a series of wind incidence angles.

Instantaneous pressure differences between the two side walls of the cube nominally parallel to the flow were shown to correlate well to mean flow direction, especially for the case of a single cube. Regions of high surface pressure standard deviation coincide with reattachment zones.

The pressure standard deviation in the staggered cube array, modelling a very rough wall boundary layer, shows that the separation region is smaller as a result of the reduced velocity caused by the blockage effect of upstream cubes. Small changes in wind incidence have no significant effect on the pressure statistics for the case of a staggered array.

Spatially resolved surface pressures were also used to approximate the instantaneous friction velocity of the cube array, and mean values correspond well with values obtained from Clauser plot estimates. The instantaneous transverse shear stress was also approximated and exhibited a bimodal behaviour consistent with flow bifurcation and outer region meandering, which is consistent with observations from previous studies.

A pollutant source was then introduced together with a traversing fast-flame ionisation detector (FFID) probe to measure concentration at multiple locations around the model. FFID measurements are much more restrictive than surface pressure measurements, so identifying a relationship between the two parameters could enhance experimental capabilities.

The correlation between the concentration in one location and surface pressure over the cube was then obtained, after demonstrating that the FFID had no measurable effect on pressures. The correlation coefficient, r_c, between pressure, p, and concentration, C, is given in equation (1). Results for the case of a single cube, of height *h,* are shown in in Figure 1, for a FFID position adjacent to the front face of the cube, offset from the centre and at a height of 2*h*/3. For this case, the source was located a distance *h* upstream on the centreline, at a height of *h*/2.

Figure 1 shows a weak negative correlation on the front face adjacent to the FFID position: a slower moving 'pocket' of air flowing past the source will collect more tracer gas, so lower pressure correlates to a higher concentration and vice versa. Correlations on opposite wall-normal faces tend to have opposite signs, suggesting that there is a link between flow direction and correlation coefficient, and that the flow meanders side to side in the tunnel.

These results demonstrate that it is possible to obtain time-resolved pressure measurements with full-scale ranges of order 1 Pa. Also, identifying that a correlation exists between concentration and surface pressure in certain situations suggests that surface pressure measurement could compliment FFID measurements in future experimental campaigns.

$$r_c = \frac{\sum(p_i - \bar{p})(C_i - \bar{C})}{\sqrt{\sum(p_i - \bar{p})^2 \sum(C_i - \bar{C})^2}} \quad (1)$$

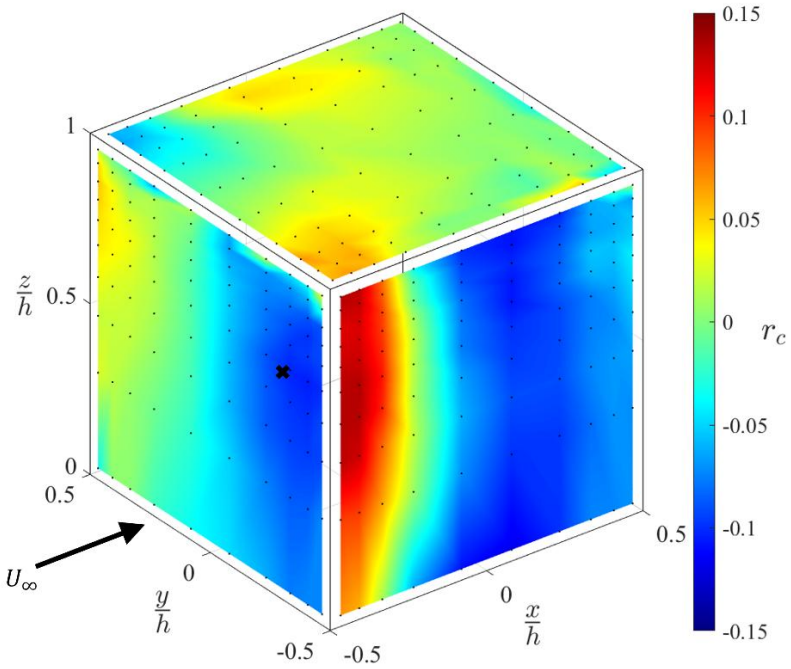

Figure 1: Single cube correlation coefficient between concentration at (x/h=-0.53, y/h=-0.33, z/h=0.67) indicated with a cross & surface pressure for a source position at (x/h=-1.5, y/h=0, z/h=0.5) where the origin of the coordinate system is the centre of the cube at floor level and h is cube height.

References

Castro, I. P., & Robins, A. G. (1977). The flow around a surface-mounted cube in uniform and turbulent streams. *Journal of Fluid Mechanics*, 79, 307-335.

Flow and dispersion in the built environement

PHYSMOD 2024 – International Workshop on Physical Modelling of Flow and Dispersion Phenomena
Ecole Centrale de Lyon, Ecully, France – August 28-30, 2024

Analyzing the influence of small fireplaces to the air quality of residential areas

F. Harms[1], B. Leitl[1]

[1]EWTL, Meteorological Institute, University of Hamburg, Bundestrasse 55, D-20146, Germany

Abstract

Pollutant emissions from private households substantially influence the air quality in Germany. Particularly in the near of emission sources high concentrations of fine particles are observed. The air quality in residential areas is not only influenced by the amounts of pollutants released, but also by individual release conditions. In order to improve the air quality in these areas by restricting release conditions, a research project was sponsored by the German Environment Agency (UBA).

As part of the research project, the EWTL at the University of Hamburg is tasked to identify parameters influencing the air quality next to a detached house. The focus of these measurements is on dispersion in the recirculation zone behind the building and close to surrounding houses. Based on systematic wind tunnel measurements the influence of selected release and dispersion parameters is tested. For example, the height and position of the stack at the building is changed systematically. Hereby typical configurations of single family houses are reflected. Furthermore, the effect of the roof structure on the amount of tracer trapped in the recirculation zone of the house is analyzed. For these measurements the slope of the roof is varied systematically. For selected parameters, also the influence of different wind directions is tested. In addition to the measurements around an isolated building, measurements within a group of buildings are carried out. Finally, the influence of a hillside building configuration on near source dispersion is investigated.

All measurements are carried out in the large boundary layer wind tunnel “WOTAN”. The 25 m long wind tunnel provides an 18 m long test section equipped with two turn tables and an adjustable ceiling. The cross section of the tunnel measures 4 m in width and 2.75 to 3.25m in height depending on the position of the adjustable ceiling. A neutrally stratified model boundary layer flow in the scale of 1:200 was generated by a carefully optimized combination of turbulence generators at the inlet of the test section, and a compatible floor roughness. The modelled boundary layer fulfils the requirements of the revised German VDI Guideline 3783/12 for wind tunnel modelling of atmospheric flow and dispersion phenomena.

Figure 1 shows the first tested model house in the scale of 1:200. The picture displays 2 stacks which can be used independently.

First results of the measurement campaign, which started in 2024, will be presented and discussed. These results will also be compared to findings of previous studies in this field. Due to the relative small size of detached houses, most wind tunnel studies use relative large scales. This typically leads to a challenge in modelling a proper boundary layer flow. Particularly the integral length scale of the modeled boundary layer tends to relative small values when large scales are used. Therefore, the

presentation will discuss the challenge to model a boundary layer flow which and is qualified to analyze dispersion processes of small fireplaces and fulfills the requirements of the revised German VDI 3783/12 guideline.

Figure 1: Model house with two stacks. One stack is located at the side of the building and the other stack is placed in the center of the roof.

References

VDI 3783/12: Physical modelling of flow and dispersion processes in the atmospheric boundary layer-Application of wind tunnels. VDI/DIN Handook Clean Air, Vol. 1b: Environmental Meteorology, VDI/Beuth (2024)

PHYSMOD 2024 – International Workshop on Physical Modelling of Flow and Dispersion Phenomena
Ecole Centrale de Lyon, Ecully, France – August 28-30, 2024

Evaluation of Taylor's hypothesis validity in urban street-canyon flows

R. Combette[1], L. Perret[1], B. Conan[1]

[1]Nantes Université, École Centrale Nantes, CNRS, LHEEA, UMR 6598, F-44 000 Nantes, France

Abstract

In experimental studies of urban flows, Particle Image Velocimetry (PIV) and its variants (2D-PIV, stereoscopic PIV, tomographic PIV, etc.) have become indispensable tools, enabling the acquisition of 2D or 3D velocity fields with increasing spatial resolution. However, these techniques cannot capture the pressure field, which is also crucial for understanding phenomena such as drag generated by immersed buildings or estimating instantaneous wind loads. This has motivated researchers to develop methods for reconstructing the pressure field from the velocity one by solving the Poisson equation derived from the conservation of momentum (in its incompressible form):

$$\frac{\partial \mathbf{u}}{\partial t} + (\mathbf{u}.\nabla)\,\mathbf{u} = -\frac{1}{\rho}\nabla p + \nu\nabla^2\mathbf{u} \qquad (1)$$

Where ***u***, *p*, *ρ*, and *v* are the velocity vector, the pressure, the density, and the kinematic viscosity, respectively. Depending on the PIV technique used, most spatial terms can be obtained or estimated. Therefore, the main challenge lies in the calculation of the acceleration (*∂**u**/∂t*), as sufficient temporal resolution cannot generally be achieved in PIV. Various methods have been proposed to estimate this term, among which figures the use of Taylor's hypothesis (TH). The assumption is made that the turbulent eddies are convected at a certain convection velocity $\mathbf{U}_c$, and the temporal term can be derived from the following relation:

$$\frac{D\mathbf{u}'}{Dt} = \frac{\partial \mathbf{u}'}{\partial t} + (\mathbf{U}_c.\nabla)\,\mathbf{u}' = 0 \qquad (2)$$

Where **u**' is the fluctuating velocity defined by Reynolds's decomposition. The choice of this convection velocity is particularly important. While the mean velocity is commonly used and leads to accurate results for pressure estimation in most regions, limitations are typically encountered in regions of high shear-layer activity (Laskari et al. 2016, Van der Kindere et al. 2019) and more specific convection velocities can be designed (de Kat and Ganapathisubramani 2012). In the context of data-driven methods, the use of TH to estimate time-derivatives could help in providing an initial dynamical model, avoiding the use of an advanced PIV setup (Perret et al. 2008).

The objective of this study is to evaluate the validity of using Taylor's hypothesis to estimate the velocity time derivative in urban street-canyon flows. The numerical simulations are obtained by performing a LES of a street canyon flow with OpenFOAM. The *buoyantBoussinesqPimpleFoam* solver is used with 2nd-order schemes for both spatial and temporal discretization. The dynamic k-equation subgrid scale model is used. For the sake of simplicity, the computational domain is composed of a single canyon, and periodic boundary conditions are applied in both the streamwise and spanwise directions. The mean velocity at the inlet is kept constant, and the results (fluctuations, time derivative, and gradient of velocity) are collected after a sufficient period of time during which the turbulent flow develops over the canyon.

First, following common practice, the time-derivative term (denoted ***a***) is estimated using the mean velocity as the convection velocity:

$$\mathbf{a} = \frac{\partial \mathbf{u}'}{\partial t} \quad ; \quad \mathbf{a}_{TH} = -\left(\bar{\mathbf{u}}.\nabla\right)\mathbf{u}' \qquad (3)$$

As shown in Figure 1, good agreement exists between the estimated and true streamwise accelerations. The largest discrepancies are observed in the shear-layer region and within the canyon, where, consistently with previous studies (Laskari et al. 2016, Van der Kindere et al. 2019), the turbulent fluctuations are no longer convected at the mean velocity, thus calling for a better choice of convection velocity. The same conclusions can be drawn for the two other velocity components (not shown here).

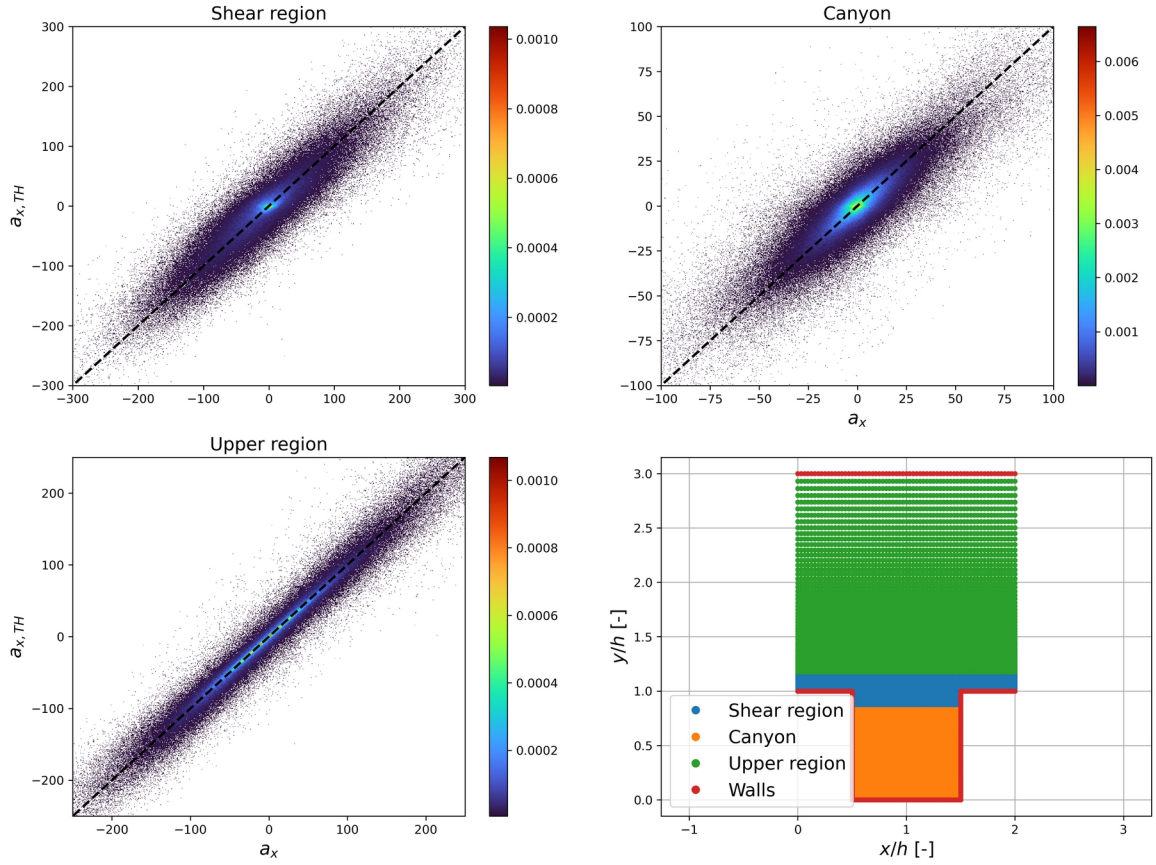

Figure 1: 2D histograms of the estimated streamwise acceleration vs the true acceleration in 3 different regions of the flow using the mean velocity as a convection velocity for TH .

In the final paper, other choices for the convection velocity will be tested, and PIV-introduced bias (such as noise, limited spatial resolution, or incomplete velocity gradient tensor) will be evaluated.

References

Perret, L., Delville, J., Manceau, R., & Bonnet, J. P. (2008). Turbulent inflow conditions for large-eddy simulation based on low-order empirical model. *Physics of Fluids*, *20*(7).

de Kat, R., & Ganapathisubramani, B. (2012). Pressure from particle image velocimetry for convective flows: a Taylor's hypothesis approach. *Measurement Science and Technology*, *24*(2), 024002.

Laskari, A., de Kat, R., & Ganapathisubramani, B. (2016). Full-field pressure from snapshot and time-resolved volumetric PIV. *Experiments in fluids*, *57*, 1-14.

Van der Kindere, J. W., Laskari, A., Ganapathisubramani, B., & De Kat, R. (2019). Pressure from 2D snapshot PIV. *Experiments in fluids*, *60*, 1-18.

PHYSMOD 2024 – International Workshop on Physical Modelling of Flow and Dispersion Phenomena
Ecole Centrale de Lyon, Ecully, France – August 28-30, 2024

Decomposition methods POD and OPD: Can they tell us something about pollutant ventilation capacity?

Z. Babuková[1, 2], Š. Nosek[1], R. Kellnerová[1], M. Jakubcová[1], Z. Jaňour[1]

[1]Institute of Thermomechanics of the CAS, Department of Fluid Dynamics, Dolejškova 1402/5, 182 00 Praha 8, Czech Republic
[2]Charles University, Faculty of Mathematics and Physics, Department of Atmospheric Physics, Ke Karlovu 3, 121 16 Praha 2, Czech Republic

Abstract

The characterization of turbulent flow within the Atmospheric Boundary Layer is still challenging. However, contemporary mathematical methodologies, such as Proper Orthogonal Decomposition (POD; Berkooz et al., 1993) or Oscillating Pattern Decomposition (OPD; Uruba, 2015), are able to reveal so called coherent structures within the complex 3D flow, owning spatio-temporal data, for instance, from the Particle Image Velocimetry (PIV).

Previous studies in the field predominantly focus on analysing the characteristics and identifying coherent structures within fluid flow, as well as evaluating the analytical potential of different methodologies (e.g., Fu et al., 2023; Li et al., 2023). However, a notable gap exists in the literature concerning the exploration of the interplay between coherent structures and pollutant transfer, despite the promising avenues offered by decomposition methods.

In this contribution, we will explore the interplay of these methods with venting capacity across two spatial contexts (street canyons and an underground room) to bolster the reliability of conclusions drawn. We delve into the variability of POD expansion coefficients a_j (see Figure 1), the stability of OPD modes given by their periodicity p, and spatial evolution of the OPD structures, all analysed using 2D data from the PIV measurements. The ventilation capacity will be assessed from the concentrations obtained either from LES simulations (street canyons) or laboratory measurements using the fast flame ionization detector (underground room).

Our findings suggest that these methods to some extent can assess pollutant ventilation capacity. In particular, greater capacity for pollutant ventilation is associated with higher standard deviations of the POD expansion coefficients, the presence of numerous OPD modes, and, for steet canyons, with the penetration of OPD structures into the canyon. However, these methods cannot accurately predict the resulting concentrations due to the significant influence of pollutant source position (Kluková et al., 2021). Moreover, a comprehensive analysis of the entire 3D space is essential to capture all potential mechanisms for pollutant removal from the studied area.

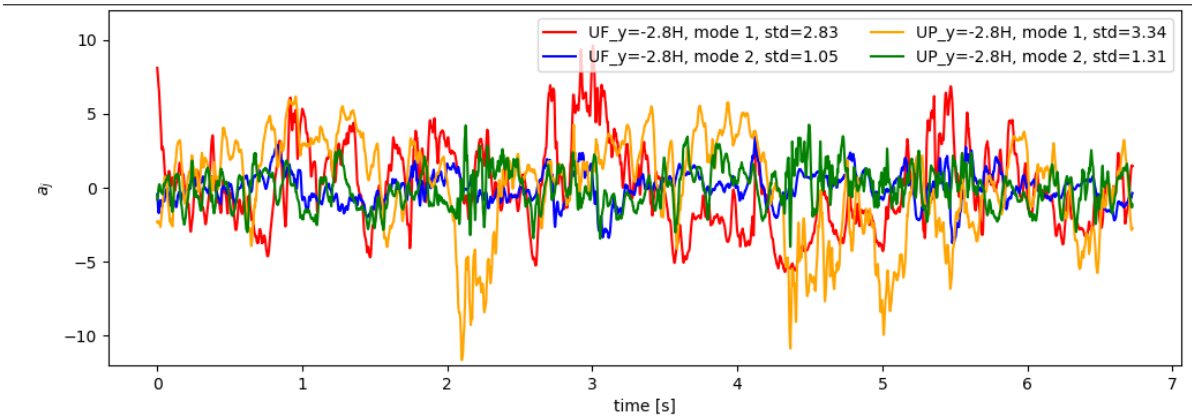

Figure 1: POD expansion coefficients a_j for the uniform street canyon with flat (UF; red and blue lines for the first and second mode, respectively) and pitched (UP; orange and green lines for the first and second mode, respectively) roofs with standard deviations of the expansion coefficients a_j labelled.

References

Berkooz, G., Holmes, P. & Lumley, J. L. (1993). The Proper Orthogonal Decomposition in the Analysis of Turbulent Flows. *Annual Review of Fluid Mechanics*, 25. 539-575

Fu, Y., Lin, X., Li, L., Chu, Q., Liu, H., Zheng, X., Liu, Ch-H., Chen, Z., Lin, Ch., Tse, T. K. T., Li, C. Y. (2023). A POD-DMD augmented procedure to isolating dominant flow field features in a street canyon. *Physics of Fluids*, 35. 025112

Kluková, Z., Nosek, Š., Fuka, V., Jaňour, Z., Chaloupecká, H. & Ďoubalová, J. (2021). The Combining Effect of the Roof Shape, Roof-height Non-uniformity and Source Position on the Pollutant Transport between a Street Canyon and 3D Urban Array. *Journal of Wind Engineering and Industrial Aerodynamics*, 208. 104468

Li, D., Zhao, B., Wang, J. (2023). Data-driven identification of coherent structures in gas–solid system using proper orthogonal decomposition and dynamic mode decomposition. *Physics of Fluids*, 35. 013321

Uruba, V. (2015). Near Wake Dynamics around a Vibrating Airfoil by means of PIV and Oscillation Pattern Decomposition at Reynolds number of 65000. *Journal of Fluids and Structures*, 55. 372-383

PHYSMOD 2024 – International Workshop on Physical Modelling of Flow and Dispersion Phenomena
Ecole Centrale de Lyon, Ecully, France – August 28-30, 2024

Reynolds number independence of approaching flow and pollutant concentration at very low wind speed in wind tunnel experiments

R. Yoshie[1], T. Tachibana[2]

[1]Tokyo Polytechnic University, Department of Engineering, Iiyama Minami 5-45-1, 243-0297 Atsugi, Japan
[2]Wind Engineering Institute Co.,Ltd., Kanda Jinbo-chou 1-14-3, 101-0051 Chiyoda, Tokyo, Japan

Abstract

Atmospheric stability has a large influence on pollutant dispersion in urban areas. We had conducted gas dispersion experiment under various atmospheric stability in thermally stratified wind tunnel, and proposed SER_C* (stability effect ratio of dimensionless pollutant concentration) (Hu and Yoshie, 2020). The SER_C* is the ratio of dimensionless concentration under non-neutral atmospheric stability condition to that under neutral condition. According to the experiment, SER_C* increased as the Bulk Richardson number (*Equation (1)*) increased, and it implied that SER_C* could be expressed by the function of R_b. By multiplying this SER_C* function by the dimensionless concentration obtained from neutral state experiments or CFD, we aim to be able to predict pollutant concentrations in non-neutral atmospheric condition. However, according to our investigation of atmospheric stability in Tokyo using observation data and analysis data by WRF, the range of R_b in actual phenomena was found to be much larger than that in our previous wind tunnel experiments (Yoshie and Tachibana, 2023). Since R_b is inversely proportional to the square of the wind speed, the range of R_b can be greatly expanded by conducting experiments at lower wind speeds. However, if the wind speed is too low, there is a risk that the Reynolds number dependence of approaching flow and pollutant concentration may occur. Therefore, in this study, we first confirmed that under neutral atmospheric condition, even when the reference wind speed was lowered to about 0.5 m/s (Reynolds number about 8000), the Reynolds number dependence on the dimensionless properties of approaching wind and the dimensionless concentration in an urban block model was small.

$$R_b = \frac{g(\theta_H - \theta_f)H}{\theta_a U_H^2} \qquad (1)$$

where g is acceleration of gravity [m s^{-2}], H is reference height [m], θ_H is air temperature at H [K] and θ_f is floor surface temperature [K], θ_a is absolute temperature of air [K], U_H is wind speed at H [m s^{-1}].

Method of Wind Tunnel Experiment

The experiments were conducted in the thermally stratified wind tunnel at Tokyo Polytechnic University. Approaching wind velocity and concentration within a regular arrayed urban block model under neutral atmospheric condition were measured. For the urban block model, 60 mm cubes (14 rows in the flow direction x 9 columns in the width direction of the wind tunnel = 126 pieces) were arranged at equal intervals of 60 mm. Assuming a situation in which gas is being emitted from a group of construction vehicles at a construction site within a urban block, a surface source (30 mm square) for tracer gas emission was placed on the floor of the 8th row. Ethylene (C_2H_4) was used as a tracer gas.

A high-speed flame ionization detector was used to measure the concentration of the tracer gas within the urban block model. The number of concentration measurement points within the urban block was 95. The measurement points were placed to cover the locations of various flow patterns (reverse flow, upward flow, downward flow, and straight flow on the roads in the urban block model). The wind speed of the approaching flow was varied from 0.4 ms^{-1} to 2.0 ms^{-1} to confirm the Reynolds number dependence. The approaching wind velocity was measured by PIV.

Results of Wind Tunnel Experiment

The dimensionless vertical profile of the mean wind velocity, standard deviations of wind velocity fluctuations σ_u (flow direction), σ_w (vertical direction) and Reynolds stress $\overline{u'w'}$ for different wind speed from 0.4 ms^{-1} to 2.0 ms^{-1} were overlapped well (not shown here).

Figure 1 shows the time-averaged value of the dimensionless concentration obtained from Equation (2) for different wind speeds.

$$C^* = CU_H H^2/Q \qquad (2)$$

where C is measured concentration [m^3 m^{-3}], Q is tracer gas emission rate [m^3 s^{-1}], H is reference height [m]. U_H is wind speed at the reference heigt [ms^{-1}]

The reference height H was 0.3 m from the wind tunnel floor. For all wind speed, the dimensionless concentrations were almost overlapped. Therefore, it was confirmed that even if the reference wind speed U_H was lowered to about 0.5 m/s (Reynolds number about 8000), the dependence of the Reynolds number on the dimensionless concentration was small.

Thus, we are currently conducting wind tunnel experiments for gas dispersion with varying atmospheric stability at lower wind speeds (at wider R_b range).

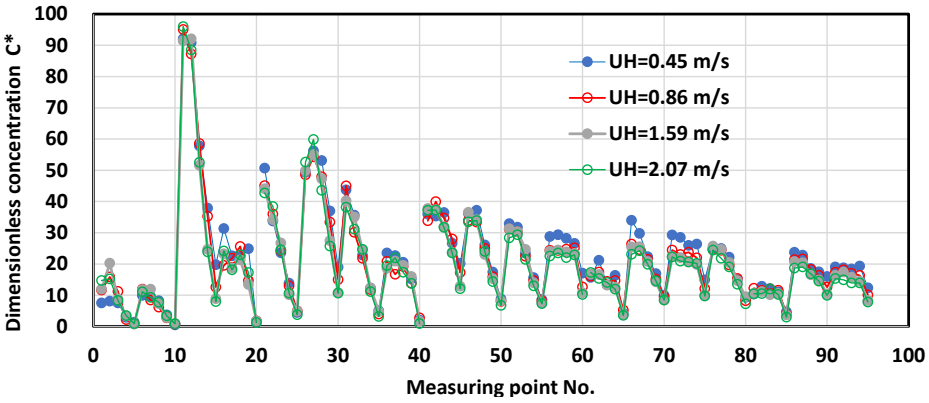

Figure 1: Dimensionless concentration at every measuring points: Reynolds number independence of dimensionless concentration

Acknowledgement

This work was supported by JSPS KAKENHI Grant Number 21H01498.

References

Hu, T., Yoshie, R. (2020). Effect of atmospheric stability on air pollutant concentration and its generalization for real and idealized urban block models based on field observation data and wind tunnel experiments. *Journal of Wind Engineering & Industrial Aerodynamics*, Vol, 207.

Yoshie, R., Tachibana T., Xuan, Y. (2023) Investigation of atmospheric stability in Tokyo using observation data and analysis data by WRF. *The 16th International Conference on Wind Engineering*.

PHYSMOD 2024 – International Workshop on Physical Modelling of Flow and Dispersion Phenomena
Ecole Centrale de Lyon, Ecully, France – August 28-30, 2024

Scale interaction between the urban boundary layer and a street canyon in a morphological model

H. Du[1], L. Perret[2], E. Savory[1]

[1]University of Western Ontario, Department of Mechanical and Materials Engineering, 1151 Richmond Street, N6A 3K7 London, Canada
[2] Nantes Université, École Centrale Nantes, CNRS, LHEEA, UMR 6598, F-44 000 Nantes, France

Abstract

The nature of the modulation mechanism between the most energetic scales of the boundary layer and that of the canopy region remains an open question for morphological urban roughness, especially when tall buildings protrude from the canopy. The presence of large-scale coherent structures in the wake of a local tall building could strongly modify the downstream boundary layer, and, therefore, potentially modify the scale interaction mechanism. In the present study, the main question to be addressed is: how do morphology and a single upstream tall building impact the scale interaction in the overlying boundary layer and the street canyon?

Tests were conducted in the Atmospheric Boundary Layer Wind Tunnel in the LHEEA at Ecole Centrale de Nantes (see Du et al., 2023 for experimental details), as shown in Figure 1(a-c). Experiments with the cathedral in a 1:200 morphological model of the Rue de Strasbourg area of Nantes were first performed. The cathedral was then replaced by square-based rectangular prisms, which were constructed with a cross-sectional area of 200 mm (W_b)×200 mm and a varying height (H_b) of 100, 200, 300, or 600 mm (AR_b = 0.5,1,1.5,3 respectively), labelled as B1h, B2h, B3h, B6h. All the experiments were conducted with the same oncoming boundary layer, developed over a fetch of cubic roughness with height h_1 = 50mm. The oncoming boundary layer statistics are given in Table 1. The street canyon ridge height was h_2 = 116mm and stereoscopic PIV measurements were conducted at the street canyon centre plane.

U_e (m s^{-1})	u^*/U_e	h_1 (m)	δ (m)	Re_{h1} (u*)	$Re_δ$ (u*)	d/h_1	z_0/h_1	$∂P/∂x$ (Pa m^{-1})
5.8	0.07	0.05	0.0975	1200	24000	0.64	0.08	-0.37

Table 1. Oncoming boundary layer characteristics

Multi-time delay Linear Stochastic Estimation (LSE), as introduced by Durgesh & Naughton (2010), is implemented in the POD-LSE method by Podvin et al. (2018). After careful consideration of the auto-correlation of the HWA measured velocities, for a single physical HWA signal in all the measured configurations, 20 time-delayed HWA signals were generated corresponding to linear time-delay increments of 0.05 s from -0.5 s to 0.5 s, where the signal with zero-time delay represents the physical signal. These time-delayed HWA signals (100 in total) could be regarded as imaginary HWA probes, either upstream or downstream of the actual array of the HWA probes. The POD-LSE method directly maps the POD amplitudes from the measurements to the desired field estimation, all in a single-step procedure. The mapping matrix is filtered at 5Hz. This method assists in separating the large and small scales and extends the large scales to a higher frequency.

A spatially-averaged two-point spatial-temporal correlation using Equation 1, where $x_L = x_S = 0$ and $z_S = 0.75h_2$, can bring insight into the temporal evolution of the interaction between the large-scale motions and the small-scale fluctuations at a fixed point in the street canyon, as shown in Figure 1(d-h).

$$R_{u_L u_S^2}(x_S, z_S, x_L, z_L, \tau) = \frac{\overline{u_L'(x_L, z_L, t+\tau) u_S'^2(x_S, z_S, t)}}{\sqrt{\overline{u_L'^2(x_L, z_L)}}\sqrt{\overline{u_S'^4(x_S, z_S)}}} \quad (1)$$

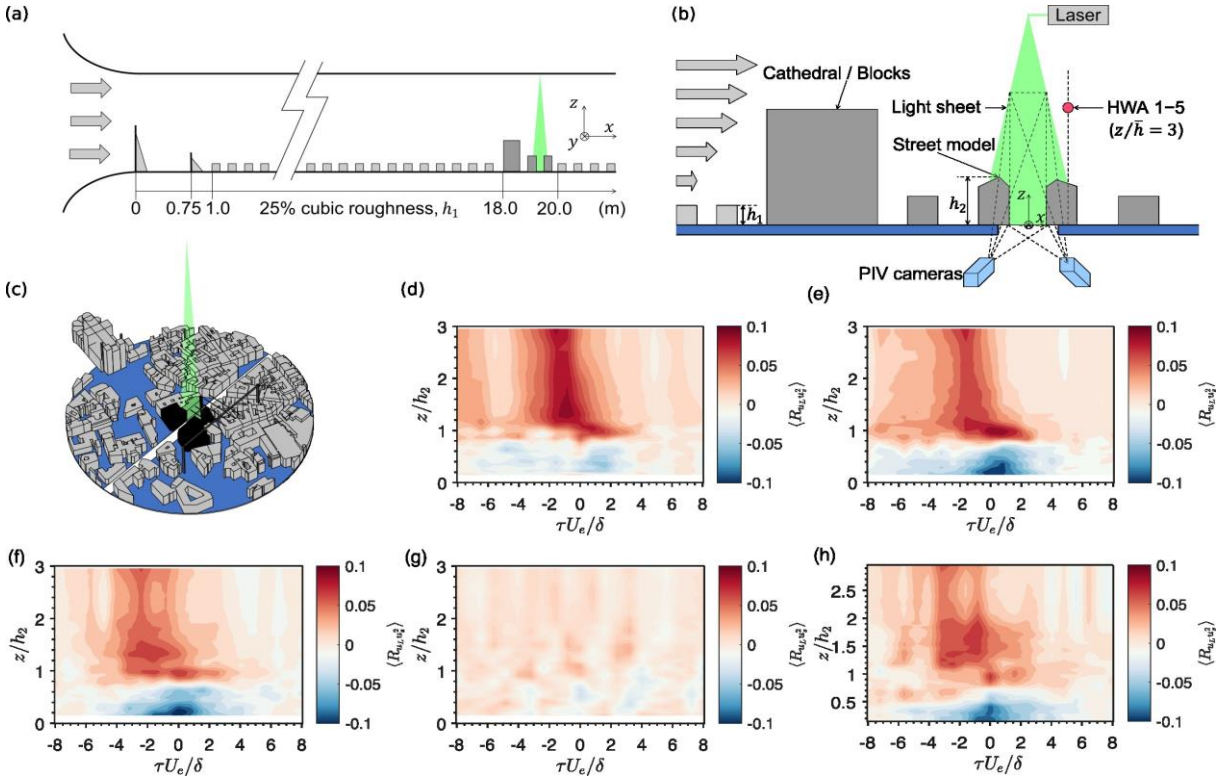

Figure 1: a) Wind tunnel set-up; b) stereoscopic PIV and HWA set-up for XZ plane; c) simplified RdS 3D model with laser sheet in XZ plane; Spatially-averaged cross-correlation coefficient $\langle R_{u_L u_S^2} \rangle$ where $x_L = x_S$ and $z_S = 0.75h_2$ for the d) B1h; e) B2h; f) B3h; g) B6h and h) Cath configurations.

It can be concluded that when there is no upstream tall building present or the upstream building height is not tall enough, the large-scale high or low momentum regions within the boundary layer have the potential to amplify or suppress small-scale fluctuations at the roof-top, respectively. Meanwhile, the boundary layer downstream of a tall building can exhibit large-scale eddies, which can amplify or suppress small-scale fluctuations at the roof-top level.

References

Du H, Savory E, Perret L (2023) Effect of morphology and an upstream tall building on the mean turbulence statistics of a street canyon flow. *Build Environ* 241(110):428

Durgesh V, Naughton J (2010) Multi-time-delay LSE-POD complementary approach applied to unsteady high-Reynolds-number near wake flow. *Exp Fluids* 49:571–583

Podvin B, Nguimatsia S, Foucaut JM, Cuvier C, Fraigneau Y (2018) On combining linear stochastic estimation and proper orthogonal decomposition for flow reconstruction. *Exp Fluids* 59:1–12

PHYSMOD 2024 – International Workshop on Physical Modelling of Flow and Dispersion Phenomena
Ecole Centrale de Lyon, Ecully, France – August 28-30, 2024

The Effects of Wind Direction on Pollutant Dispersion in Tall Building Clusters

D.Bi[1], A. Mishra[1], M. Carpentieri[1], M.Placidi[1], A.Robins[1]

[1]Environmental Flow Research Centre (EnFlo), School of Mechanical Engineering Sciences, University of Surrey, Guildford, Surrey, GU2 7XH, UK

Abstract

Tall building clusters, which are common in mega-cities such as London and New York, efficiently address the demands of rapid global urbanization; however, the presence of tall buildings can also have negative effects on air quality levels on-site due to pollutants released from different sources (such as vehicle emissions, emissions from heating systems, accidental fires, etc) and modifications of the wind flow field. Understanding how pollutant concentrations develop in urban environments offers insights into mitigation strategies and reducing health risks associated with poor air quality. Wind direction significantly impacts the dispersion of scalar contaminants and their downward transport into the wakes of tall building clusters. This experimental study, conducted in the meteorological wind tunnel at the EnFlo Laboratory of the University of Surrey, investigates how various wind directions influence dispersion characteristics, focusing on pollution plume development and its interaction with turbulent wakes. Velocity and concentration measurements were conducted using three-component Laser Doppler Anemometry (LDA) and Fast-response Flame Ionization Detectors (FFID), respectively. The building models, clusters of wooden cylinders with a square cross-section measuring 60 mm in width and 240 mm in height arranged in regular arrays, were oriented at angles of 0°, 22.5°, and 45° to the bulk flow. Notably, the lateral profiles in the near-wake region of symmetrical cluster layouts at 0° and 45° displayed a bimodal distribution, which diminished in the asymmetrical cluster at 22.5°, where the concentration peaks deviated from the centerline location. For the wind incidence angle of 45°, slight variations in lateral concentration profiles were observed at the middle height of the buildings except for the near-wake region, which can also be corroborated in the vertical profiles showing minimal change for the plume height. Furthermore, as the wind incidence angle increased, the plume boundary width widened. Passive scalar transport was also examined. Compared to the 0° cluster, where a distinct channelling effect in the spacing between the buildings is evident, the turbulent flux in the horizontal plane of the 22.5° and 45° clusters showed minimal variation across the width of the cluster's windward side in different streamwise positions. Meanwhile, in the vertical plane, turbulent flux peaks occurred near the cluster canopy, indicating a stronger uplift of the plume when the wind direction was not perpendicular to the cluster.

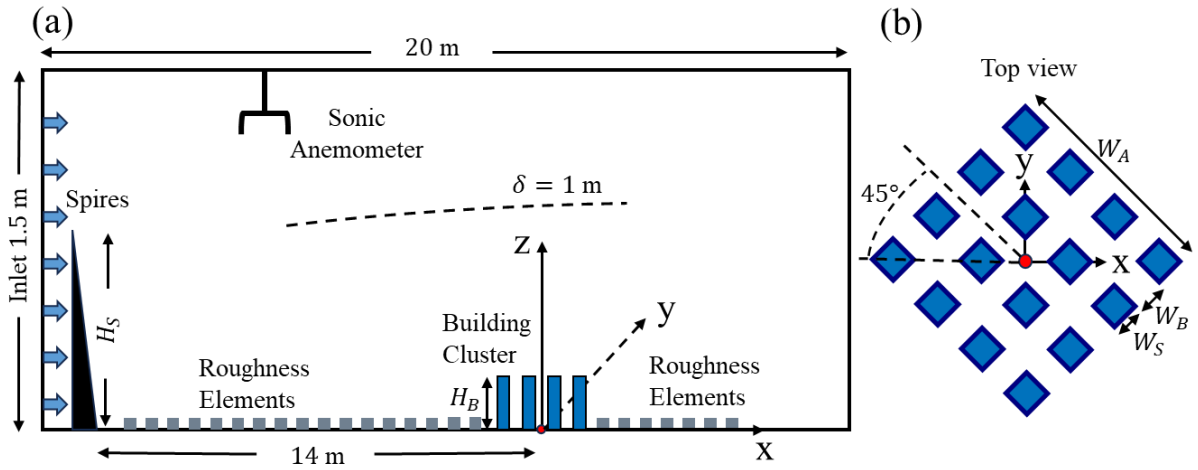

Figure 1: Schematic of the experiment setup: (a) wind tunnel layout; (b) top view of the building models with an orientation angle of 45°.

PHYSMOD 2024 – International Workshop on Physical Modelling of Flow and Dispersion Phenomena
Ecole Centrale de Lyon, Ecully, France – August 28-30, 2024

VALIDATION OF WIND TUNNEL MEASUREMENTS WITH AIR QUALITY MEASUREMENTS ON A SHIP

S.P.M. van den Akker[1]
[1]Peutz BV, Department of Environmental Engineering, Lindenlaan 41, 6584 AC Molenhoek, the Netherlands

Abstract

Wind tunnel dispersion measurements

A wind tunnel study of the dispersion of diesel engine exhaust gas on a scale model of an offshore support vessel was conducted in 2014. The aim of the investigation was to optimize the funnel design. For the study a maritime medium roughness lead-in area was used. The atmospheric boundary layer profile in the wind tunnel fulfils the reference specification of NEN-EN-ISO 19901-1, for U_{10} = 7.7 ms^{-1} (15 kt).

The emission speed of the exhaust gas increases with the engine power output. For the chosen funnel design for this vessel the emission speed is V_s = 23 ms^{-1} at 100% power output. The relative wind speed varied between U = 0 ms^{-1} to U = 20 ms^{-1}. An important similarity parameter for the dispersion of engine exhaust gas is the dimensionless relative emission speed W(t), defined as:

$$W(t) = \frac{V_s(t)}{U(t)} \qquad (1)$$

It was observed that measured concentrations decrease with increased W. For W < 0.5 the measured concentrations are nearly constant. For W > 1.8 all concentrations approach 0. Dispersion measurements where therefore conducted in the wind tunnel for W = 0.4, W = 0.9 and W = 1.8. Plume buoyancy was not included in the wind tunnel modelling as kinetic plume rise was assumed to be dominant for the short dispersion distances involved in this study.

On-board measurements

During a test run in 2015 the air quality was measured on board of the finished vessel in the crew accommodations. The levels of nitrogen oxides (NO_X) and carbon dioxide (CO_2) were recorded using passive electrochemical sensors with a sampling interval of 15 seconds. Additionally, questionnaires were distributed to the crew to record any odour nuisance complaints during the test run.

The ships computer logs provided detailed time series of the engine power output as well as wind data measured by 4 different on-board sonic anemometers. The engine manufacturer provided exhaust gas flow (Φ_v, in m^3s^{-1}), CO_2 and NO_X emission data as a function of the engine power output.

Carbon dioxide is commonly used as a marker for indoor air quality. Finding correlations between CO_2 levels and diesel engine odour complaints is a matter of ongoing research. However, due to the abundance of secondary sources of indoor CO_2 on the ship, the influence of the engine exhausts was indistinguishable in the measurement data. It was decided to validate the wind tunnel model using

the NO_x measurements and then use the validated model to distinguish between the influence of the engine exhausts and the influence of secondary sources of CO_2.

Initial validation failure

In situ meteorological measurements and emission data were combined with the concentration coefficients measured in the wind tunnel to produce time series of CO_2 and NO_x concentrations from the engine exhausts. However, this initial attempt to reproduce the on-board NO_x measurements was unsuccessful. The correlation between the engine CO_2 levels and engine odour complaints was poor.

A close examination of ships logs revealed that the meteorological measurement results diverged significantly between the 4 on-board anemometers. This divergence can be caused by the influence of the ships superstructure on the air flow near the anemometers. Similar problems occur in urban situations (see Schliffke et al., 2017). It was proposed that this divergence in the measured meteorological data could be a dominant source of the inaccuracy.

Additional wind tunnel study to improve wind data

An additional wind tunnel study was conducted on the scale model of the vessel. In the locations of the sonic anemometers the local deviations from the undisturbed wind speed and wind direction were measured. These wind tunnel measurements were used to correct the meteorological data from the ships logs to obtain an improved estimate of the "true" (undisturbed) wind speed and wind direction.

Using this improved estimate of the wind speed and wind direction the on-board measurements could be reproduced satisfactorily (see figure 1), and the correlation between engine CO_2 and engine odour complaints was strong.

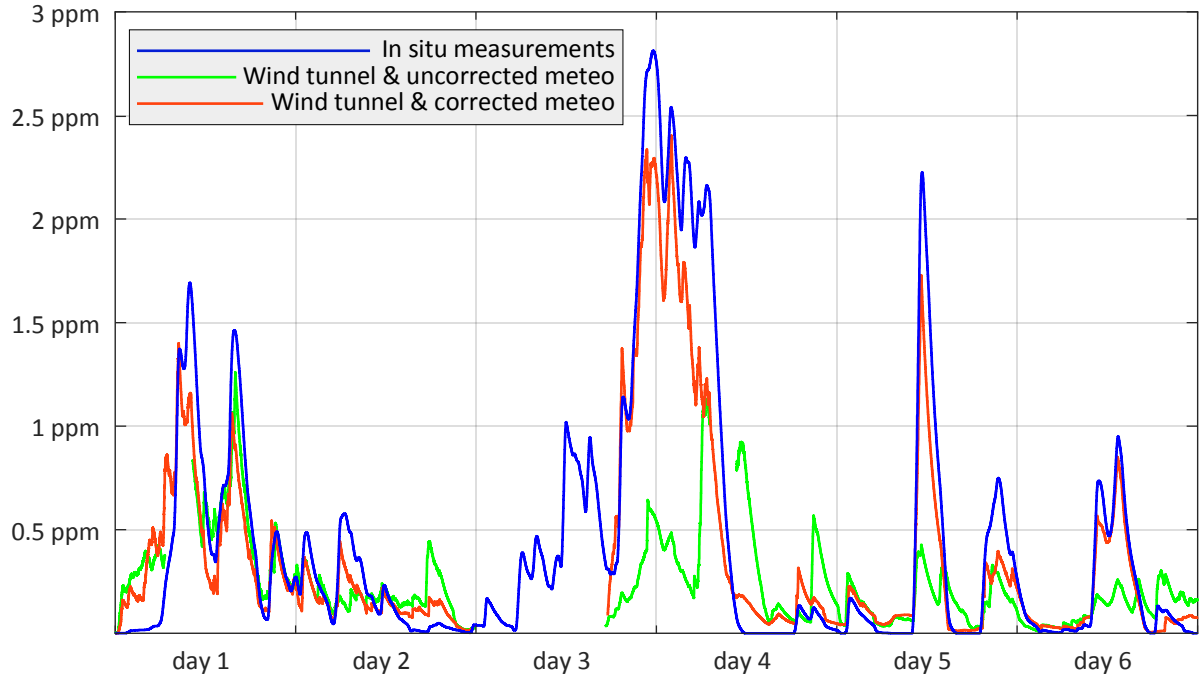

Figure 1: In situ NOx concentrations and wind tunnel results

References

Schliffke, B., Schäfer, K., Harms, F. & Leitl, B. (2017). How representative are urban wind measurements? *Physmod 2017.*

PHYSMOD 2024 – International Workshop on Physical Modelling of Flow and Dispersion Phenomena
Ecole Centrale de Lyon, Ecully, France – August 28-30, 2024

Wind Tunnel Modeling in Support of the Evaluation of an Urban Radiation Protection Model

B. Leitl[1], F. Harms[1]

[1]University of Hamburg, Faculty of Mathematics, Informatics and Natural Science, Earth System Sciences Department, Bundesstrasse 55, 20246 Hamburg, Germany

Abstract

Implementing the European Council Directive 2013/59/Euroatom in Germany resulted in a new radiation protection law, now requesting a "realistic calculation of the exposure of a single person in the population due to releases from nuclear facilities". Releases from larger sources as for example from the dismantling of nuclear powerplants are treated with established atmospheric transport models already validated for longer transport distances. However, since a number of rather small emission sources is operated also in urban environments, the German Federal Radiation Protection Agency (BfS) decided to modify its standard Lagrangian dispersion model for use with wind fields generated by an obstacle resolving microscale flow model (MISKAM). The new combination of models now needs to be verified and validated before routine use.

Within a consortium of experienced microscale atmospheric dispersion modelers, the EWTL at the University of Hamburg is tasked to provide dedicated qualified reference data in order to estimate possible uncertainties in radiation exposure calculations for time periods of up to one year. Jointly it was decided to generate new data for comparison because none of the existing data sets is providing the desired systematic variation in the parameters driving urban dispersion with sufficient detail. Furthermore, the updated VDI 3783/12 guideline for wind tunnel modelling of atmospheric flow and dispersion should now be considered in Germany, which makes the generation of new validation data sets even more challenging.

The new set of reference data for urban-type dispersion from local sources was designed with reference to a typical German city district layout. A first set of dispersion experiments is carried out in a simplified, yet complex urban structure with buildings being replicated at Level of Detail 1 (LOD1). Systematic variations in this configuration consider building density, roof shape, release location/height, approach flow conditions, building heights or urban greenery for example. A second model configuration, using the same building layout but with a realistic heterogeneity of roof shapes (LOD2) will be used as basis for generating a 'synthesized annual dispersion/exposure data set' based on wind tunnel dispersion measurements for at least 18 wind directions and a realistic dispersion category statistic as used for air quality modelling regularly.

As for all wind tunnel test series, in the planning of systematic experiments for the provision of reference data for numerical modelling, a number of decisions must be taken or trade-offs must be made when deciding on the number of individual measurements. In the presentation the often

critical way to a proper wind tunnel setup and qualified experiments will be described by following the revised VDI 3783/12 guideline as close as possible within the scope of a time-limited project.

Experimental work started in February 2024 with the development and documentation of qualified model boundary layer flows at a geometric scale of 1:400. First systematic data sets compiled with a simplified LOD1 geometry include a building density variation is investigated. Figure 1 exemplarily shows a plan view of the model configuration for the densest and the coarsest building arrangement measured in the wind tunnel. Results of the generic experiments will be presented and discussed with respect to the more challenging requirements for the generation of reference data sets according to VDI 3783/12. Furthermore, the contribution intends to trigger a lifely discussion on wind tunnel data quality requirements, ensuring confidence in laboratory experiments as reference for modern atmospheric flow and dispersion modelling also in the future.

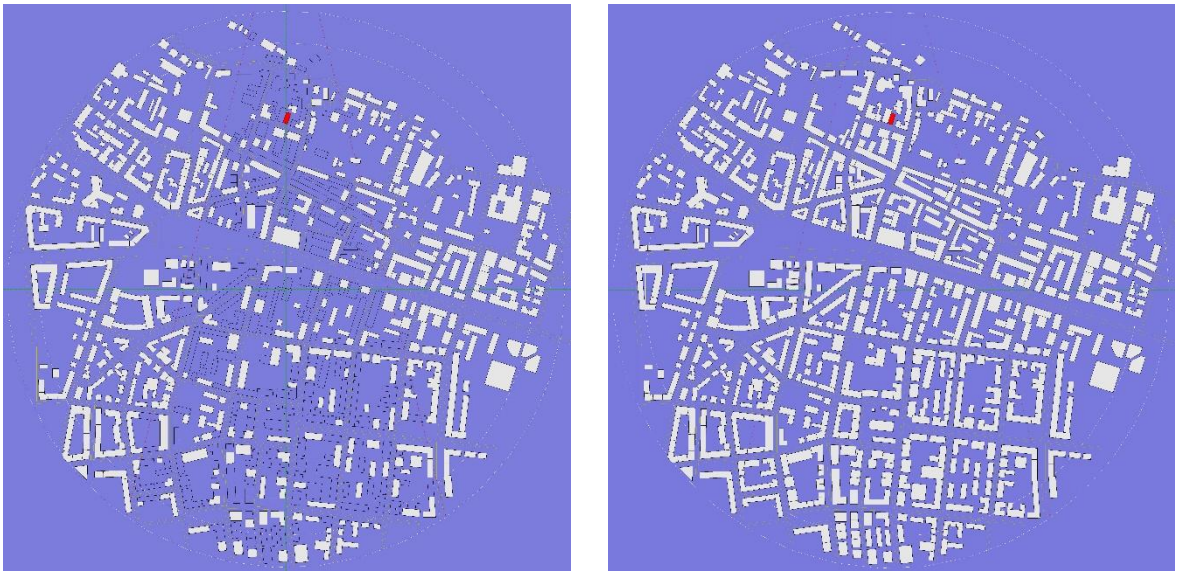

Figure 1: Exemplary LOD1 model layout for testing dependence of roof level emission dispersion from the red building on downwind building density (left: coarse, right: high).

References

Council Directive 2013/59/Euroatom laying down basic safety standards for protection against the dangers arising from exposure to ionising radiation, and repealing Directives 89/618/Euratom, 90/641/Euratom, 96/29/Euratom, 97/43/Euratom and 2003/122/Euratom (2013) Official Journal L13/1 (17.01.2014)

VDI 3783/12: Physical modelling of flow and dispersion processes in the atmospheric boundary layer - Application of wind tunnels. VDI/DIN Handook Clean Air, Vol. 1b: Environmental Meteorology, VDI/Beuth (2024

PHYSMOD 2024 – International Workshop on Physical Modelling of Flow and Dispersion Phenomena
Ecole Centrale de Lyon, Ecully, France – August 28-30, 2024

Turbulence characteristics within an idealized urban canopy layer

Fei Li[1], Naoki Ikegaya[2], Chun-Ho Liu[1,*]

[1]Department of Mechanical Engineering, The University of Hong Kong, Hong Kong, China
[2]Faculty of Engineering Sciences, Kyushu University, Japan

Abstract

Turbulent flow in urban areas is essential for comfortable pedestrian space. To understand the characteristics of its characteristics within an idealized urban canopy layer (UCL) and to scrutinize the relationship between the large- and small-scale turbulence, particle image velocimetry (PIV) was employed to measure the velocities within the idealized UCL consisting of staggered cubes of 25% packing density. The amplitude modulation (AM) is adopted to explore the scale interaction at the pedestrian level. The empirical mode decomposition (EMD) is used to investigate the turbulent scale characteristics in the UCL. The negative AM coefficient is likely correlated with positive skewness. On the other hand, the positive AM coefficient almost appears in the regions where skewness is negative and vice versa. Hence, the supressing effect between the large- and small-scale turbulence would result in a positive extreme wind fluctuation. In contrast, acceleration would cause a negative, extreme wind fluctuation. The joint probability function (JPDF) of the frequency and amplitude of fluctuating winds is calculated to illustrate the probability of occurrence for different turbulent fluctuation amplitude at various scales. The ridge line of the JPDF increases first then decreases with increasing frequency. The most frequent event occurs at around 10-Hz frequency. These results reveal the most frequent turbulent scales within UCLs whose scale interaction would influence the turbulence structures so do the comfort of pedestrian-level urban environment.

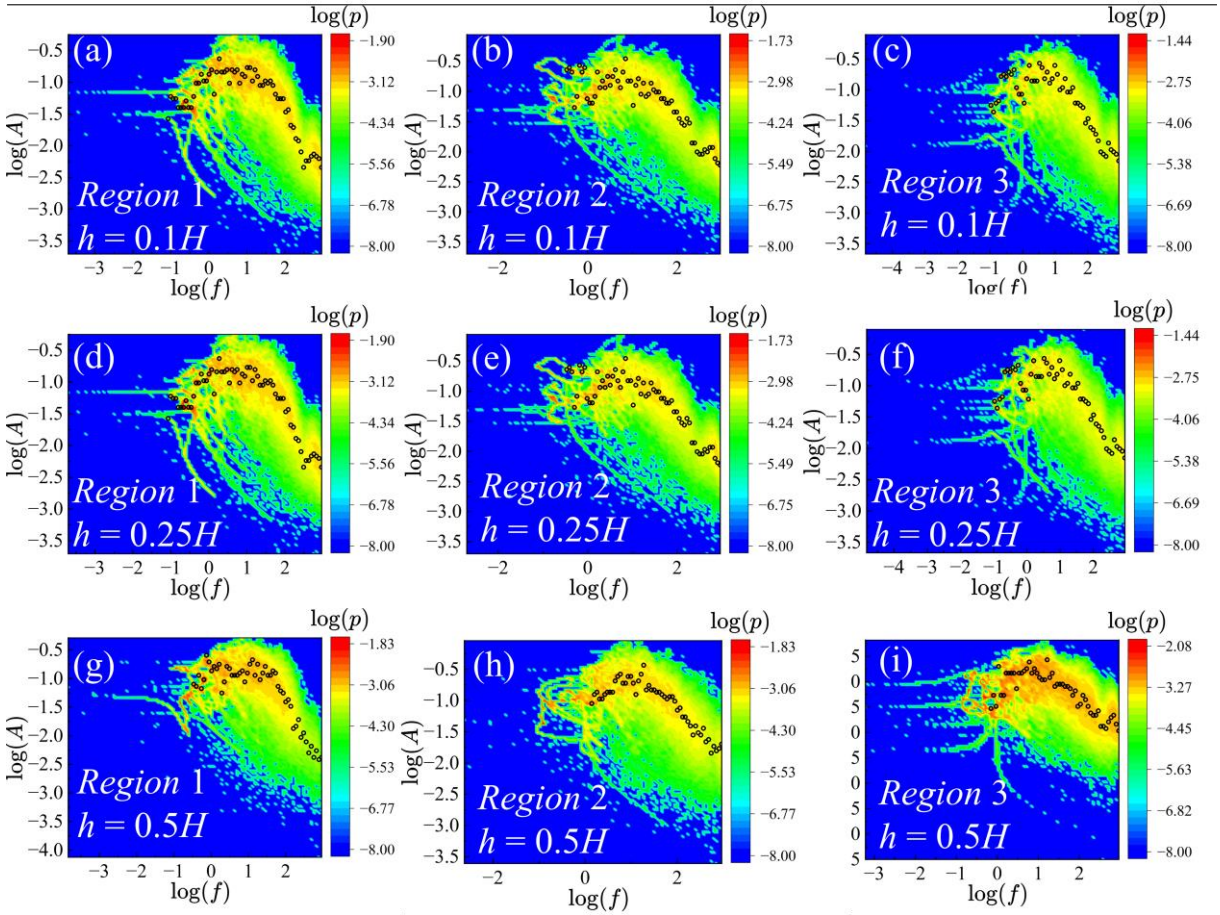

Figure 1: JPDF in terms of amplitude and frequency at the center of Region 1 (a)(d)(g), Region 2 (b)(e)(h), and Region 3 (c)(f)(i) at h = 0.1H (a)-(c), h = 0.25H (d)-(f), and h = 0.5H (g)-(i), respectively. The black dot is the ridge value of the contour.

30 Aug 2024

Validation and intercomparison of numerical, analytical and physical models

PHYSMOD 2024 – International Workshop on Physical Modelling of Flow and Dispersion Phenomena
Ecole Centrale de Lyon, Ecully, France – August 28-30, 2024

Validation of LES with Coarser and Finer Resolutions against the Wind Tunnel Study

R. Kellnerová[1], K. Jurčáková[1], V. Fuka[2], Š. Nosek[1]

[1]Institute of Thermomechanics of the CAS, Department of Fluid Dynamics, Prague, 182 00, Czech Republic
[2]Faculty of Mathematics and Physics, Department of Atmospheric Physics, CU, Prague, 180 00, Czech Republic

Abstract

The advanced statistical techniques for qualitative and quantitative validations of Large Eddy Simulations (LES) of turbulent flow within and above a two-dimensional street canyon are presented. Time-resolved data from 3D LES with a coarser and a finer resolution are compared with those obtained from time-resolved 2D Particle Image Velocimetry (TR PIV) measurements. We have extended a standard validation approach based solely on time-mean statistics by a novel approach based on analyses of the intermittent flow dynamics.

While the standard Hit rate validation metric indicates not so good agreement between compared values of both the stream-wise and vertical velocity within the canyon canopy for the coarser LES resolution due to mild differences in small structures, the Fourier, quadrant and Proper orthogonal decomposition (POD) analyses demonstrate very good prediction of larger characteristic structures in the flow (see the result for smaller and larger patterns in Fig. 1).

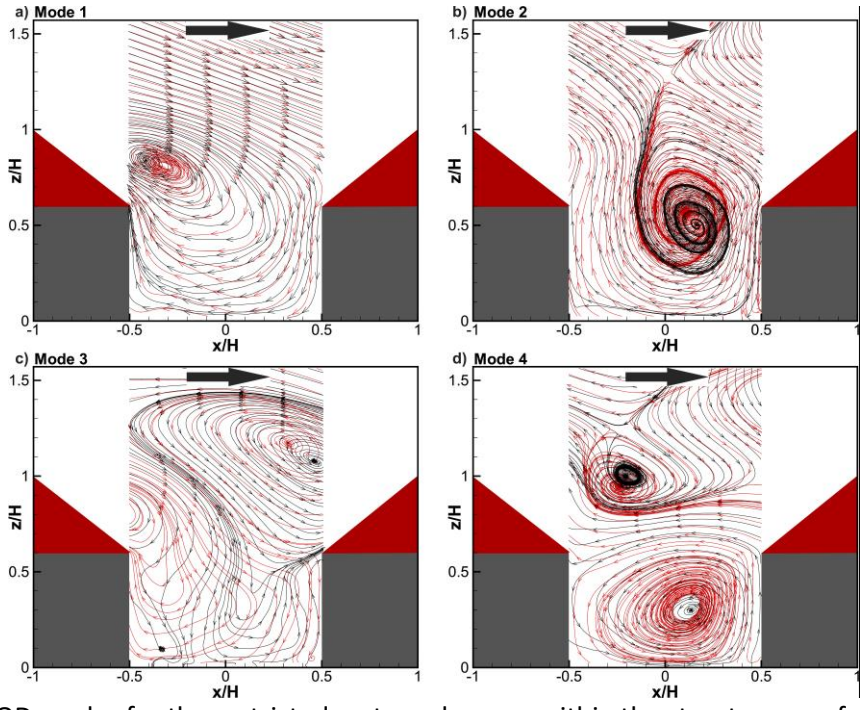

Fig. 1: The POD modes for the restricted rectangular area within the street canyon for PIV and LES (coarser). (**a**–**d**) correspond to Mode 1–4. The black streamlines denote PIV, the red streamlines denote LES (coarser). The LES modes are interpolated on the PIV grid.

Using the quadrant analysis, we demonstrated similarity between the model with the coarser resolution and the experiment with respect to the typical shape of large intensive sweep and ejection events and their frequency of appearance.

The finer LES resolutions data matched with the experimental even better, for both the smaller and larger turbulent scales. These findings indicate that although the mean values predicted by the LES do not meet the criteria of all the standard validation metrics, the dominant coherent structures are simulated well.

Acknowledgements: The financial support for the project was provided by GA-22-14608S.

PHYSMOD 2024 – International Workshop on Physical Modelling of Flow and Dispersion Phenomena
Ecole Centrale de Lyon, Ecully, France – August 28-30, 2024

Assessing the capability of Large-Eddy Simulation in reproducing stable atmospheric boundary layers

M. Barulli[1], M. Cassiani[2], A. Emmanuelli[1], M. Marro[1], P. Salizzoni[1]

[1]Ecole Centrale de Lyon, CNRS, Universite Claude Bernard Lyon 1, INSA Lyon, LMFA, UMR5509, 69130, Ecully, France
[2]NILU-Norwegian Institute for Air Research, 2007, Kjeller, Norway

Abstract

While strict neutral stability conditions are quite rare in atmosphere, stable boundary layers are typically common at night, when a thermal gradient between a cooling surface and a warmer adjacent air layer develops. Understanding stable stratified atmospheric boundary layers is crucial for several reasons including climate modeling, weather prediction and pollutant dispersion.

The interplay between the mechanical generation of turbulence and its damping due to buoyancy effect represents a challenge when trying to understand the dynamics of the stable boundary layer (SBL). The balance of these two aspects results in SBLs exhibiting a wide spectrum from well-mixed to non-turbulent flows. Despite numerous investigations of turbulence structure and transport processes, a complete understanding has not been achieved due to measurement complexities and the intricate nature of factors such as unsteadiness, non-uniformity, and sensitivity to terrain features. Consequently, a unified conceptual framework or theory for SBLs is lacking.

In this work Large Eddy Simulation (LES) using the PALM model system (Maronga et al., 2020) are performed to investigate neutral and stable boundary layers dynamics. The simulations are rigorously validated against wind tunnel experiments (Salizzoni et al., 2021). Both periodic and non-periodic boundary conditions along the streamwise direction are considered, with the latter precisely replicating the wind tunnel setup. The buoyancy effect on the turbulent boundary layer developed over a rough surface is investigated for different stability conditions. Stably stratified flows are created by cooling the bottom boundary using a Dirichlet boundary condition. Different bulk Richardson numbers are simulated ranging from neutral boundary layer to weak and moderate stable boundary layers. A good agreement between simulation and experimental data is observed for both periodic and non-periodic boundary conditions, affirming the fidelity of the computational approach. *Figure 1* shows vertical profiles of second order statistics. These results show that the fluctuation variances decrease with increasing bulk Richardson number, as expected from a SBL which tends to suppress turbulent fluctuations.

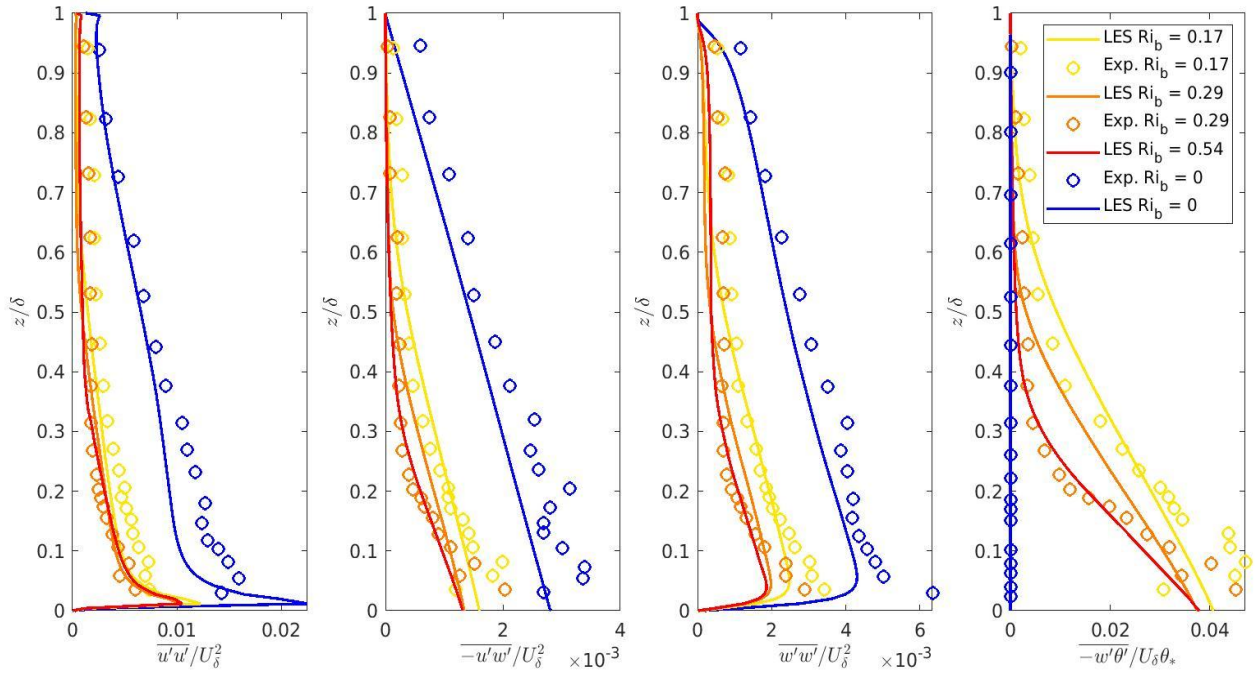

Figure 1: Vertical profiles of Reynolds stresses and kinematic heat flux obtained from LES simulations with periodic boundary conditions (lines) and wind-tunnel measurements (Salizzoni et al., 2021) (dots).

Moreover, even though the two boundary condition types do not seem to significantly affect first and second order statistics, the Eulerian integral length scales show a significant difference depending on the boundary condition used. This may be due to the fact that in the non-periodic case the length of the domain is of fundamental importance in the development of turbulent scales. For this reason periodic boundary conditions may offer a valid alternative by removing the constraint of overly long domains.

The results demonstrate that LES are capable of faithfully reproducing the dynamics of neutral and stably stratified boundary layers. Hence, the next stage involves releasing a passive scalar from a point source to investigate the effects of stratification on the dispersion and meandering of a plume.

References

B. Maronga et al. (2020). Overview of the PALM model system 6.0. Geoscientific Model Development, vol. 13, pp. 1335–1372, 2020.

P. Salizzoni et al. (2021). Passive scalar dispersion in slightly stable boundary layers. AGU Fall Meeting Abstracts, vol. 2021, pp. NG35B-0447.

PHYSMOD 2024 – International Workshop on Physical Modelling of Flow and Dispersion Phenomena
Ecole Centrale de Lyon, Ecully, France – August 28-30, 2024

Integrating wind tunnel, numerical model and measurement data for ship plume assignment

R. Badeke[1], V. Matthias[1], A. Sankaran[2], C. Kähler[2], J. Schade[3,4], S. Jeong[4], and T. Adam[4]

[1]Institute of Coastal Environmental Chemistry, Helmholtz-Zentrum hereon GmbH, 21502 Geesthacht, Germany
[2]Department of Aerospace Engineering, Institute of Fluid Mechanics and Aerodynamics, University of the Bundeswehr Munich, 85577 Neubiberg, Germany
[3]Joint Mass Spectrometry Center (JMSC), Chair of Analytical Chemistry, Faculty of Mathematics and Natural Sciences, University of Rostock, 18059 Rostock, Germany
[4]Faculty of Mechanical Engineering, Institute of Chemistry and Environmental Engineering, University of the Bundeswehr Munich, 85577 Neubiberg, Germany

Abstract

This study focuses on a combined approach of wind tunnel measurements, numerical modeling and real-world observations of ship exhaust plumes for source assignment (Fig. 1). Using a 1:500 scale replica of a generic cruise ship in the atmospheric wind tunnel at the University of the Bundeswehr Munich, various wind and exhaust velocities were considered, with particular attention to vertical wind velocity profiles and concentration distributions. Wind tunnel data were derived by Sankaran et al (2024). A comparison between wind tunnel data and microscale model simulations with MITRAS (Badeke et al., 2021, 2022) was conducted. Wind tunnel data aided in assessing the range of plume dispersion patterns, providing insights into the accuracy of the model results and for validation purposes. Urban-scale numerical modeling using the urban-scale EPISODE-CityChem model (Karl et al., 2019) that incorporated near-field plume profiles from the wind tunnel and MITRAS was performed for real-world comparisons. Particle measurements conducted at three locations along the German coast of the Baltic Sea (Lübeck Bay, Darßer Ort and Rostock Hohe Düne) complemented this study (Rosewig et al., 2023). Ship plumes were measured at varying distances, from few hundred meters to several kilometers. Utilizing instruments such as Single-Particle Mass Spectrometer and a Scanning Mobility Particle Sizer, a variety of plume events were classified as ship plumes and assigned by comparing measurements with Automatic Identification System (AIS) data on ship traffic. The Moving Point Source Algorithm (Pan et al., 2021) was used to represent the dispersion of a moving ship plume in EPISODE-CityChem. The 3D wind field was preprocessed with MCWIND (Hamer et al., 2020) based on wind data from local weather stations at 10 min resolution. The model chain successfully replicated measured plume events at a the same high temporal resolution of 10 min. An interpolation procedure was applied to derive modeled plume arrival times at a minute level. Model predictions showed events appearing 5 to 10 minutes earlier on average compared to measurements. Possible reasons for this include model and wind tunnel differences due to stability and scaling, measurement time delay and small-scale variations in the modeled wind field. The results of this study support air quality compliance monitoring for individual ships, especially within emission control areas like the Baltic Sea.

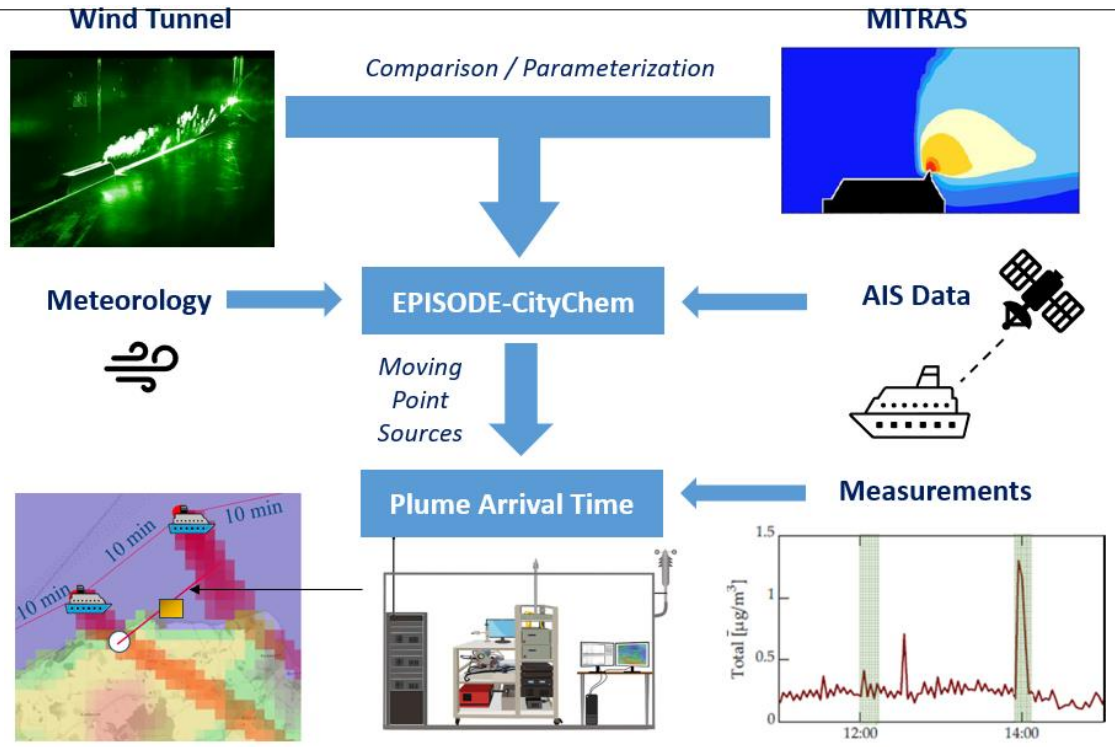

Figure 1: Integration scheme for ship plume assignment.

Acknowledgement

This research is funded by dtec.bw – Digitalization and Technology Research Center of the Bundeswehr (project LUKAS). dtec.bw is funded by the European Union – NextGenerationEU.

References

Badeke, R., Matthias, V., & Grawe, D. (2021). Parameterizing the vertical downward dispersion of ship exhaust gas in the near field. *Atmos. Chem. Phys.,* 21, 5935–5951.

Badeke, R., Matthias, V., Karl, M., & Grawe, D. (2022). Effects of vertical ship exhaust plume distributions on urban pollutant concentration – a sensitivity study with MITRAS v2.0 and EPISODE-CityChem v1.4. *Geosci. Model Dev.,* 15, 4077–4103.

Hamer, P. D., Walker, S.-E., Sousa-Santos, et al. (2020). The urban dispersion model EPISODE v10.0 - Part 1: An Eulerian and sub-grid-scale air quality model and its application in Nordic winter conditions. *Geosci. Model Dev.*, 13, 4323–4353, https://doi.org/10.5194/gmd-13-4323-2020, 2020.

Karl, M., Walker, S.-E., Solberg, S., & Ramacher, M. O. P. (2019). The Eulerian urban dispersion model EPISODE - Part 2: Extensions to the source dispersion and photochemistry for EPISODE-CityChem v1.2 and its application to the city of Hamburg. *Geosci. Model Dev.,* 12, 3357–3399.

Pan, K., Lim, M. Q., Kraft, M., & Mastorakos, E. (2021). Development of a moving point source model for shipping emission dispersion modeling in EPISODE-CityChem v1.3. *Geosci. Model Dev.,* 14, 4509−4534.

Rosewig, E.I., Schade, J., Passig, J., et al. (2023). Remote detection of different marine fuels in exhaust plumes by onboard measurements in the Baltic Sea using Single-Particle Mass Spectrometry. *Atmosphere,* 14, 849.

Sankaran, A., Hain, R. & Kähler, C. (2024). Assessing the Dispersion Characteristics of Ship Exhausts in Neutral Boundary Layers: Wind Tunnel Testing, PHYSMOD conference presentation.

PHYSMOD 2024 – International Workshop on Physical Modelling of Flow and Dispersion Phenomena
Ecole Centrale de Lyon, Ecully, France – August 28-30, 2024

Comparison between simulation and wind-tunnel experiment for an idealised industrial site

Claudia Schiavini[1, 2], Massimo Marro[2], Pietro Salizzoni[2], Lionel Soulhac[2], Marco Ravina[1], Deborah Panepinto[1], Mariachiara Zanetti[1]

[1]Politecnico di Torino, Dipartimento di ingegneria per l'ambiente, il territorio e le infrastrutture (DIATI), Corso Duca degli Abruzzi 24, 10129 Turin, Italy
[2]Ecole Centrale de Lyon, CNRS, Universite Claude Bernard Lyon 1, INSA Lyon, LMFA, UMR5509, 69130, Ecully, France

Abstract

Introduction

Industrial sites can be subject to accidents such as leaks or fires which lead to potential environmental and sanitary risks. To monitor preventively such risks at the local scale fast operational models able to consider the impact of the site geometry are needed. In this study, we evaluated the performances of one of such models, namely PMSS, by comparing simulations to wind tunnel measurements taken on the small-scale model of an idealised industrial site.

Methods

We simulated pollutant dispersion on an idealised industrial site including elements of interest in its geometry such as a courtyard, zones of storing of tanks and groups of elements forming a complex porous structure, representing for instance a piping system. We chose a neutral incident boundary layer and a passive scalar in order to neglect stratification and buoyancy effects.

This study focuses on simulations obtained with PMSS (Parallelised Micro SWIFT SPRAY) which is a modelling system able to simulate pollutant dispersion at microscale (resolution lower than 10 m). The model is composed of a wind and turbulence model based on empirical laws named PSWIFT, and a Lagrangian dispersion model named PSPRAY (Tinarelli et al, 2012). Both PSWIFT and PSPRAY consider obstacles and are parallelised in order to reduce computation times (Oldrini et al, 2017).

Concentration and velocity measurements were performed in the wind tunnel of the Ecole Centrale de Lyon on a model of the industrial site at a scale 1/200 using a boundary layer of 0.8 m high with a free-stream velocity of 5 ms^{-1}. More details about the boundary layer can be found in Nironi et al (2015). Concentration and velocity were respectively measured with a flame ionisation detector (FID) and a laser doppler anemometer (LDA). Both measurement methods are described in Marro et al (2020).

Numerical simulations compared to wind tunnel experiments

Results of the comparison of simulations and wind tunnel experiments are shown in Figure 1.

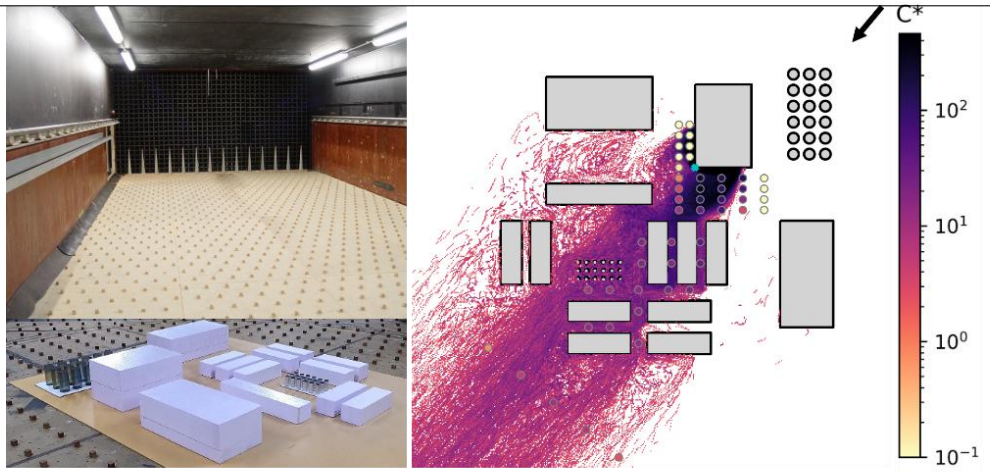

Figure 1: (a) View of the wind tunnel and small scale model of the industrial site. (b) Map of the simulated dimensionless concentration field and measurement points (filled dots). Source position and incoming wind direction are indicated by the blue cross and the arrow.

Plume shapes are correctly reproduced in the simulations even though local discrepancies appear within the recirculation zone of the highest obstacle (see the light dots close to the source in Figure 1). Differences may be due to approximations of the velocity field in the PSWIFT computation. Model to experiment agreement increases with the distance to the source, the impact of recirculation being less significant in the far field.

Conclusion

We compared simulations from the dispersion model PMSS to wind tunnel measurements of concentration with a focus on how the impact of complex geometry is reproduced in the simulations. Recirculations are globally well considered in the simulations despite inaccuracies due to local impacts of some obstacles. Further analysis would consider more configurations of the site notably to deepen the analysis of complex porous elements.

Computational resources were provided by HPC@POLITO (http://www.hpc.polito.it)

References

Marro, M., Gamel, H., Méjean, P., Correia, H., Soulhac, L., & Salizzoni, P. (2020). High-frequency simultaneous measurements of velocity and concentration within turbulent flows in wind-tunnel experiments. *Experiments in Fluids*, *61*(12), 245. https://doi.org/10.1007/s00348-020-03074-7

Nironi, C., Salizzoni, P., Marro, M., Mejean, P., Grosjean, N., & Soulhac, L. (2015). Dispersion of a Passive Scalar Fluctuating Plume in a Turbulent Boundary Layer. Part I : Velocity and Concentration Measurements. *Boundary-Layer Meteorology*, *156*(3), 415-446. https://doi.org/10.1007/s10546-015-0040-x

Oldrini, O., Armand, P., Duchenne, C., Olry, C., Moussafir, J., & Tinarelli, G. (2017). Description and preliminary validation of the PMSS fast response parallel atmospheric flow and dispersion solver in complex built-up areas. *Environmental Fluid Mechanics*, *17*(5), 997-1014. https://doi.org/10.1007/s10652-017-9532-1

Tinarelli, G., Mortarini, L., Castelli, S. T., Carlino, G., Moussafir, J., Olry, C., Armand, P., & Anfossi, D. (2012). Review and Validation of MicroSpray, a Lagrangian Particle Model of Turbulent Dispersion. In *Lagrangian Modeling of the Atmosphere* (p. 311-328). American Geophysical Union (AGU). https://doi.org/10.1029/2012GM001242

PHYSMOD 2024 – International Workshop on Physical Modelling of Flow and Dispersion Phenomena
Ecole Centrale de Lyon, Ecully, France – August 28-30, 2024

Do the wind profiles shown in the guidelines exist in reality?

K. Jurčáková[1], R. Kellnerová[1]

[1]Institute of Thermomechanics of the Czech Academy of Sciences, Dolejškova 5, 182 00, Praha, Czech Republic

Introduction

The modeling of the atmospheric boundary layer (ABL) in the wind tunnel is based on the assumption that different boundary layers are self-similar. This assumption is only valid under many conditions, which are rarely fulfilled in both the wind tunnel and the atmosphere. The conditions that are most often not fulfilled in ABL are a constant forcing and a homogeneous long fetch, which causes great difficulties in comparing wind tunnel and in situ measurements. We will show the comparison of wind tunnel and in-situ measurements at the meteorological observatory Kopisty (Czech Republic).

Methods and materials

The meteorological observatory Kopisty is located in the northwest of the Czech Republic. The observatory is located in an industrial region where there are huge industrial parks and remnants of open-cast coal mines. The ridge of the Krušné hory (Ore Mountains) is located to the northwest at a distance of 10 km. The difference in altitude is about 600 meters. In addition to measuring basic meteorological data, the observatory is equipped with a unique 80-meter mast. The mast is equipped with 3D sonic anemometers at four heights (20, 40, 60 and 80 m). We have 4 years of measurements with a sampling frequency of 10 Hz. Only the days with strong winds, almost neutral stratification and negligible vertical wind shear were considered.

The model of the meteorological observatory landscape was manufactured at a scale of 1:1333. The landscape model with a diameter of 2 km was inserted into the wind tunnel. Based on the mast measurements at 80 m, the wind rose was evaluated and three prevailing wind directions (60°, 220° and 300°) were selected for measurements in the wind tunnel. The development section of the wind tunnel was filled with turbulence generators and roughness elements to create a boundary layer profile over a moderately rough surface according to the guideline (VDI 3783, 2000). The measurement was performed using the Particle Image Velocimetry (PIV) system. The data were measured with a sampling frequency of 200 Hz and a spatial resolution of approximately 3 mm.

Comparison of in-situ and wind-tunnel profiles

A total of 240 two-hour periods were selected by objective criteria (neutral stratification, strong wind, no vertical wind shear). The time series were linearly detrended and converted to natural coordinates. There is a large variability in the magnitude and shape of the individual profiles. The most common averaging period for meteorological wind data is 30 minutes. It is clearly shown that this period is insufficient for representative averaging – the profile scatter is higher than for two-hour profiles. The dimensionless profiles of turbulence intensities in the longitudinal and vertical directions do not follow the tabulated profiles. The integral length scales (based on the time when

the autocorrelation curve reaches the value e^{-1} and the local wind speed) increase with the altitude, but again the variability is large.

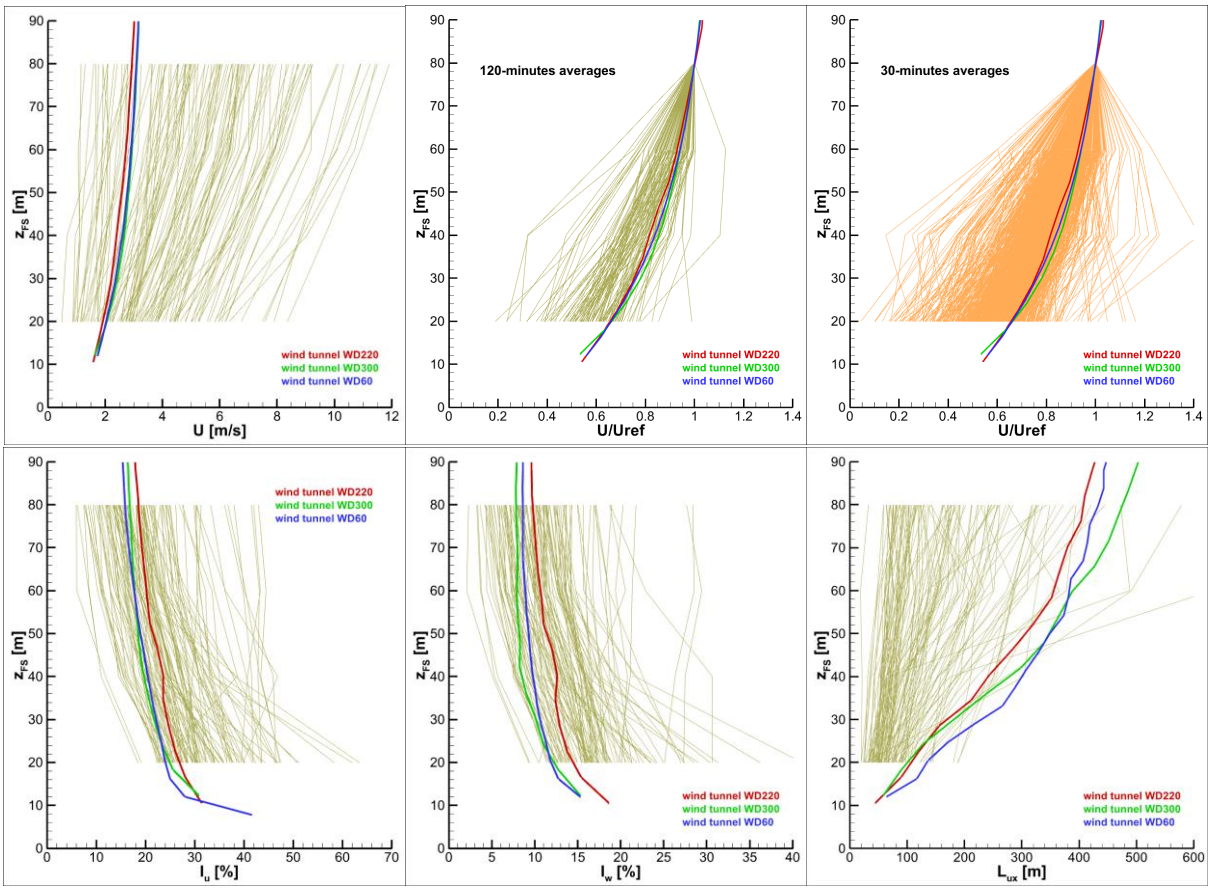

Figure 1: Comparison of the wind tunnel data (red, green, and blue lines) with the ensemble of the in-situ measurements. Variables shown from the top left: mean wind speed, normalized wind speed, normalized wind speed (30 minutes averaging time), longitudinal turbulence intensity, vertical turbulence intensity, longitudinal integral length scale.

Conclusion

We compared wind tunnel and in situ measurements without success. We were unable to select a period with a well-developed boundary layer based on objective criteria such as strong wind and negligible vertical wind shear. The 4-point mast measurements are insufficient for any profile fitting. The best agreement was obtained by comparing dimensionless spectra.

We will continue with in-situ data processing and search for a useful strategy. Our goal is to establish a best practice guideline for in-situ data requirements, revisiting the work of Counihan, 1975, and extending it to include the data from modern instruments such as Doppler wind lidars and sodars.

References

Counihan, J. (1975): Adiabatic atmospheric boundary layers: A review and analysis of data from the period 1880-1972. Atmospheric Environment, 9, 871-905.

VDI – Verein Deutcher Ingenier. (2000) Environmental meteorology. Physical modeling of flow and dispersion processes in the atmospheric boundary layer. Application of wind tunnels, VDI-Standards: VDI 3783, Part 12, Dusserdorf.

PHYSMOD 2024 – International Workshop on Physical Modelling of Flow and Dispersion Phenomena
Ecole Centrale de Lyon, Ecully, France – August 28-30, 2024

Reciprocity principle and application to inverse modelling

J. Salles Loustau[1, 2], L. Soulhac[1], A. Emmanuelli[1], O. Duclaux[2], R. Nammour[3], C.V. Nguyen[1]

[1]Ecole Centrale de Lyon, CNRS, Universite Claude Bernard Lyon 1, INSA Lyon, LMFA, UMR5509, 69130, Ecully, France
[2]Laboratoire Qualité de l'Air, TotalEnergies, 69360 Solaize, France
[3]E&P Research & Technology USA, TotalEnergies, 77002-5605 Houston (Texas), USA

Abstract

Characterizing atmospheric pollutant sources is a major worry in an industrial context to improve on site security and environmental impact, but it can be challenging, especially under time constraint. To tackle this issue, the inverse modelling approach is often used to obtain the model parameters m_s of a source s, i.e. its strength and position. Classically, an optimization problem is solved, minimizing a cost function J depending on m_s, depicting the gap between the concentration observations d and the modelled ones provided by a forward transport and dispersion model of pollutants C_s originating from s. It is an iterative algorithm, relying on optimization methods computing the gradient ∇J and updating the m_s values at each iteration. Among these techniques, the adjoint efficiently calculates ∇J at each iteration, by avoiding computing the full Jacobian matrix, such that $\nabla J(m_s) = \left(\frac{dC_s}{dm_s}\right)^* [C_s(m_s) - d]$. The adjoint term $\left(\frac{dC_s}{dm_s}\right)^*$ represents the sensitivities of the model outputs, i.e. the concentrations at receivers, to the input variables, i.e. the source parameters m_s.

However, these sensitivities are valid only for a unique value set of m_s, computed at a given iteration i of the minimization algorithm. Indeed, for each i, a new forward model run with the updated m_s values is needed to compute an adjoint field featuring these sensibilities, leading to large simulation costs. Alternatively, switching source and sensor positions, one can consider a backward model, i.e. a direct model with both time and wind field reversed, to compute a retro-plume. The retro-modelling idea comes from the adjoint method application to the instantaneous advection-diffusion equation (ADE), highlighting the reciprocity principle (Pudykiewicz, 1998). For any turbulent incompressible flow in the domain $\Omega \subset \mathbb{R}^3$ over the time interval $[0, T]$ and any steady/unsteady, fixed/mobile source s of passive scalar, the ADE is, considering $C_s(\boldsymbol{x}, t)$ the concentration field, D the constant diffusion coefficient and $\boldsymbol{u}(\boldsymbol{x}, t)$ the advection velocity field (wind velocity):

$$\frac{\partial C_s(\boldsymbol{x},t)}{\partial t} + \boldsymbol{u}(\boldsymbol{x}, t) \cdot \nabla_{\boldsymbol{x}} C_s(\boldsymbol{x}, t) = D\Delta_{\boldsymbol{x}} C_s(\boldsymbol{x}, t) + s(\boldsymbol{x}, t) \quad (1)$$

where $s(\boldsymbol{x}, t)$ is the forcing term depicting emissions. Equation (1) being linear for the concentration, C_s can be computed as the convolution of a Green function a and s, such that, for any fixed/mobile sensor r, $C_s(\boldsymbol{x_r}, t_r) = \int_T \int_\Omega a(\boldsymbol{x}, t, \boldsymbol{x_r}, t_r)\, s(\boldsymbol{x}, t)\, dv\, dt$, with $C_s(\boldsymbol{x_r}, t_r)$ the concentration at sensor position $\boldsymbol{x_r}$ at time t_r from a source shot s at position $\boldsymbol{x_s}$ and time t_s. The Green function $a(\boldsymbol{x}, t, \boldsymbol{x_r}, t_r)$ is solution of a unit ADE, i.e. the concentration at $\boldsymbol{x_r}$ and t_r for a unit instantaneous point at $\boldsymbol{x_s}$ and t_s. The reciprocity principle states that a is also solution of the unit backward ADE, i.e. the unit ADE with reversed flow and time, associated with a unit instantaneous point release at $\boldsymbol{x_r}$ and t_r. By linearity, the adjoint state C_s^* associated with source s is obtained such that

$C_s^*(\boldsymbol{x_r}, t_r) = \int_{-T}\int_{\Omega} a(\boldsymbol{x_s}, t_s, \boldsymbol{x}, t)p(\boldsymbol{x}, t)\, dv\, dt$, with $C_s^*(\boldsymbol{x_r}, t_r)$ the concentration at $\boldsymbol{x_s}$ and t_s from a source shot at $\boldsymbol{x_r}$ and t_r, solution of the adjoint equation:

$$\frac{\partial C_s^*(\boldsymbol{x},t)}{\partial(-t)} - \boldsymbol{u}(\boldsymbol{x},t)\cdot\nabla_{\boldsymbol{x}} C_s^*(\boldsymbol{x},t) = \nabla_{\boldsymbol{x}}\cdot(D\Delta C_s^*(\boldsymbol{x},t)) + p(\boldsymbol{x},t) \quad (2)$$

where $p(\boldsymbol{x},t)$ is the forcing term of the adjoint equation, such that $p(x,t) = C_s(\boldsymbol{x},t) - d(\boldsymbol{x},t)$. It means that, as shown in Figure 1-a), the concentration at $\boldsymbol{x_r}$ and t_r (purple point) coming from a source s at x_s and t_s (red point) equals, in Figure 1-b), the concentration at $\boldsymbol{x_s}$ and t_s (red point) coming from the same source s but at x_r and t_r (purple point) transported in both flow and time reversed.

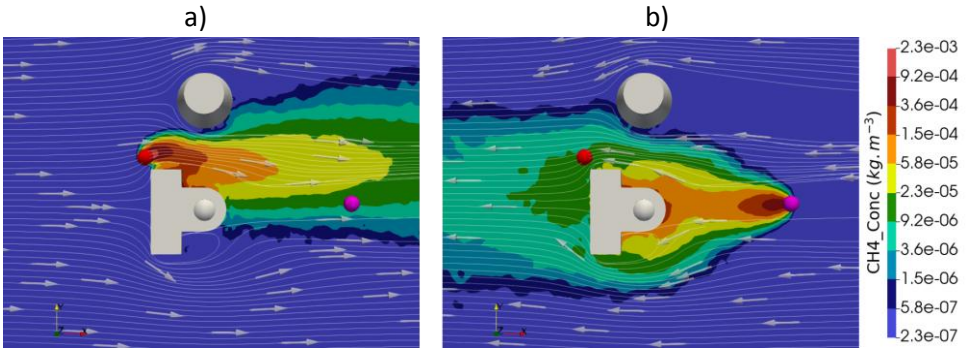

Figure 1: In log. scale: a) Direct concentration field with wind streamlines; b) Inverse concentration field, with wind streamlines

This reciprocity principle remains valid for the RANS advection-diffusion equation and is equivalent to the well-mixed condition criteria (Thomson, 1987). In this study, a Lagrangian Stochastic (LS) model is used instead, as it accurately models turbulent dispersion in a complex environment while still providing reasonable computational cost, but the principle remains the same and is still valid.

The reciprocity principle is of great interest for inverse modelling. Indeed, in a steady case with fixed sensors, as the Green functions can be calculated by reverse dispersion from the sensor positions with equation (2), computing a new adjoint field at each iteration of the optimization algorithm is not necessary anymore, only requiring calculating a unique adjoint field by sensor and, at each iteration, picking the field value at the newly computed source position. Hence, if the number of receivers is smaller than the iteration number of the optimization algorithm, using a backward model is more efficient than using a forward one. Also, if there are more sources than receivers, the concentration computation is quicker using a backward model. Besides, the convolution of the forward and backward fields could increase the statistical power (for the LS model), improving the reliability of the modelled concentrations and hence of the inverse modelling. Finally, new measurement techniques appeared recently, such as the Particle Tracking Velocimetry (PTV), could experimentally verify the reciprocity.

In this study, the reciprocity principle is presented and applied to the inverse modelling workflow by using the adjoint method to a LS backward model. The approach benefits and implications will be highlighted. Finally, some validations with experimental results and applications to both academic and industrial cases are presented, on diverse datasets configurations with increasing complexity.

References

Pudykiewicz, J. A. (1998): Application of adjoint tracer transport equations for evaluating source parameters. *Atmospheric Environment*, 32. 3039-3050.

Thomson, D. J. (1987): Criteria for the selection of stochastic models of particle trajectories in turbulent flows. *Journal of Fluid Mechanics*, 180. 529–556.

Atmospheric boundary layer flow

PHYSMOD 2024 – International Workshop on Physical Modelling of Flow and Dispersion Phenomena
Ecole Centrale de Lyon, Ecully, France – August 28-30, 2024

Characterisation of the boundary layer wind tunnel facility at the University of Bristol

Nada Taouil[1], H.D. Lim[1], B. Zang[1], Mahdi Azarpeyvand[1]

[1]School of Civil, Aerospace and Design Engineering, University of Bristol, UK

Abstract

The Boundary Layer Wind Tunnel (BLWT) at the University of Bristol is a new national wind tunnel facility that was recently commissioned. With an 18m long, 2m wide and 1m high test section, it is envisaged to be a pivotal enabler for environmental fluid dynamics research in the UK. To fully harness its capabilities for urban flow research, the use of appropriate flow conditioners, as shown in Fig. 1(a), is needed to accurately simulate an atmospheric boundary layer flow.

As a new wind tunnel facility, thorough measurements of the empty wind tunnel are essential to validate the flow uniformity and quality. Hot wire anemometry was used to characterise the vertical profiles of the smooth-wall turbulent boundary layer flow at 14 meters from the entrance of the test section. Key parameters were established, including the boundary layer thickness (δ=200 mm) which is within 10% of theoretical estimates, the free-stream turbulence intensity (0.13%) and the friction velocity (u^*=0.64 m/s), which was estimated using the law of the wall based on wall similarity:

$$\frac{u}{u^*} = \frac{1}{k}\ln\left(\frac{y.u^*}{v}\right) + C \; . \qquad (1)$$

where k=0.42 is the von Karman constant and C=5 is the smooth-wall intercept. Figure 1(b) shows that the mean velocity profiles are reasonably homogeneous at three spanwise locations, and although there are slight deviations, these are within acceptable range (<3%) (Wittwer and Möller, 2000).

Precise simulation of an atmospheric boundary layer flow is necessary to enable air pollution research. This is achieved by adopting the Counihan's methodology (Counihan, 1969) in the present study, which utilises 900 mm tall quarter-elliptic wedge spires as vortex generators, a castellated barrier wall to introduce momentum deficit at the near-wall region, and a fetch of roughness elements strategically arranged for an upstream fetch of 10 meters, as illustrated in Figure 1(a). By adjusting the design of these flow conditioners, different types of terrain flow, i.e. rural or urban can be simulated.

Figure 1(c) shows the velocity profile of one of the rough wall configurations with the roughness elements and the barrier installed. As expected, in contrast to the smooth-wall data, the boundary layer thickness of the rough-wall data is significantly larger. This, along with the roughness elements

creating additional flow turbulence and disruption, may explain the differences in the outer wake region.

Figure 1(d) shows the power law exponent (α) of the velocity profile, given by

$$\frac{u}{u_1} = (\frac{y}{y_1})^{\alpha} \quad (2)$$

to understand the impact of roughness elements and the barrier wall. From the analysis of these plots, it appears that adjustments to the configuration of the roughness elements is necessary to reach a power index of α=0.29, which is typical for urban flows. Additionally, further investigation into the effects of the quarter-elliptic wedge spires will be conducted to understand their impact on boundary layer characteristics. The thickness of the boundary layer generated depends on the height of the spires, which is estimated to be around 90% of the height of the spires.

In the conference presentation, further results and discussions will be provided, including mean velocity distributions, turbulence intensity, Reynolds shear stresses and power spectrum density and their comparison for both the smooth and rough configurations, with measurements taken closer to the wall to get lower values of y^+. Moreover, comparisons with established datasets such as Engineering Sciences Data Unit (ESDU) will be conducted to validate the accuracy of the BLWT's simulations and confirm its suitability for atmospheric flow studies.

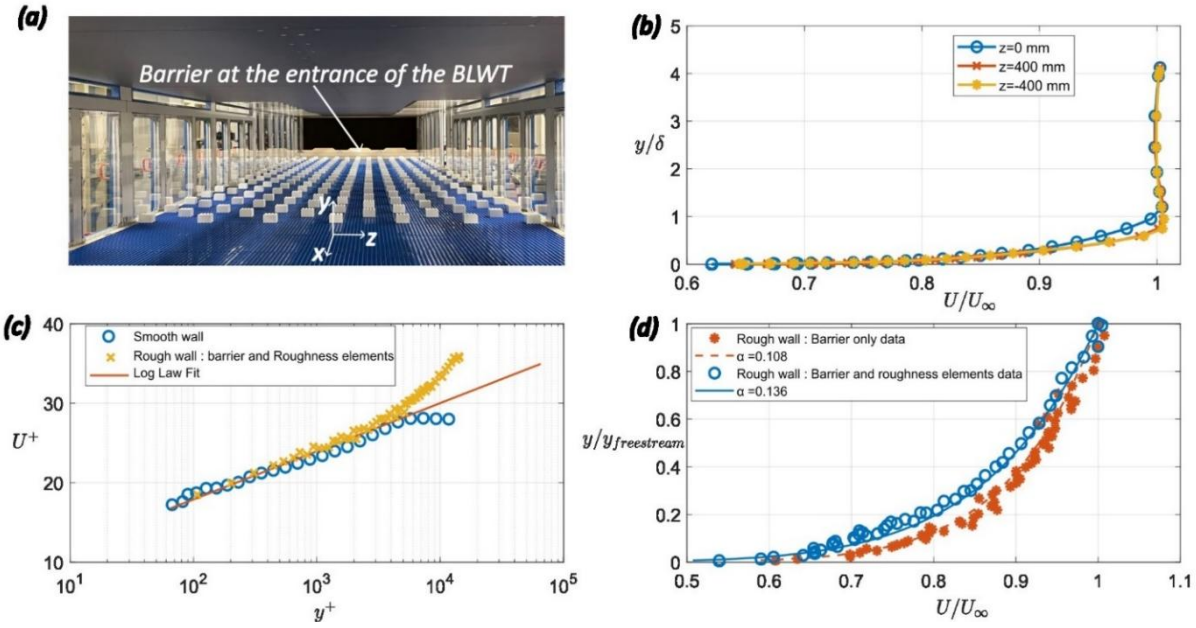

Figure 1: (a) BLWT with roughness elements (Lego blocks) and barrier installed. (b) Spanwise homogeneity analysis at three positions. (c) Log-law fit for smooth wall and rough wall data. (d) Mean velocity with power law exponent fit for two different rough wall configurations.

References

Counihan, J., 1969. An improved method of simulating an atmospheric boundary layer in a wind tunnel. *Atmospheric Environment*, 3(2), pp.197-214.

Wittwer, A. R., & Möller, S. V. (2000). Characteristics of the low-speed wind tunnel of the UNNE. *Journal of Wind Engineering and Industrial Aerodynamics*, *84*(3), 307–320.

PHYSMOD 2024 – International Workshop on Physical Modelling of Flow and Dispersion Phenomena
Ecole Centrale de Lyon, Ecully, France – August 28-30, 2024

Wake characteristics of a model wind turbine immersed in a boundary layer

V. Babin[1], Y. Bohbot-Raviv[1], L. Shmuel Sabban[2], and J. Alisse[2]

[1]Israel Institute for Biological Research, Environmental Sciences, Department of Applied Mathematics, P.O.B 19, 7410001 Ness-Ziona, Israel
[2]Noga - Israel Independent System Operator Ltd., 8 Moshe Fliman St., Haifa, Israel

Abstract

Wind energy, alongside other renewable sources, has experienced significant growth in recent years, with the expectation of a sharp rise in the number of wind farms in the coming decades. This investigation is part of a broader project initiated by Noga – Israel Independent System Operator, Ltd. – aimed at determining the optimal distance needed between wind farms and high-voltage transmission lines.

A turbulent wake generated by a scaled-down wind turbine has been modeled and analyzed at the Environmental Wind Tunnel Laboratory (EWTL) of the Israel Institute for Biological Research (IIBR). The turbine was immersed in a scaled-down boundary layer that was slightly rough and neutrally stable. Modeling and characterizing the wake under idealized wind tunnel conditions serve as important tools for enhancing field measurements and numerical evaluations of field-scale wakes. The forthcoming presentation will primarily focus on the experimental details and the mean and instantaneous flow properties, while the spectral properties of the wake will be discussed separately by Bohbot-Raviv et al. in another presentation.

Our wake model is generated based on an incoming boundary layer with a scaling-length factor of approximately 400. The in-house scaled-down miniature wind turbine, utilizing a rotor design by Bastankhah and Porté-Agel (2017a,b), stands at 195 mm tall with a 3-blade rotor diameter of 150 mm (refer to Figure 1, left). The wake, observed up to 10 rotor diameters downstream, was generated under 10% streamwise turbulence intensity of the incoming flow, maintaining a mean tip-speed ratio of 5. The boundary layer's thickness at the turbine's location is estimated to be approximately 600 mm, roughly three times the height of the rotor's top tip. We conducted quantitative and qualitative spatial flow visualization employing double-pulsed plane two-component Particle Image Velocimetry (PIV). Additionally, velocity field mapping along the wake was performed through point-measurements using hot-wire anemometry (HWA) for two velocity components.

The mean velocity deficit, turbulence intensity, vertical Reynolds shear stress, and their evolution along the vertical axial mid-plane are analyzed. At least three distinct regions of the wake were identified based on the flow properties: the very-near wake (0<x<2D), near wake (2D<x<10D), and far wake (x>10D), where similarity is expected to hold. The wake deficit persists as far as 11D downstream from the turbine. These findings align well with previous experimental works (Barlas et al., 2016 and others) and Large Eddy Simulation (LES) (Wu and Porté-Agel, 2012).

Analyses of the PIV data in the vertical axial mid-plane along the wake (x,0,z) will also be presented. Signatures of the root and hub vortices are identified at the center of the very-near wake, creating layers of positive and negative vorticity that quickly diffuse along a 1D distance from the turbine. A vortex strip with high negative vorticity values at the top-tip height is clearly observed. Top-tip vortices and their persistence are discernible in the instantaneous vorticity field (blue circles in Figure 1, right), originating from the 3D helicoidal vortices produced by each blade of the rotor during rotation.

A comparison of wake characteristics with previous studies involving similar physical models from single wind turbines characterized by low inlet turbulence is presented (Barlas et al., 2016, among others). Future stages of the project plan will be discussed to conclude the presentation.

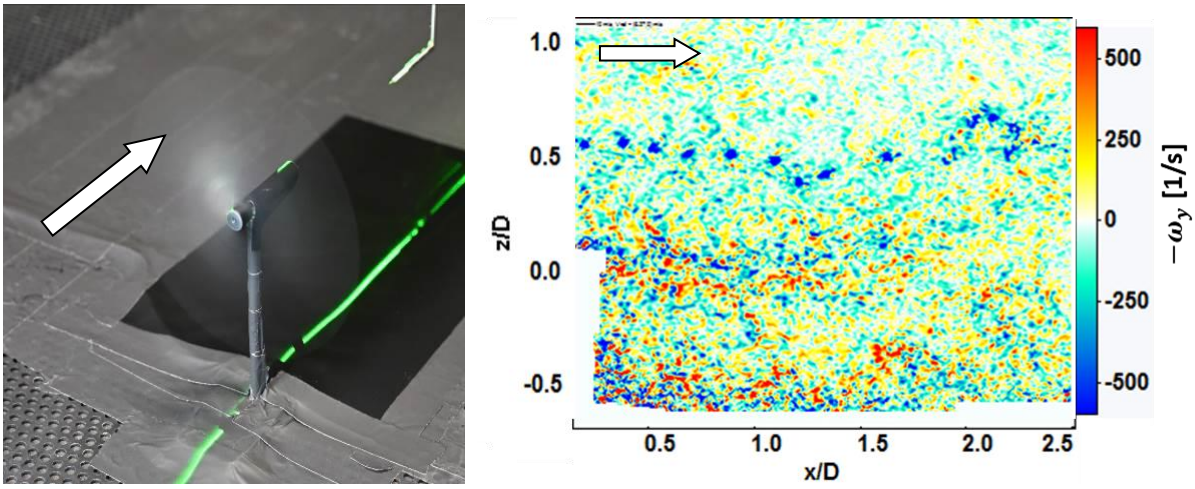

Figure 1: (left) depicts the scaled-down wind turbine, HWA and illuminated strip from the PIV laser sheet in the vertical axial mid-plane along the wake (x,0,z) from the experiment setup in the wind tunnel; (right) The instantaneous vorticity component of the wake in the very-near wake (0<x<2.5D), as measured by Particle Image Velocimetry (PIV) in the vertical axial mid-plane.

References

Bastankhah, M., Porť e-Agel F. (2017). A new miniature wind turbine for wind tunnel experiments. Part i: Design and performance. *Energies*, 10(7) 908.

Bastankhah, M., Porť e-Agel F. (2017). A new miniature wind turbine for wind tunnel experiments. Part ii: wake structure and flow dynamics. *Energies* 10(7) 923.

Barlas, E., Buckingham, S., van Beeck, J. (2016). Roughness effects on wind-turbine wake dynamics in a boundary-layer wind tunnel. *Boundary-Layer Meteorology* 158(1):27–42.

Wu, Y.T., Porť e-Agel, F. (2012). Atmospheric turbulence effects on wind-turbine wakes: An LES study. *Energies* 5(12):5340–5362.

PHYSMOD 2024 – International Workshop on Physical Modelling of Flow and Dispersion Phenomena
Ecole Centrale de Lyon, Ecully, France – August 28-30, 2024

Turbulent scales in the wake of a model wind turbine immersed in a boundary layer

Y. Bohbot-Raviv[1], V. Babin[1], L. Shmuel Saban[2] and J. Alisse[2]

[1]Israel Institute for Biological Research, Environmental Sciences, Department of Applied Mathematics, P.O.B 19, 7410001 Ness Ziona, Israel
[2] NOGA - Israel Independent System Operator LtD, 8 Moshe Fliman St., Haifa Israel

Abstract

The wake generated by a scaled-down horizontal axis wind turbine immersed in a slightly rough boundary layer (at a scale ratio of 1:400) is examined at the Environmental Wind Tunnel Laboratory at IIBR. Spectral analyses of the modeled wake provide a scale-by-scale energetic description of the flow within the turbine wake. This examination is part of a broader project initiated by Noga – Israel Independent System Operator, Ltd. – aimed at investigating the optimal distance needed between wind farms and high-voltage transmission lines. Identifying dominant frequencies and understanding their signatures under idealized wind tunnel conditions are important tools for enhancing field-scale measurements and numerical investigations of field-scale wakes.

The forthcoming presentation will primarily focus on the spectral properties of the modelled wake, while the experimental details and mean flow properties will be presented separately by Babin et al. in another presentation.

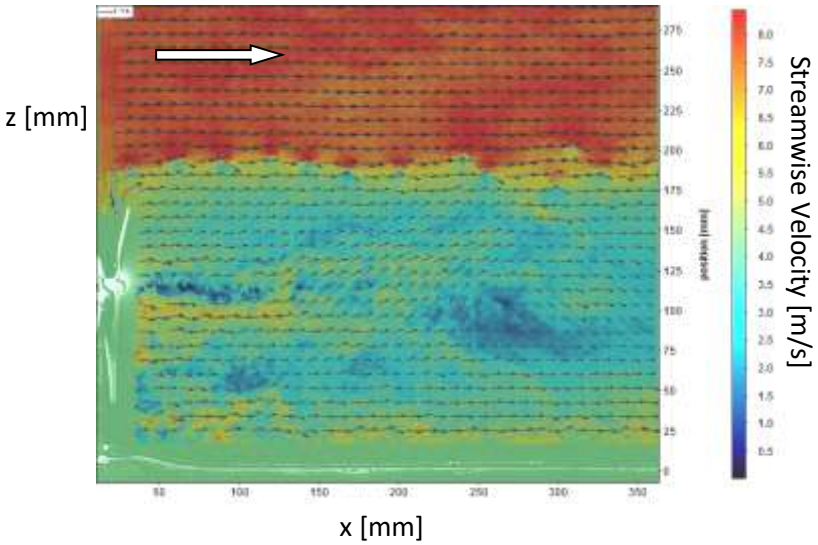

Figure 1: Instantaneous velocity field (u,w) and mean streamwise velocity (color) by particle image velocimetry in the axial mid-plane along the very-near wake.

In the relatively high-frequency range, the turbine induces strong turbulent energy into the wake. The dominant frequencies of the flow and their evolution in the vertical axial mid-plane along the wake are identified and examined. Our spectral analysis confirms small scales (high frequencies) induced by the rotating turbine in the top and bottom tip heights and additional large scale (low frequency) of the flow in the wake. The evolution of the energy deficit (i.e., relative to the incoming energy) in the large-scale turbulent kinetic energy partially confirms the concept proposed by Chamorro et al. (2012) viewing the turbine acting as a 'low-pass filter'. Several terms in the turbulent kinetic energy budget are also explored to identify dominant physical processes in the near wake.

In an attempt to associate the dominant large-scale frequencies with flow structure, particle image velocimetry qualitatively infers on a meandering motion of the wake as a whole at approximately $0.2f_T$, where f_T is the mean rotation frequency. Such low frequencies correspond to a few hundredths of Hertz in full scale (i.e., hundreds of meters). Similar meandering frequencies have been observed in similar studies in the laboratory (Barlas et al., 2016 and Chamorro et al., 2012) and in the field (Heisel et al., 2018). Future stages of the project will conclude the presentation.

References

Chamorro, L., Guala, M., Arndt, R., & Sotiropoulos, F. (2012). On the evolution of turbulent scales in the wake of a wind turbine model. *Journal of Turbulence*, 13:27.

Barlas, E., Buckingham, S., & van Beeck, J. (2016). Roughness effects on wind-turbine wake dynamics in a boundary-layer wind tunnel. *Boundary-Layer Meteorology*, 158(1):27–42.

Heisel, M., Hong, J., & Guala, M. (2018). The spectral signature of wind turbine wake meandering: A wind tunnel and field-scale study. *Wind Energy*, 21(9):715–731.

PHYSMOD 2024 – International Workshop on Physical Modelling of Flow and Dispersion Phenomena
Ecole Centrale de Lyon, Ecully, France – August 28-30, 2024

Wake Characteristics of Multi-scale Buildings in a Turbulent Boundary Layer

C. Southgate-Ash[1], A. Mishra[1], S. Grimmond[2], A. Robins[1], M. Placidi[1]

[1] University of Surrey, Faculty of Engineering and Physical Sciences, Centre for Aerodynamics and Environmental Flow, Guildford, GU2 7XH, United Kingdom

[2] University of Reading, Department of Meteorology, Brian Hoskins Building, University of Reading, Whiteknights campus, RG6 7BE, United Kingdom

Introduction

Urban forms characterised by multi-scale roughness can drastically modify the wind structure within cities affecting both pedestrian comfort and air quality at street level. Despite the multiscale nature of modern cities, for simplicity, most urban flow studies focus on cuboid buildings with a single length scale (Cheng and Castro, 2002; Coceal et al., 2006; Castro, 2007; Leonardi and Castro, 2010; Castro et al., 2017). Although this is effective for certain simplified morphologies, it is often an oversimplification compared with real urban data (Grimmond and Oke, 1999; Barlow and Coceal, 2009; Makedonas et al., 2021). To study how significant additional length scales are in urban flow modelling, six multiscale forms are considered: reference cuboids for two aspect ratio (mean building height to width) cases (standard, 1; tall, 3) plus two fractal iterations of each. Although the six models have the same mean building width, height (H_B), and frontal area, their length scales characteristics differ, isolating the effect of progressively smaller length scales. These are used in wind tunnel experiments within a deep turbulent boundary layer.

Experimental set up

The experiments were carried out in the University of Surrey Environmental Flow Research Centre (EnFlo) 'A' wind tunnel. This tunnel's working section covers 5000 mm (length) x 900 mm (width) x 600 mm (height). It is a blowdown, open-circuit wind tunnel with a maximum velocity of 25 ms^{-1} and a free-stream turbulence intensity below 0.1%. We consider a range of velocities, resulting in a Reynolds number range $Re_L = 6.7 \times 10^3 - 8.2 \times 10^4$, based on the building height. Three-dimensional Laser Doppler Anemometry (LDA) measurements were taken to measure the vertical and lateral mean velocity profiles in the building model wakes at several downstream locations (Figure 1). Irwin spires, along with floor roughness elements were employed to produce a thick velocity profile, similar to that of an urban boundary layer with a relative boundary layer depth at the building location of $\delta/H_B \approx 0.24$ and 0.41 for the standard and tall models respectivelty and $u_\tau = 0.45$ ms^{-1}.

Key Findings

The vertical and lateral wake spreads behind each building model were examined via 3D LDA measurements. For both sets of models (standard and tall), a linear lateral spreading with the downstream location was found following the extent of a region characterised by strong recirculation. For the standard models, the base iteration model showed the most amount of lateral spreading and

the opposite was true for the tall. Vertically, any significant wake spreading was hindered by the roof-level shear layer growth. The vertical spread seemed to scale with the maximum building height in the nearwake ($X < H_B$), but with the average building height for $X > H_B$. For the base iteration models, all three velocity fluctuation components were observed to be higher in the near-wake but to decay faster than in the fractal models. Finally, the introduction of progressively smaller scales was found not to modify the shedding frequency of the models, but to affect its strength with the intensity of the shedding decreasing with each fractal iteration (i.e. length scale).

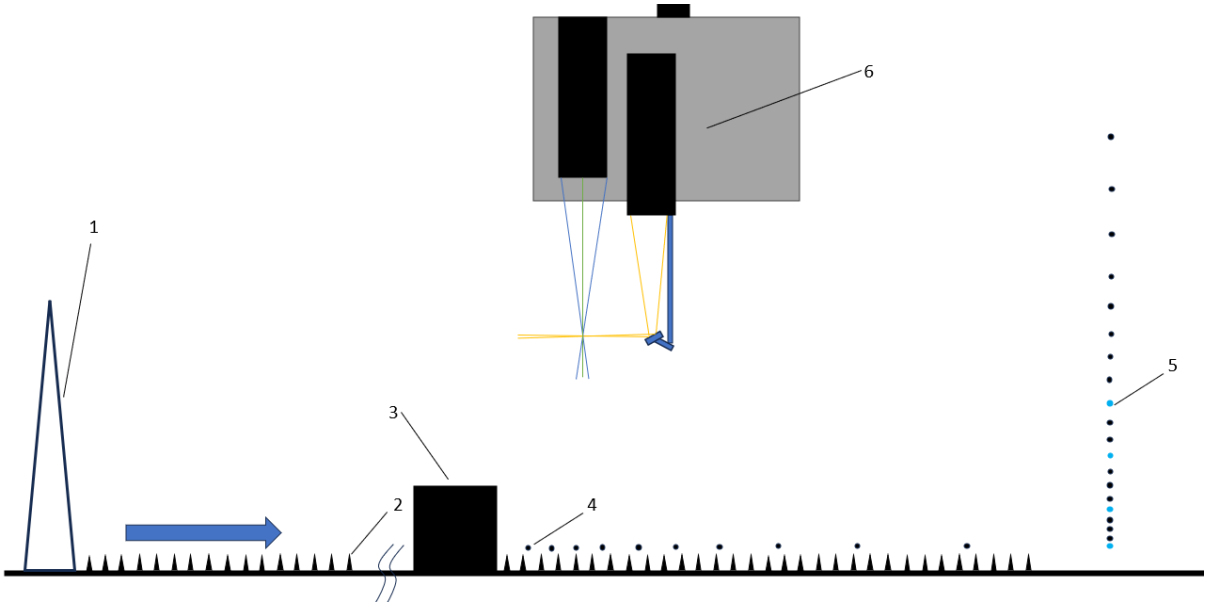

Figure 1: Wind tunnel and LDA set up showing [1] Irwin spires, [2] floor roughness, [3] building model, [4] streamwise location of vertical and lateral profiles, [5] Example of vertical measurement profile with the blue dots showing the height at which lateral profiles were taken, [6] LDA probes. Not to scale.

References

Barlow, J. F. and Coceal, O. (2009). "A review of urban roughness sublayer turbulence". In: Reading: Met Office 10, pp. 216–240.

Castro, I. et al. (2017). "Measurements and Computations of Flow in an Urban Street System". In: Boundary-Layer Meteorology 162, pp. 207–230.

Cheng, H. and Castro, I. P. (2002). "Near Wall Flow over Urban-like Roughness". In: Boundary-Layer Meteorology 104.2, pp. 229–259.

Castro, I. P. (2007). "Rough-wall boundary layers: mean flow universality". In: Journal of Fluid Mechanics 585, pp. 469–485.

Coceal, O. et al. (2006). "Mean Flow and Turbulence Statistics Over Groups of Urban-like Cubical Obstacles". In: Boundary-Layer Meteorology 121.3, pp. 491–519.

Leonardi, S. and Castro, I. P. (2010). "Channel flow over large cube roughness: a direct numerical simulation study". In: Journal of Fluid Mechanics 651, pp. 519–539.

Grimmond, C. S. B. and Oke, T. R. (1999). "Aerodynamic Properties of Urban Areas Derived from Analysis of Surface Form". In: Journal of Applied Meteorology 38.9, pp. 1262–1292.

Makedonas, A. , Carpentieri, M. and Placidi, M. (2021). "Urban Boundary Layers Over Dense and Tall Canopies". In: Boundary-Layer Meteorology 181.1, pp. 73– 93.

PHYSMOD 2024 – International Workshop on Physical Modelling of Flow and Dispersion Phenomena
Ecole Centrale de Lyon, Ecully, France – August 28-30, 2024

Roughness Sublayer Flows over Cubes with Uniform and Non-uniform Height: A Wind Tunnel Study

Ziwei Mo[1], Chun-Ho Liu [2]

[1]School of Atmospheric Sciences, Sun Yat-sen University, & Southern Marine Science and Engineering Guangdong Laboratory (Zhuhai), Zhuhai, China
[2]Department of Mechanical Engineering, The University of Hong Kong, Hong Kong

Abstract

Atmospheric surface layer (ASL) consists of inertial sublayer (ISL) and roughness sublayer (RSL). In view of the presence of roughness elements, RSL extends and become increasingly important in the mass and energy exchange between the atmospheric boundary layer and land surface. This study investigates the RSL flows over different configurations of arrays constructed by LEGO® bricks using wind tunnel measurements. Constant-temperature (CT) hot-wire anemometry (HWA) is used to measure the flows in the turbulent boundary layer (TBL). The effects of uniform and non-uniform roughness element height are examined to demystify the aerodynamic properties and turbulence structure in the RSLs. The results show that roughness element height increases the RSL thickness. Drag coefficient C_d is elevated over higher, non-uniform-height elements. We propose that the RSL-to-turbulent-boundary-layer-height ratio (Z_{RSL}/Z_{TBL}) could be parameterized by C_d, which would benefit the RSL parameterization in meso-scale meteorological models. Compared with that in the ISL, the vertical gradient of mean wind speed is smaller in the RSL that is well predicted by our modified analytical model. The mixing length l_m is also calculated to contrast the RSL and ISL turbulent length scale. It is found that the mixing length l_m is proportional to the vertical height z (i.e., $l_m = \kappa z$; where κ is the von Kármán constant). However, κ is equal to 0.2 in this study that is different from other studies over staggered cube arrays. As the canopy roof is difficult to be determined over arrays of non-uniform roughness elements, air exchange rate (ACH) induced by RSL turbulence, ACH_{RSL}'', is introduced to assess the RSL ventilation capacity analogous to the roof-level ACH. A tight correlation is found between the square root of C_d and ACH_{RSL}'', suggesting a potential parameterization for evaluating the RSL ventilation. These findings demonstrate the importance of RSL flow parametrization and the implication to ventilation assessment over urban areas, facilitating sustainable urban environment development.

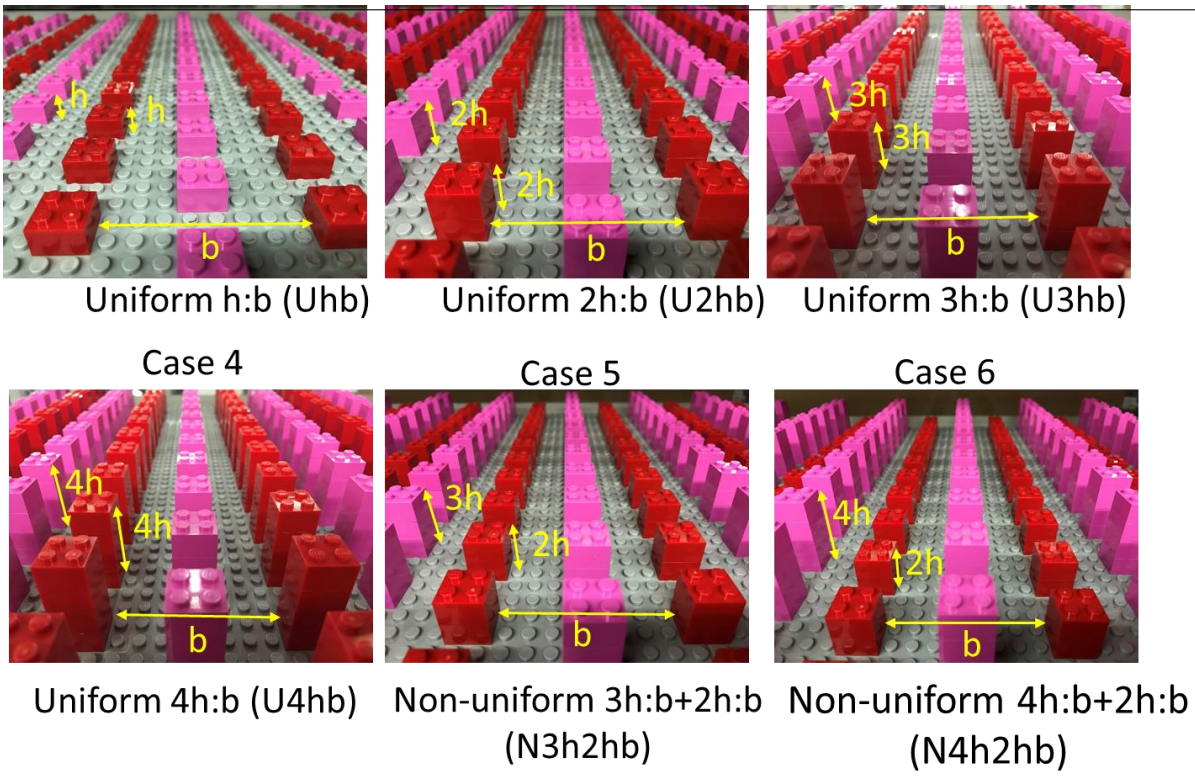

Figure 1: The photos of the configurations of the cube arrays

PHYSMOD 2024 – International Workshop on Physical Modelling of Flow and Dispersion Phenomena
Ecole Centrale de Lyon, Ecully, France – August 28-30, 2024

Assessing the Dispersion Characteristics of Ship Exhausts in Neutral Boundary Layers: Wind Tunnel Testing

A. Sankaran, R. Hain, C. Kähler

Department of Aerospace Engineering, Institute of Fluid Mechanics and Aerodynamics, University of the Bundeswehr Munich, 85577 Neubiberg, Germany

Abstract

The objective of this study is to model a neutral atmospheric boundary layer over sea/seashore conditions in wind tunnel and utilize it for dispersion study of ship exhaust. Counihan type spires in conjunction with a barrier are utilized to mimic the atmospheric boundary layer in the sea and shore conditions with neutral conditions. Stereoscopic Particle Image Velocimetry (sPIV) measurements were conducted to clarify if there is span–wise variation due to the presence of the spire system with spire height H = 900 mm.

The experimental condition with the barrier and spires to simulate the atmospheric boundary layer in the wind tunnel (Eiffel type atmospheric wind tunnel located at the University of the Bundeswehr Munich). The stereoscopic PIV setup for corresponding measurements is shown in Fig. 1. The modelled boundary layer characteristics like the mean wind profile, turbulent intensities, roughness length, and integral length scale are quantified and compared with the expected conditions at marine conditions available (Hsu et al., 1994; VDI, 2000). The average velocity profile in the main flow direction (U along x), fitted using power law (equation 1) and log-law (equation 2) formulations can be expressed as follows:

$$U = a(z-b)^{\alpha} \tag{1}$$

$$U = U_0 \log\left(\frac{z-b}{z_0}\right) \tag{2}$$

Here, z is the direction perpendicular to the surface, a, b, α, U_0, and z_0 are fitting parameters. b is referred to as displacement height, and z_0 represents the roughness length. For a free stream velocity of 10 ms^{-1}, the obtained fitting parameters are depicted in Table 1.

a (ms^{-1})	b (mm)	α	U_0 (ms^{-1})	z_0 (mm)
4.66	8.43	0.088	0.566	0.0126

Table 1. Velocity profile fitting parameters

A generic cruise ship model (using a scale 1:500) is positioned 9H downstream of the spire setup. The flow characteristics and Reynolds number independence of the flow characteristics are confirmed for the velocities studied by the sPIV measurements.

Subsequently, experiments for concentration measurements with the exhaust flow were conducted. The exhaust flow is seeded with the flow tracers of DEHS particles with average diameter of 0.4 µm. Here, we apply an optical-based particle counting method in conjunction with particle counter calibration to determine spatially resolved particle concentration measurements to evaluate the exhaust dispersion characteristics (Sankaran et al., 2024).

The inset in Fig. 1 illustrates the average concentration profile for a free stream velocity of 10 ms^{-1} and exhaust velocity of 13 ms^{-1} at 90° yaw angle of the ship.

The obtained results are intended for validation and comparison with numerical models with controlled incoming wind conditions.

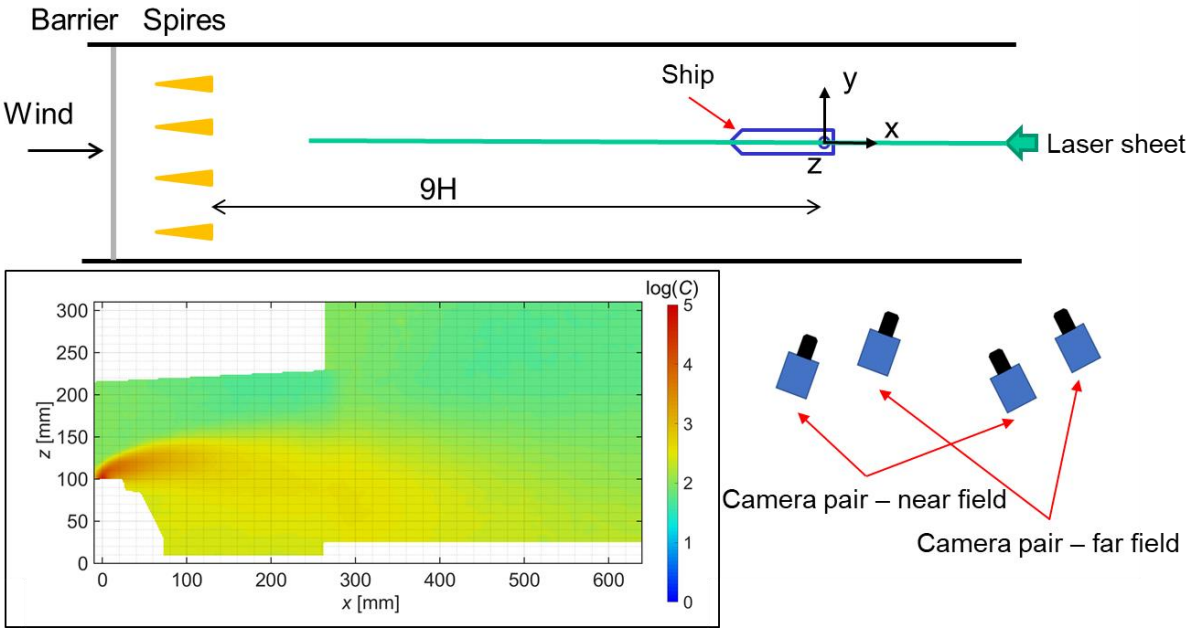

Figure 1: Top view of the experimental setup to measure the velocity field and concentration field with the exhaust flow. The inset shows the average concentration field with 10 ms^{-1} far-field velocity and 13 ms^{-1} exhaust velocity at 90° ship yaw angle. Note that the concentration contour is in log scale with C in particles per cm^3.

Acknowledgement

This research is funded by dtec.bw – Digitalization and Technology Research Center of the Bundeswehr. dtec.bw is funded by the European Union – NextGenerationEU.

References

Hsu, S. A., Meindl, E. A., & Gilhousen, D. B. (1994). Determining the power-law wind-profile exponent under near-neutral stability conditions at sea. *Journal of Applied Meteorology and Climatology*, 33(6), 757-765.

Verein Deutscher Ingenieure (2000). Environmental Meteorology, Physical Modelling of Flow and Dispersion Processes in the Atmospheric Boundary Layer, Application of Wind Tunnels (VDI 3783-12).

Sankaran, A., Hain, R., & Kähler, C. J. (2024). Particle image based simultaneous velocity and particle concentration measurement. *Measurement Science and Technology*, 35(6), 065206.

PHYSMOD 2024 – International Workshop on Physical Modelling of Flow and Dispersion Phenomena
Ecole Centrale de Lyon, Ecully, France – August 28-30, 2024

Intermittency Analysis of the Turbulence over Idealized Urban Areas Based on Empirical Mode Decomposition

Ruiqi Wang [1], Chun-Ho Liu [1]

[1] The Department of Mechanical Engineering, The University of Hong Kong, Pokfulam Road, Hong Kong, China

Abstract

Turbulence intermittency is a unique characteristic of dynamical motions, which spans in time and space, that has attracted a lot of attention. Numerous studies have demonstrated the positive influence of turbulence intermittency in vertical transport (Wei et al., 2018) as well as near-ground air quality (Ren et al., 2019). Intermittency is observed in the probability distribution of energy dissipation, momentum fluxes, and enstrophy, suggesting the implicit technical limitation of the Kolmogorov theory. Our previous works showed that sweep Q4 ($u'' > 0$ and $w'' < 0$) occurs intermittently but contributes more, especially in the roughness sublayer (RSL) that dominates the near-ground transport (Mo and Liu, 2023). This study is therefore conceived to examine the interactions among attention surface roughness, intermittency, and transport processes. It is the first one to reveal the intermittent properties of coherent structures and energy transfer processes over idealized urban areas. In the experiments, the rough surfaces in the wind tunnel are fabricated by plastic LEGO® blocks to represent idealised urban areas. Vertical profiles of velocity and turbulence statistics are sampled by a hot-wire anemometer (HWA) to sample the flows over urban canopies of different surface roughness. In order to identify intermittent structures of all sizes and obtain their phase information, two conventional methods, empirical mode decomposition (EMD) and wavelet analysis of velocity fluctuations, are used for complementary solution. The former decomposes the turbulent wind fields into a series of intrinsic mode functions (IMFs). The latter, on the other hand, utilizes the local intermittency measure (LIM) to detect the intermittent structures and energy transfer in the flows. The joint probability density functions (JPDFs) of fluctuating velocities are expressed in terms of instantaneous frequency and instantaneous amplitude that demonstrate the most frequent dynamical events (Figure 1a). To detect intermittency, LIM and the flatness factor (FF) are calculated by wavelet coefficients. Apparently, intermittency is more significant among the small-scale motions (IMF2 and IMF3) than the large-scale ones (IMF7 and IMF8; Figure 1b). In addition, intermittency diminishes with increasing wall-normal distance. Furthermore, simultaneous LIM peaks with phase synchronization can only be found between two adjacent IMFs (i.e. similar time scales). It is in turn indicated that energy transfer processes are intermittent that tend to occur in-between adjacent time scales. The finding contributes to an in-depth understanding of the nature of intermittent wind fluctuations and turbulence kinetic energy (TKE) cascade mechanisms.

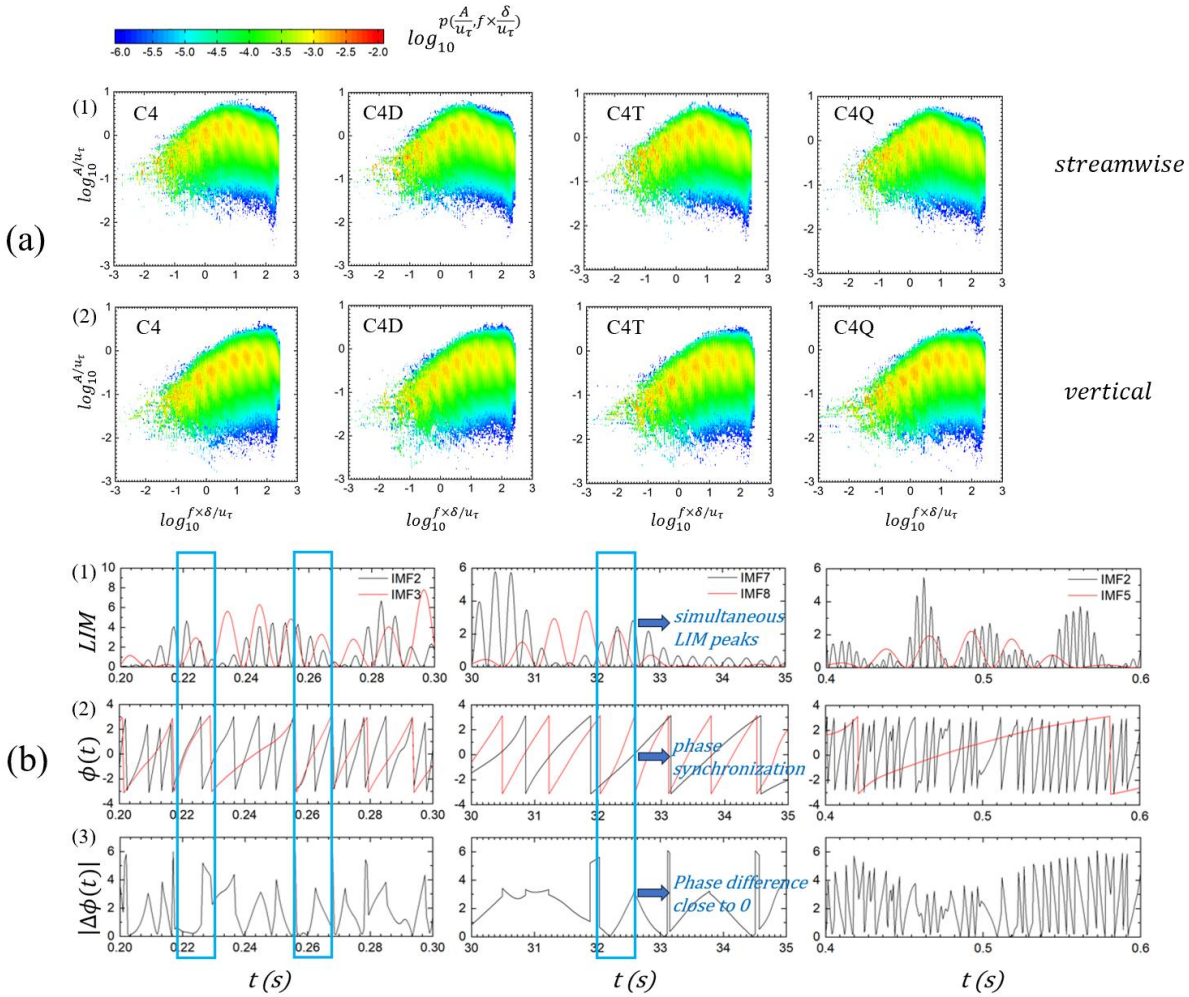

Figure 1: (a) JPDF of (1) streamwise u'' and (2) vertical w'' velocity fluctuations in the amplitude–frequency space in log scale (C4; C4D; C4T; and C4Q are arrays of roughness elements of different densities). (b) Time traces of (1) LIM; (2) phase difference; and (3) absolute phase difference of IMF pairs (IMF2 & IMF3; IMF7 & IMF8; and IMF2 & IMF5).

References

Mo, Z., Liu, C.-H., 2023. Inertial and roughness sublayer flows over real urban morphology: A comparison of wind tunnel experiment and large-eddy simulation. Urban Climate 49, 101530. https://doi.org/10.1016/j.uclim.2023.101530

Ren, Y., Zhang, H., Wei, W., Wu, B., Liu, J., Cai, X., Song, Y., 2019. Comparison of the turbulence structure during light and heavy haze pollution episodes. Atmospheric Research 230, 104645. https://doi.org/10.1016/j.atmosres.2019.104645

Wei, W., Zhang, H., Wu, B., Huang, Y., Cai, X., Song, Y., Li, J., 2018. Intermittent turbulence contributes to vertical dispersion of $PM_{2.5}$ in the North China Plain: cases from Tianjin. Atmospheric Chemistry and Physics 18, 12953–12967. https://doi.org/10.5194/acp-18-12953-2018

Committees

Organising committee

Marilina Barulli (Ecole Centrale Lyon - LMFA)
Perrine Charvolin-Volta (Centrale Innovation - LMFA)
Ariane Emmanuelli (Ecole Centrale Lyon - LMFA)
Sofia Fellini (Politecnico di Torino)
Louis Gostiaux (CNRS - LMFA)
Livia Grandoni (Ecole Centrale Lyon - LMFA)
Stefano Lanzini (Ecole Centrale Lyon - LMFA)
Marie-Noëlle Pailhès (CNRS - LMFA)
Marie Poulain-Zarcos (Ecole Centrale Lyon - LMFA)
Emelyne Rabany (CNRS - LMFA)
Pietro Salizzoni (Ecole Centrale Lyon - LMFA)
Jean Salles-Loustau (Ecole Centrale Lyon - LMFA)
Claudia Schiavini (Ecole Centrale Lyon & Politecnico di Torino - LMFA)

Scientific committee

Ariane Emmanuelli (Ecole Centrale Lyon - LMFA)
Sofia Fellini (Politecnico di Torino)
Livia Grandoni (Ecole Centrale Lyon - LMFA)
Christof Gromke (Karlshrue Insitut für Technology)
Klára Jurčáková (Institute of Thermomechanics of the Czech Academy of Sciences)
Bernd Leitl (University of Hamburg - Meteorological Institute)
Massimo Marro (CNRS - LMFA)
Paolo Monti (Roma La Sapienza)
Marie Poulain Zarcos (Ecole Centrale Lyon - LMFA)
Pietro Salizzoni (Ecole Centrale Lyon - LMFA)
Eric Savory (University of Western Ontario) Lionel Soulhac (INSA - LMFA)

List of participants

- Ahmad Khurshid
- Alexandrou Giorgos
- Babin Valery
- Babuková Zuzana
- Badeke Ronny
- Balczo Marton
- Barulli Marilina
- Bi Dianfang
- Birch David
- Bohbot-Raviv Yardena
- Bouris Demetri
- Carpentieri Matteo
- Chaloupecka Hana
- Charvolin Perrine
- Combette Robin
- Deebank Charles
- Del Ponte Annika Vittoria
- Di Renzo Teresa
- Du Haoran
- Emmanuelli Ariane
- Esposito Antonio
- Fellini Sofia
- Gillmeier Stefanie
- Gostiaux Louis
- Grandoni Livia

- Gromke Christof
- Guoliang Chen
- Harms Frank
- Hayden Paul
- Huret Thomas
- Jakubcová Michala
- Janke David
- Jurcakova Klara
- Kellnerova Radka
- Lanzini Stefano
- Lawton Tom
- Leitl Bernd
- Li Fei
- Lim Desmond
- Liu Chun-Ho
- Márton Koren
- Marro Massimo
- Michard Marc
- Monti Paolo
- Mouzourides Petros
- Nguyen Chi Vuong
- Nosek Štěpán
- Papp Balint
- Pappa Vasiliki
- Perret Laurent
- Pini Agnese
- Poulain-Zarcos Marie
- Rabany Emelyne
- Rico Orero Joan
- Robins Alan
- Salizzoni Pietro
- Salles Loustau Jean

- Sankaran Abhilash
- Savory Eric
- Schiavini Claudia
- Schmeer Joy
- Sedlak Pavel
- Soulhac Lionel
- Southgate-Ash Cameron
- Spicer Tom
- Takumi Tachibana
- Taouil Nada
- Van Den Akker Stephan
- Vuillermoz Samuel
- Wang Ruiqi
- Wu Xuefei
- Xue Yunpeng
- Yoshie Ryuichiro

Author Index